UNIVERSITY OF CALIFORNIA,
IRVINE

Constraining Marine Refractory Dissolved Organic Carbon Cycling Using Carbon Isotopes

DISSERTATION

submitted in partial satisfaction of the requirements
for the degree of

DOCTOR OF PHILOSOPHY

in Earth System Science

by

Christian Blair Lewis

Dissertation Committee:
Professor Ellen R. M. Druffel, Chair
Professor Claudia Czimczik
Professor Brett D. Walker, University of Ottawa

2021

DEDICATION

To my supportive parents, family, wonderful wife Sammy, and pet-in-law Bruno.
Thank you.

TABLE OF CONTENTS

LIST OF FIGURES

LIST OF TABLES

LIST OF TERMS

ACKNOWLEDGEMENTS

There are many people who have influenced my life and work over the past six years, and helped shape my dissertation into a successful work. Foremost, I must thank my thesis advisor Dr. Ellen Druffel. Ellen is an inspirational scientist and role model, who helped shape the field of marine geochemistry. Ellen has always demonstrated hard-work and persistence and promoted optimism, even when road-blocks appear in the course of research. Thank you, Ellen, for supporting me over the last six years, being a constant source of encouragement, and believing in me.

My dissertation also would not have been realized without the ever-present support of our Lab Manager, Sheila Griffin. Sheila's deep knowledge of the methods behind radiocarbon analysis is instrumental in all research undertaken in the Druffel Lab. Her unique ability to light up a room with her laugh keeps the lab a fun place to work. Thank you for your support over these last few years, as a colleague and friend. I was always encouraged by you to pursue creative endeavors outside of work and to stay balanced in life; and I will always be inspired by, and look forward to your unparalleled bakes!

Dr. Brett Walker was the first person I met in the Druffel-family at UCI, and he has since always been a source of support for me. As a postdoctoral scholar in our lab, Brett always found time in a jam-packed schedule of research, undergraduate mentorship, and writing publications, to listen to my ideas and provide essential guidance. Brett is authentic, and has a way of getting to the heart of a problem and finding innovative solutions. His passion for science is always at the fore, and I am grateful to have had the opportunity to be mentored by him.

This work was also made possible by all of our collaborators who study radiocarbon in the Department of Earth System Science, and the Keck Carbon Cycle Accelerator Mass Spectrometry Lab. Thank you to my thesis committee member Dr. Claudia Czimczik, for providing guidance since my first year of graduate school. I am grateful for our lab-neighbor, Dr. Xiaomei Xu, who has not only opened up her lab to share equipment with us, but provided vital advice about experimental design, and how to ensure the proper standards and blanks are analyzed for proper data reduction. Xiaomei is known for the high standard of her data, a benchmark to work towards. I am also thankful to Dr. Guaciara dos Santos for providing essential feedback about how to approach the difficult task of constraining carbon blanks in systems with small-samples. I am also thankful for Dr. John Southon, the backbone of the Keck CCAMS Lab. Through the consistent advancement and complex maintenance of the AMS, John's work lies humbly in the background of every radiocarbon data-point in this dissertation! Thank you to Chanda Bertrand, Hector Martinez, Nassib Shammas, Megha Rudesh, and many others who make the Radiocarbon Prep Lab a positive, collaborative space where amazing science is done.

I must also thank the many other Earth System Science faculty, graduate students, and staff who have influenced my path here at UCI. Thank you to all faculty members for creating a department that continues to inspire with groundbreaking environmental research, and an emphasis on environmentalism, and understanding anthropogenic impacts on our planet. I want to thank the faculty I have had the honor of working alongside as a Teaching Assistant including Dr. Julie Ferguson, Dr. François Primeau and Dr. Ellen Druffel. Thank you to the faculty members who taught our first-year graduate level courses, establishing the groundwork upon which good ESS research could thrive, and thank you to my first-year cohort.

Finally, I thank my friends and family who have been a constant source of support during the past six years. Thank you especially to Sammy, who has supported me through high and low moments unconditionally, and has put up with many moments of stress. Thank you for listening to me rant about all things science, space, and ocean, and encouraging me to have more work-life balance.

Christian B. Lewis

Education:

2015-2021 Ph.D. in Earth System Science, University of California, Irvine

2017 M.S. in Earth System Science, University of California, Irvine

2014 B.S. in Chemistry, Loyola University Maryland

Research Experience:

2015-Present Graduate Research Assistant, University of California, Irvine, Department of Earth System Science, advised by Dr. Ellen Druffel

- Specialized in stable ($\delta^{13}C$) and radiocarbon ($\Delta^{14}C$) isotope measurements of dissolved organic carbon
- Responsible for the maintenance, calibration, and use of preparative capillary GC-FID to isolate pyrogenic compounds for isotopic characterization
- Participated in two international field campaigns to collect dissolved organic carbon and biomarker samples for carbon cycle studies

2014-2015 Fulbright U.S. Student Program Research Grantee, GEOMAR Helmholtz Centre for Ocean Research Kiel, Department of Chemical Oceanography, advised by Dr. Christa Marandino

- Used GC-MS to measure the production of dimethyl sulfide gases in the Kiel Fjord
- Collected trace gas samples aboard the Japanese research vessel Hakuho Maru on a method intercomparison project
- Collected trace gas samples monthly at the Boknis Eck Time Series Station

2013-2014 Hauber Research Fellow, Department of Chemistry, Loyola University Maryland, advised by Dr. Elizabeth Dahl

- Used GC-MS to measure the biological production of alkyl nitrate gases
- Cultured diatoms and cyanobacteria for chemostat experiments

Publications:

1. **Lewis, C.B.** Walker, B.D., Druffel, E.R.M., (2020) Isotopic and optical heterogeneity in solid-phase extracted dissolved organic carbon. *Marine Chemistry* 219 (February): 103752. https://doi.org/10.1016/j.marchem.2020.103752.

2. **Lewis, C.B.** Walker, B.D., Druffel, E.R.M., (2021) Constraining the cycling of global solid-phase extracted dissolved organic carbon using radiocarbon measurements. In review at *Geophysical Research Letters*

Meeting Presentations:

1. **Lewis, C.B.** (2020) Understanding the Ocean Carbon Cycle using Radiocarbon. Talk. February 5, 2020. Jet Propulsion Laboratory, California Institute of Technology.

2. **Lewis, C.B.,** Walker, B.D., Druffel, E.R.M., (2020) Isotopic Measurements of Solid-Phase Extracted Dissolved Organic Matter in the Eastern Pacific Ocean. Ocean Sciences Meeting. Poster. February 16-21, 2020. Portland, Oregon.

3. **Lewis, C.B.** Walker, B.D., Druffel, E.R.M., (2019), Pacific Ocean refractory dissolved organic carbon, Radiocarbon Short Course. Talk. August 12-16, Irvine, California.

4. **Lewis, C.B.** (2019). Compound specific radiocarbon analyses: approach and applications for the environment. 2019 Radiocarbon Short Course, University of California, Irvine, August 2019.

5. **Lewis, C.B.** (2019) A deeper understanding of the microbial carbon pump: collaborative ideas for Earth System Science. Crystal Cove Biogeochemistry Workshop, June 2019.

6. **Lewis, C.B.** Walker, B.D., Druffel, E.R.M., (2018) Isotopic heterogeneity within solid-phase extracted DOC elutions from seawater. Ocean Sciences Meeting. Talk. February 11-16, 2018. Portland, Oregon.

7. **Lewis, C.B.** Walker, B.D., Druffel, E.R.M., (2017) Assessing a new method of marine dissolved organic carbon (DOC) analysis using radiocarbon. The Fourteenth International AMS Conference (AMS14). Invited Talk. August 14-18, 2017. Ottawa, Canada.

Field Experience:

2018 NOAAS Ronald H. Brown, GO-SHIP IO7N – *Radiocarbon of Dissolved Organic Carbon, Dissolved Organics, Biomarkers* (36 days)

2016-2017 NOAAS Ronald H. Brown, GO-SHIP P18N/S – *Radiocarbon of Dissolved Organic Carbon, Dissolved Organics, Biomarkers, Helium/Tritium Sampling* (69 days)

2015 Hakuho Maru, KH1501 - *Distribution of volatile organic compounds in the air-sea boundary during phytoplankton bloom in Oyashio region* (30 days)

2014-2015 R/V Littorina, Boknis Eck Coastal Time Series – *Trace Gas Sampling for measurement of biological production of DMS in the Kiel Fjord* (1 day/month)

Awards and Fellowships:

2020 Graduate Dean's Dissertation Year Fellowship Award

2017 AMS14 Student Travel Grantee – *Student travel grant for the AMS14, the 14th International Radiocarbon Conference*

2017 Antarctica Service Medal – *awarded for service greater than ten days stationed south of 60 degrees of latitude*

2014-2015 Fulbright U.S. Student Program Research Grantee, GEOMAR Helmholtz Centre for Ocean Research Kiel, Department of Chemical Oceanography

Teaching Experience:

2019 Lecturer for Earth System Science Summer Session I, ESS 3, *Oceanography*

2017-Present Teaching Assistant, University of California Irvine. Courses: *Introduction to Earth System Science*, *Oceanography*, *Terrestrial Hydrology*, *Earth System Chemistry*

Outreach:

2019-2020 Graduate InterConnect Peer Mentor – *Serving as a mentor for incoming international graduate students; connecting them to resources on campus, community on and off campus, and facilitating adjustment to graduate student life*

2020 Orange County Chapter Science Olympiad Graduate Student Advisor – *Dynamic Planet B and C – advised undergraduate students on the development of a test focusing on oceanography for middle and high-school aged students*

2019 Mentor Excellence Program – *A 5-session program focused on developing effective mentoring skills, including mentor/mentee relationship lifecycle, ethics in academia, mentoring across differences, conflict resolution and wellness*

2018 UCI Graduate Student Orientation Volunteer

2017-2018 Elected Graduate Student Representative – *Served as temporary liaison between faculty and graduate students in the Earth System Science Department*

2016-2017 CLEAN Education (Climate, Literacy, Empowerment and iNquery) – *Monthly educational workshops about climate and earth science to elementary school students in Costa Mesa, CA.*

2010-2014 Evergreen Orientation Leader (Loyola University Maryland) – *Small-group facilitation of first-year students through orientation and fall-semester. Evergreens receive training in small group facilitation, mentorship, diversity training, and more.*

Memberships:

2017-Present The Oceanography Society

2014-Present American Geophysical Union

ABSTRACT OF THE DISSERTATION

Constraining marine refractory dissolved organic carbon cycling using carbon isotopes

by

Christian B. Lewis

Doctor of Philosophy in Earth System Science

University of California, Irvine, 2021

Professor Ellen R. M. Druffel, Chair

Dissolved organic carbon (DOC) is the largest exchangeable pool of organic carbon in the ocean, and is similar in size to atmospheric carbon. DOC is formed during surface ocean primary production by marine phytoplankton and can survive on average >6000 ^{14}C years in the deep ocean. This residence time greatly exceeds that of dissolved inorganic carbon (DIC), and indicates that a majority of DOC is refractory, or unreactive. Even though previous estimates of refractory DOC (RDOC) abundance is ~95% of total DOC, the mechanisms that facilitate its formation, cycling, and sinks are still poorly understood. A better understanding of these mechanisms is important because the ocean's role in the global carbon cycle, and global physical climate, may link closely to the strength of the biological pump and DOC storage.

This dissertation research characterizes the stable and radiocarbon isotopic compositions ($\delta^{13}C$ and $\Delta^{14}C$) of solid-phase extracted DOC (SPE-DOC), which is representative of RDOC. First, the mass and isotopic composition of extraneous carbon (C_{ex}) in the SPE method is analyzed. This study identifies that one SPE resin commonly used to extract DOC from seawater (Bond Elut PPL) elutes SPE-DOC with isotopic heterogeneity. Incomplete elution may exclude terrestrial-like organic matter that elutes later. An updated protocol including an extended elution is developed to ensure no fractionation of SPE-DOC occurs.

This updated protocol is used to characterize SPE-DOC $\delta^{13}C$ and $\Delta^{14}C$ values at the highest latitudinal resolution to date, using samples from three GO-SHIP Repeat Hydrography Cruises spanning the central and eastern Pacific Ocean and a portion of the western Indian Ocean. SPE-DOC $\delta^{13}C$ and $\Delta^{14}C$ values are significantly lower than those for total DOC. Low $\delta^{13}C$ values relative to total DOC indicate preferential respiration of large biomolecules with high $\delta^{13}C$ values. An additional product of this heterotrophic respiration is carboxy-rich alicyclic matter, which is known to be extremely recalcitrant (C-rich and low in oxygen and hydrogen). These low SPE-DOC $\delta^{13}C$ and $\Delta^{14}C$ values point to the microbial carbon pump (MCP) as a major driver of the marine carbon cycle through the removal of biomolecules with high $\delta^{13}C$, and addition of refractory products that resist degradation. This increases DOC residence time and drives low $\Delta^{14}C$ values. The large meridional span in this $\Delta^{14}C$ dataset also allows for the first regional estimates of RDOC abundance. These estimates match the simple yet powerful "two-pool" model of DOC cycling proposed in 1987, in which the deep ocean is a well-mixed pool of old RDOC, and the surface is a mixture of RDOC from depth and labile DOC from recent photosynthesis.

Although the importance of the MCP, and the two-pool model are not new ideas, sampling has been spatially and temporally sparse. This dissertation research provides a high-resolution isotopic perspective from under-sampled regions in the open ocean that supports these concepts.

Chapter 1: Introduction

1.1 Using carbon isotopes to study the global carbon cycle

The global carbon cycle refers to the exchange of carbon between Earth's atmosphere, land, oceans, and geological reservoirs. Processes such as chemical weathering of rock act on timescales of millions of years, while processes, such as photosynthesis, heterotrophic respiration, air-sea gas exchange, and many others, act on timescales of days to thousands of years. The movement of carbon among Earth's reservoirs influences the atmospheric concentration of carbon dioxide (CO_2), which plays a significant role in global climate. Since the beginning of industrialization, humans have altered the natural carbon cycle by burning fossil fuels at unprecedented rates. In order to understand how each of the Earth systems will respond to increased atmospheric CO_2 concentrations, it is important to study the natural systems, such as the global carbon cycle.

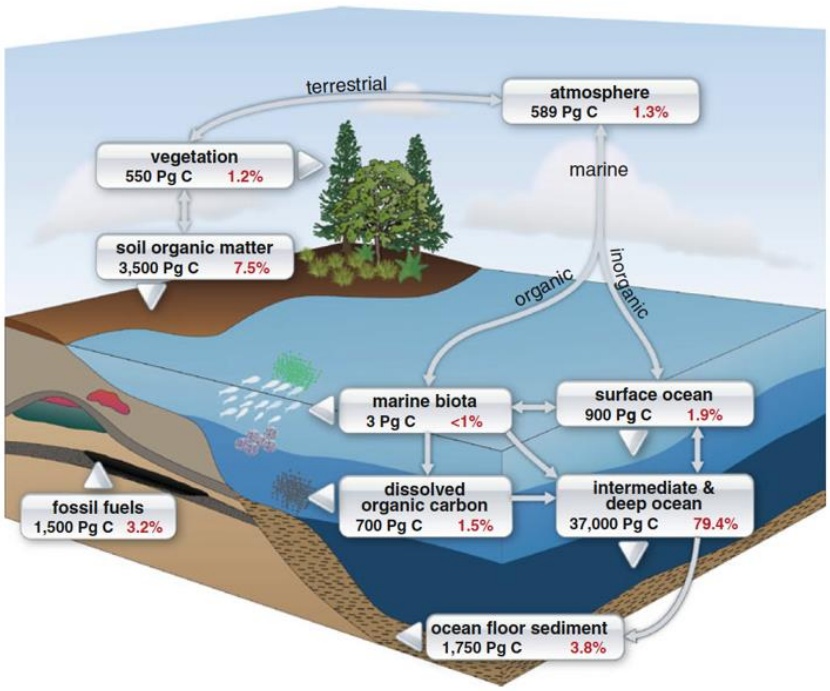

Figure 1. Adapted from Schuur (2016), this diagram shows the different major carbon reservoirs in terms of size (Pg C, black numbers) and fraction of total carbon (percent, red numbers).

Earth's oceans contain the largest reservoir of carbon active on "short" timescales, with 36,000 Pg of dissolved inorganic carbon (DIC) stored primarily in the deep ocean (Takahashi et al., 1981). The oceans also contain 662 Pg of dissolved organic carbon (DOC), which is similar in size to atmospheric carbon (700 Pg) (Hansell et al., 2009). Isotope analyses are a powerful way to trace carbon exchange through these different reservoirs. An isotope is an atom that contains a different number of neutrons than another atom of the same element. Carbon has three naturally occurring isotopes. The most abundant, ^{12}C (98.89%) and ^{13}C (1.11%)) are stable and are created during nucleosynthesis in stars. The least abundant is the radioactive isotope ^{14}C, which is a cosmogenic radionuclide. Cosmic rays interacting with Earth's atmosphere create neutrons that collide with ^{14}N atoms, producing radiocarbon (^{14}C). After a few weeks, ^{14}C is oxidized to carbon monoxide (^{14}CO) and then carbon dioxide ($^{14}CO_2$), mixes throughout the atmosphere and becomes part of the global carbon cycle (Trumbore et al. 2016). Biogeochemical processes such as photosynthesis, or surface ocean dissolution, equilibrate $^{14}CO_2$ between the atmosphere and other reservoirs. When this equilibration is interrupted or stopped, the ^{14}C in a given substance will decay by beta-decay with a half life of 5730 years. This reduces the amount of ^{14}C relative to the atmosphere. Measuring the ratio of ^{14}C to ^{12}C relative to an oxalic acid standard and correcting for isotope fractionation yields a $\Delta^{14}C$ value, defined by (Stuiver & Polach, 1977), and described by the equation below (Beaupré, 2015).

$$\Delta^{14}C = \delta^{14}C - 2(\delta^{13}C + 25)(1 + \left(\frac{\delta^{14}C}{1000}\right))$$

$\Delta^{14}C$ values are useful for determining reservoir ages of carbon in soils, atmospheric CO_2, and ocean water, the latter of which is the focus of this dissertation. The book *Radiocarbon and Climate Change* (2016) provides more information about the history, technical development, calibration, and other uses of radiocarbon in earth science that are not covered in this Introduction.

The heavier stable isotope (^{13}C) is used in different ways to trace the carbon cycle. During physical and chemical transformations (such as phase changes or biosynthesis), the ratio of ^{13}C to ^{12}C can

change, due to the tendency for lighter atoms (^{12}C) to react more quickly than heavier ones (^{13}C). The ratio $^{13}C/^{12}C$ (R) is measured relative to that of a known standard ("PDB" Pee Dee Belemnite), and expressed as "$\delta^{13}C$".

$$\delta^{13}C = \left(\frac{R_{sample}}{R_{standard}} - 1\right) 1000‰$$

In this notation, lower values represent more depletion of ^{13}C in the sample. This isotope fractionation varies depending on the processes occurring during synthesis. Terrestrial photosynthetic pathways each yield different $\delta^{13}C$ values in bulk and compound specific organic matter. C_3 photosynthesis results in organic matter that is lower in $\delta^{13}C$ (depleted in ^{13}C) relative to C_4 photosynthesis (-30‰ to -25‰ versus -16‰ to -10‰, respectively). There is an extensive body of literature on this topic, and is summarized in multiple review papers (Hobbie & Werner, 2004; Hayes, 2001). Marine phytoplankton have distinct $\delta^{13}C$ signatures (-24‰ to -19‰) that are dependent on growth rate, water temperature, and CO_2 concentration (Goericke and Fry 1994; Hinga et al., 1984.; Rau et al. 1982; Rau et al. 1989; Wilkes et al. 2018; Williams and Gordon 1970).

Specific biosynthetic pathways in phytoplankton, such as amino acid production, can be traced using $\delta^{13}C$ values as well (Abelson and Hoering 1961; Close 2018; Macko et al. 1987). Heterotrophic remineralization generally imparts less fractionation than photosynthesis (<1‰ (Shaffer et al., 1999, Beaupre 2015). However, the contribution of microbes to marine organic matter characteristics and their $\delta^{13}C$ values are active areas of research (Close, 2018), and may depend on oxygen availability and substrate composition (Abraham et al. 1998; Close 2018; Gong and Hollander 1997; Macko and Estep 1984; Teece et al. 1999). Measured $\delta^{13}C$ values from primary production and secondary remineralization can often overlap, making $\delta^{13}C$ values of organic matter difficult to interpret. For example, a mixture of organic matter produced by both C_3 and C_4 pathways may combine to resemble the $\delta^{13}C$ value of marine phytoplankton (Pancost & Boot, 2004). However, in well constrained systems, and in parallel with $\Delta^{14}C$

and molecular-level characterization, $\delta^{13}C$ values can be used for source appropriation and in mixing models used to trace carbon flow.

Table 1. List of reported $\delta^{13}C$ values of bulk and compound specific organic matter in marine and terrestrial systems.

Photosynthetic Pathway or Compound Class	$\delta^{13}C$ (‰)	Source
C3	-30‰ to -25‰	Hayes 2001, Hobbie and Werner 2004
C4	-16‰ to -10‰	Hayes 2001, Hobbie and Werner 2004
Phytoplankton	-24‰ to -19‰	Williams and Gordon, 1970
Proteins	Slightly enriched relative to bulk biomass (~1‰)	Abelson and Hoering, 1961, Degens 1968, summarized in Close 2018
Carbohydrates	Slightly enriched relative to bulk biomass (~1‰)	Degens 1968, van Dongen 2002, summarized in Close 2018
Lipids	Depleted relative to bulk biomass (~4‰)	Abelson and Hoering, 1961, Degens 1968, summarized in Close 2018
Lignin	Depleted relative to bulk biomass (~4‰)	Benner et al. 1987

1.2 The role of marine dissolved organic carbon (DOC) in the global carbon cycle

According to Sarmiento & Gruber (2006), "the greatest puzzle in ocean carbon research is our inability to explain the large glacial-interglacial variations in atmospheric CO_2". The oceans are widely accepted as facilitating the changes in atmospheric carbon dioxide during these interglacial cycles because it is the largest of the "fast-changing reservoirs". Changes in the strength of the biological pump, and deep ocean storage of DOC may have played a role (Solomon et al., 2007). The mechanisms behind the cycling and long-term storage of DOC in the global ocean are still under investigation, and are the subject of this dissertation work.

DOC is primarily produced during surface ocean phytoplankton photosynthesis, with a small amount entering via rivers (Opsahl & Benner, 1997). Surface DOC concentrations are high in downwelling regions of the surface ocean (~70-80 µM DOC), such as the subtropical gyres, where water masses converge. Concentrations are low in upwelling zones, where DOC depleted waters mix upwards (~40-50 µM DOC). In the deep ocean, concentrations decrease along the thermohaline circulation, from 50 µM in the North Atlantic Ocean to 36 µM DOC in the deep North Pacific (Hansell et al., 2009).

Early $\Delta^{14}C$ measurements of total DOC in seawater revealed ^{14}C ages of 4000-6500 years (Williams & Druffel, 1987). This result was significant because it showed DOC ^{14}C ages are thousands of years older than those of DIC (see Figure 2), which have ages of ~800-2400 ^{14}C years and are controlled by the global overturning circulation (Stuiver et al., 1983). This implied that a large fraction of DOC has remained undegraded long enough to become well-mixed in the ocean. A simple "two-pool model" of DOC cycling was proposed by (Williams & Druffel, 1987). The surface pool consists of younger, labile DOC mixed with older, refractory DOC (RDOC), while the deeper layer is well-mixed RDOC. Although this simple model explained observations, the mechanisms driving total DOC age and concentrations were still uncharacterized.

1.3 Low molecular weight and solid-phase extracted DOC (SPE-DOC)

To understand the mechanism that drives this long-term storage, and increased age relative to DIC, much effort has been put into molecular characterization of DOC. Are some molecules within DOC more labile or more refractory than others? Are some molecules longer-lived than others? To answer these questions, DOC must first be concentrated and separated based on size, polarity, or compound class. High molecular weight DOC (HMW DOC) is isolated by tangential flow ultrafiltration (1-100 nm, (Benner et al., 1997)), while hydrophobic solid-phase extraction (SPE) resins are used to isolate typically lower molecular weight DOC (LMW DOC) based on polarity. DOC isolated using SPE is known as SPE-DOC. HMW DOC contains the large biomolecules produced by phytoplankton during photosynthesis, including carbohydrates, proteins, nucleic acids, and lipids (Aluwihare & Repeta, 1999; Aluwihare et al., 2002; Benner et al., 1992; Sannigrahi et al., 2005; Zigah et al., 2014). These labile and semi-labile compounds are degraded on timescales from days to decades (Walker et al., 2016a) and used as substates for heterotrophic remineralization. Due to their faster turnover rates than RDOC, these compounds constitute a minority of the total pool (24-28%) (Benner et al. 1997; Skoog and Benner 1997).

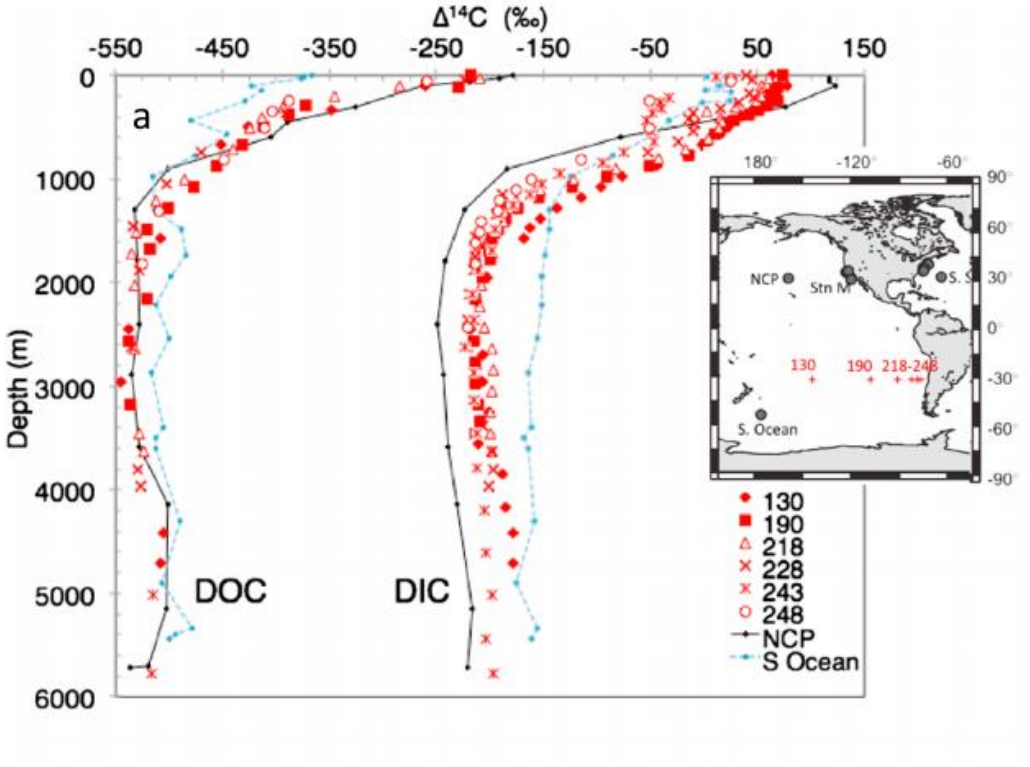

Figure 2. Adapted from Druffel and Griffin (2015), a depiction of the common offset in $\Delta^{14}C$ values between DIC (higher $\Delta^{14}C$, younger ^{14}C age) and DOC (lower $\Delta^{14}C$, higher ^{14}C age), indicating that DOC survives multiple ocean mixing cycles and is important for long-term carbon storage.

The majority of DOC is LMW DOC (Benner et al. 1992; Ogawa and Ogura 1992; Amon and Benner 1994). Relationships between DOC size and age (Walker et al., 2016a, 2016b; Guo et al., 1996; Walker et al., 2011; Loh et al., 2004), and size and polarity (Koch et al., 2008), have established that LMW DOC is older (low $\Delta^{14}C$) and more hydrophobic than HMW DOC. This is shown conceptually in Figure 3. Hydrophobicity of LMW DOC makes SPE on non-polar resins an efficient way to study the cycling of LMW DOC. Molecular characterizations of LMW DOC isolated on XAD and C18 resins showed high abundances of double-bonds, and little difference between the surface and deep ocean, or marine and terrestrial waters. This was indicative of a consistent background material (Koch et al., 2005) soon identified as carboxyl-rich alicyclic molecules (CRAM) (Hertkorn et al. 2006). Bond Elut PPL was identified as the most efficient SPE resin (Dittmar et al., 2008), and has replaced XAD and C18 resins in recent studies. SPE-DOC isolated using PPL resins have led to many recent discoveries about the molecular characteristics of LMW DOC. Studies in the Eastern Atlantic and Southern Oceans have found that CRAM and ketones increase with depth, and a robust relationship between $\Delta^{14}C$, H/C and O/C ratios can be used to predict degradation indexes (Flerus et al. 2012; Hertkorn et al. 2013; Lechtenfeld et al. 2014). Low $\Delta^{14}C$ values as a characteristic trait of SPE-DOC has also been shown in subsequent work (Broek et al., 2017, 2020; Coppola & Druffel, 2016; Zigah et al., 2017). These characteristics all point toward SPE-DOC, and LMW DOC, being refractory in nature, and potentially representative of RDOC. Finally, a landmark study from (Lechtenfeld et al., 2015) found that heterotrophic bacteria create DOC similar to that of RDOC in marine systems (such as CRAM) from simple substrates. This is strong evidence to support the idea that heterotrophic bacteria and the microbial carbon pump (MCP) play a key role in driving the long-term storage of RDOC (Jiao et al., 2010). (This complex history of LMW DOC characterization is summarized in Table 1).

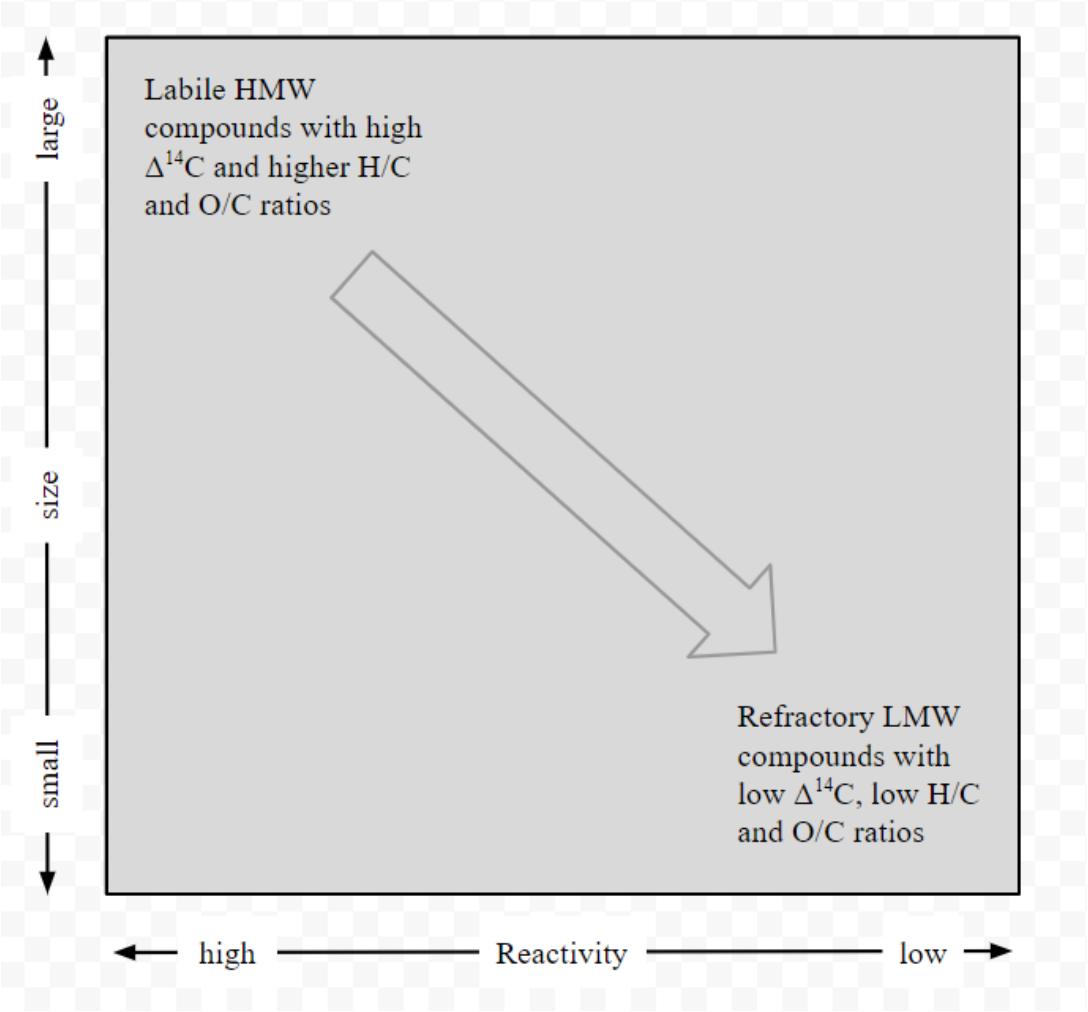

Figure 3. Conceptual diagram of the size-age continuum of DOC adapted from Amon and Benner (1996). Compounds in the top left, typically produced during phytoplankton photosynthesis are larger, have higher H/C and O/C ratios, and are degraded on timescales of years to decades. Compounds in the lower-right are hypothesized to be products of the MCP. These transformed organics have lower H/C and O/C ratios, and often contain CRAM, which contribute to their refractory nature, and low $\Delta^{14}C$.

Table 2. An abbreviated history of the last 15 years of DOC characterization using SPE-DOC and related techniques. Columns filled in gray indicate which analyses were made.

Study	Main Takeaway	Extraction Method	FT-ICR MS	C/N	NMR	$\Delta^{14}C$ (‰)	$\delta^{13}C$ (‰)
Koch et al., 2005	High abundance of double bonds in SPE-DOM; microbial degradation leads to similar features of refractory DOM	XAD and C18 resins					
Hertkorn et al., 2005	Carboxyl-rich alicyclic molecules (CRAM) are a major component of refractory DOM	ultrafiltration					
Koch et al., 2008	There is a relationship between polarity and molecular size; fresh DOM contains peaks absent from old DOM	Reverse-phase LC					
Dittmar et al., 2008	PPL provides efficient extraction of DOM (>40% in marine samples)	PPL +other resins					
Flerus et al., 2012	Correlation between SPE-DOC Δ14C (‰) and H/C ratios results in degradation index model	PPL					
Hertkorn et al., 2013	CRAM increases with depth; surface SPE-DOM has reduced concentrations of methyl esters due to photodegradation; carboxylic acids and ketons increase from surfae to depth	PPL					
Lechtenfeld et al., 2014	Most persistent compounds inhabit an "island of stability" of H/C and O/C ratios	PPL					
Lechtenfeld et al., 2015	Bacteria rapidly uptake simple precursor molecules and produce a wide variety of compounds similar in structure to that of marine DOM. Complex refractory molecules in the environment are driven by bacteria	PPL					
Broek et al., 2017	HMW and LMW DOM have different Δ14C and different elemental and stable carbon isotopic characteristics at all depths	PPL and ultrafiltration					
Broek et al., 2020	LMW DOC is stable through the water column and similar to CRAM, with some additions of HMW DOC to the deep ocean	PPL and ultrafiltration					
Lewis et al., 2020	Bond Elut PPL elutes "marine-like" SPE-DOC followed by "terrestrial-like" SPE-DOC along a hydrophobicity continuum	PPL					

Despite the recent progress in molecular characterization of marine DOC, large spatial gaps in SPE-DOC sampling remain. The Pacific Ocean is largely under sampled save a few measurements from Station ALOHA and the North Pacific Ocean (Bercovici et al., 2018; Broek et al., 2020) and the Indian Ocean contains no measurements prior to this work. Additionally, very few studies (Broek et al., 2017, 2020; Zigah et al., 2017) provide SPE-DOC isotopic measurements relative to total DOC, which allows a more in-depth understanding of LMW DOC cycling . This dissertation aims to characterize the cycling of SPE-DOC in the central and eastern Pacific Ocean and the western Indian Ocean using the highest resolution dataset available to date, using direct comparisons between SPE-DOC and total DOC $\delta^{13}C$ and $\Delta^{14}C$

1.4 Summary of the dissertation

This dissertation uses the isotopic characterization of SPE-DOC in the Pacific and Indian Ocean to provide new constrains to the two-pool model, and support the hypothesis that the MCP may be a driving force in the ocean carbon cycle. SPE-DOC measurements presented in this dissertation were made on DOC that was initially concentrated using Bond Elut PPL SPE resins. Although these resins were in wide use before this research project was started, there were few published studies on carbon blank

characterization. Chapter 2 of this work aims to show how $\delta^{13}C$ and $\Delta^{14}C$ values change over the course of a typical methanol elution of SPE-DOC. Additionally, the magnitude and isotopic signature of blank carbon associated with this SPE method is quantified using an indirect isotopic approach (Santos et al., 2010).

Chapter 3 and Chapter 4 focus on the isotopic characterization of SPE-DOC samples collected aboard three GO-SHIP Repeat Hydrography Cruises in the Eastern and Central Pacific Ocean, and the Western Indian Ocean. Chapter 3 reports SPE-DOC $\Delta^{14}C$ values in direct comparison with total DOC $\Delta^{14}C$ signatures to make the first regional estimates of RDOC abundance. These new data support the original two-pool model of DOC cycling, where the deep ocean background pool is stable and the surface pool is a two-component mixture of RDOC and labile DOC. Chapter 4 uses $\delta^{13}C$ SPE-DOC measurements to suggest that preferential remineralization of biomolecules with high $\delta^{13}C$ values may be a major mechanism through which the ocean's MCP drives marine carbon cycling. Finally, Chapter 5 summarizes the main conclusions of this work, and outlines new questions that arose, and potential areas of future research.

1.5. References

Abelson, P., & Hoering, T. C. (1961). Carbon isotope fractionation in formation of amino acids by photosynthetic organisms. *Proceedings of the National Academy of Sciences*, *47*(5), 623–632.

Abraham, W.-R., Hesse, C., & Pelz, O. (1998). Ratios of Carbon Isotopes in Microbial Lipids as an Indicator of Substrate Usage. *Applied and Environmental Microbiology*, *64*(11), 4202–4209. https://doi.org/10.1128/AEM.64.11.4202-4209.1998

Aluwihare, L. I., & Repeta, D. J. (1999). A comparison of the chemical characteristics of oceanic DOM and extracellular DOM produced by marine algae. *Marine Ecology Progress Series*, *186*, 13.

Aluwihare, L. I., Repeta, D. J., & Chen, R. F. (2002). Chemical composition and cycling of dissolved organic matter in the Mid-Atlantic Bight. *Deep Sea Research Part II: Topical Studies in Oceanography*, *49*(20), 4421–4437. https://doi.org/10.1016/S0967-0645(02)00124-8

Amon, R. M. W., & Benner, R. (1994). Rapid cycling of high-molecular-weight dissolved organic matter in the ocean. *Letters to Nature*, *369*, 549–551.

Beaupré, S. R. (2015). The Carbon Isotopic Composition of Marine DOC. In *Biogeochemistry of Marine Dissolved Organic Matter* (pp. 335–368). Elsevier. https://doi.org/10.1016/B978-0-12-405940-5.00006-6

Benner, R., Pakulski, J. D., McCarthy, M. D., Hedges, J. I., & Hatcher, P. G. (1992). Bulk Chemical Characteristics of Dissolved Organic Matter in the Ocean. *Science*, *255*(5051), 1561–1564.

Benner, R., Biddanda, B., Black, B., & McCarthy, M. (1997). Abundance, size distribution, and stable carbon and nitrogen isotopic compositions of marine organic matter isolated by tangential-flow ultrafiltration. *Marine Chemistry*, *57*, 243–263.

Bercovici, S. K., Koch, B. P., Lechtenfeld, O. J., McCallister, S. L., Schmitt-Kopplin, P., & Hansell, D. A. (2018). Aging and Molecular Changes of Dissolved Organic Matter Between Two Deep Oceanic End-Members. *Global Biogeochemical Cycles*, *32*(10), 1449–1456. https://doi.org/10.1029/2017GB005854

Broek, T. A. B., Walker, B. D., Guilderson, T. P., & McCarthy, M. D. (2017). Coupled ultrafiltration and solid phase extraction approach for the targeted study of semi-labile high molecular weight and refractory low molecular weight dissolved organic matter. *Marine Chemistry*, *194*, 146–157. https://doi.org/10.1016/j.marchem.2017.06.00

Broek, T. A. B., Walker, B. D., Guilderson, T. P., Vaughn, J. S., Mason, H. E., & McCarthy, M. D. (2020). Low Molecular Weight Dissolved Organic Carbon: Aging, Compositional Changes, and Selective Utilization During Global Ocean Circulation. *Global Biogeochemical Cycles*, *34*(6), 1–20. https://doi.org/10.1029/2020GB006547

Close, H. G. (2018). Compound-Specific Isotope Geochemistry in the Ocean. *Annual Review of Marine Science*, *11*, 27–56. https://doi.org/10.1146/annurev-marine-121916-063634

Coppola, A. I., & Druffel, E. R. M. (2016). Cycling of black carbon in the ocean. *Geophysical Research Letters*, *43*(9), 4477–4482. https://doi.org/10.1002/2016GL068574

Dittmar, T., Koch, B., Hertkorn, N., & Kattner, G. (2008). A simple and efficient method for the solid-phase extraction of dissolved organic matter (SPE-DOM) from seawater. *Limnology and Oceanography: Methods*, *6*(6), 230–235.

Flerus, R., Lechtenfeld, O. J., Koch, B. P., McCallister, S. L., Schmitt-Kopplin, P., Benner, R., Kaiser, K., & Kattner, G. (2012). A molecular perspective on the ageing of marine dissolved organic matter. *Biogeosciences*, *9*(6), 1935–1955. https://doi.org/10.5194/bg-9-1935-2012

Goericke, R., & Fry, B. (1994). Variations of marine plankton δ^{13} C with latitude, temperature, and dissolved CO_2 in the world ocean. *Global Biogeochemical Cycles*, *8*(1), 85–90. https://doi.org/10.1029/93GB03272

Gong, C., & Hollander, D. J. (1997). Differential contribution of bacteria to sedimentary organic matter in oxic and anoxic environments, Santa Monica Basin, California. *Organic Geochemistry*, *26*(9), 545–563.

Guo, L., Santschi, P. H., Cifuentes, L. A., Trumbore, S. E., & Southon, J. (1996). Cycling of high-molecular-weight dissolved organic matter in the Middle Atlantic Bight as revealed by carbon isotopic 13C and 14C signatures. *Limnology and Oceanography*, *41*(6), 1242–1252. https://doi.org/10.4319/lo.1996.41.6.1242

Hansell, D. A., Carlson, C. A., Repeta, D. J., & Schlitzer, R. (2009). Dissolved organic matter in the ocean: A controversy stimulates new insights. *Oceanography*, *22*(4), 202–211.

Hayes, J. M. (2001). Fractionation of the Isotopes of Carbon and Hydrogen in Biosynthetic Processes. *Mineralogical Society of America*, 31. https://doi.org/nosams.whoi.edu/jmh/

Hertkorn, N., Benner, R., Frommberger, M., Schmitt-Kopplin, P., Witt, M., Kaiser, K., Kettrup, A., & Hedges, J. I. (2006). Characterization of a major refractory component of marine dissolved

organic matter. *Geochimica et Cosmochimica Acta*, *70*(12), 2990–3010. https://doi.org/10.1016/j.gca.2006.03.021

Hertkorn, N., Harir, M., Koch, B. P., Michalke, B., & Schmitt-Kopplin, P. (2013). High-field NMR spectroscopy and FTICR mass spectrometry: Powerful discovery tools for the molecular level characterization of marine dissolved organic matter. *Biogeosciences*, *10*(3), 1583–1624. https://doi.org/10.5194/bg-10-1583-2013

Hinga, K. R., Arthur, M. A., Pilson, M. E. Q., & Whitaker, D. (1994). Carbon isotope fractionation by marine phytoplankton in culture: The effects of CO2 concentration, pH, temperature, and species. *Global Biogeochemical Cycles*, *8*(1), 91–102.

Hobbie, E. A., & Werner, R. A. (2004). Intramolecular, compound-specific, and bulk carbon isotope patterns in C $_3$ and C $_4$ plants: A review and synthesis. *New Phytologist*, *161*(2), 371–385. https://doi.org/10.1111/j.1469-8137.2004.00970.x

Jiao, N., Herndl, G. J., Hansell, D. A., Benner, R., Kattner, G., Wilhelm, S. W., Kirchman, D. L., Weinbauer, M. G., Luo, T., Chen, F., & Azam, F. (2010). Microbial production of recalcitrant dissolved organic matter: Long-term carbon storage in the global ocean. *Nature Reviews Microbiology*, *8*, 539–599.

Koch, B. P., Ludwichowski, K.-U., Kattner, G., Dittmar, T., & Witt, M. (2008). Advanced characterization of marine dissolved organic matter by combining reversed-phase liquid chromatography and FT-ICR-MS. *Marine Chemistry*, *111*(3–4), 233–241. https://doi.org/10.1016/j.marchem.2008.05.008

Koch, B. P., Witt, M., Engbrodt, R., Dittmar, T., & Kattner, G. (2005). Molecular formulae of marine and terrigenous dissolved organic matter detected by electrospray ionization Fourier transform ion cyclotron resonance mass spectrometry. *Geochimica et Cosmochimica Acta*, *69*(13), 3299–3308. https://doi.org/10.1016/j.gca.2005.02.027

Lechtenfeld, O. J., Hertkorn, N., Shen, Y., Witt, M., & Benner, R. (2015). Marine sequestration of carbon in bacterial metabolites. *Nature Communications*, *6*(1), 8. https://doi.org/10.1038/ncomms7711

Lechtenfeld, O. J., Kattner, G., Flerus, R., McCallister, S. L., Schmitt-Kopplin, P., & Koch, B. P. (2014). Molecular transformation and degradation of refractory dissolved organic matter in the Atlantic and Southern Ocean. *Geochimica et Cosmochimica Acta*, *126*, 321–337. https://doi.org/10.1016/j.gca.2013.11.009

Loh, A. N., Bauer, J. E., & Druffel, E. R. M. (2004). Variable ageing and storange of dissolved organic components in the open ocean. *Letters to Nature*, *430*, 877–881.

Macko, A., Fogel, L., Hare, P. E., & Hoering, T. C. (1987). Isotopic fractionation of nitrogen and carbon in the synthesis of amino acids by microorganisms. *Chemical Geology*, *65*, 14.

Macko, S. A., & Estep, M. L. F. (1984). Microbial alteration of stable nitrogen and carbon isotopic compositions of organic matter. *Organic Geochemistry*, *6*, 787–790.

Ogawa, H., & Ogura, N. (1992). Comparison of two methods for measuring dissolved organic carbon in sea water. *Letters to Nature*, *356*, 696–698.

Opsahl, S., & Benner, R. (1997). Distribution and cycling of terrigenous dissolved organic matter in the ocean. *Nature*, *386*(6624), 480–482. https://doi.org/10.1038/386480a0

Pancost, R. D., & Boot, C. S. (2004). The palaeoclimatic utility of terrestrial biomarkers in marine sediments. *Marine Chemistry*, *92*, 239–261. https://doi.org/doi:10.1016/j.marchem.2004.06.029

Rau, G. H., Sweeney, R. E., & Kaplan, I. R. (1982). Plankton 13C:12C ratio changes with latitude: Differences between northern and southern oceans. *Deep-Sea Research*, *29*(8A), 1035–1039.

Rau, G. H., Takahashi, T., & Marais, D. J. D. (1989). Latitudinal Variations in plankton d13C: implications for CO2 and productivity in past oceans. *Letters to Nature*, *341*, 516–518.

Sannigrahi, P., Ingall, E. D., & Benner, R. (2005). Cycling of dissolved and particulate organic matter at station Aloha: Insights from 13C NMR spectroscopy coupled with elemental, isotopic and molecular analyses. *Deep-Sea Research I*, *52*, 1429–1444. https://doi.org/doi:10.1016/j.dsr.2005.04.001

Santos, G. M., Southon, J. R., Drenzek, N. J., Ziolkowski, L. A., Druffel, E., Xu, X., Zhang, D., Trumbore, S., Eglinton, T. I., & Hughen, K. A. (2010). Blank Assessment for Ultra-Small Radiocarbon Samples: Chemical Extraction and Separation Versus AMS. *Radiocarbon*, *52*(03), 1322–1335. https://doi.org/10.1017/S0033822200046415

Sarmiento, J. L., & Gruber, N. (2006). *Ocean biogeochemical dynamics*. Princeton University Press.

Schuur, E. A. G., Druffel, E. R. M., & Trumbore, S. E. (Eds.). (2016). *Radiocarbon and climate change*. Springer Berlin Heidelberg.

Skoog, A., & Benner, R. (1997). Aldoses in various size fractions of marine organic matter: Implications for carbon cycling. *Limnology and Oceanography*, *42*(8), 1803–1813. https://doi.org/10.4319/lo.1997.42.8.1803

Solomon, S., Qin, D., Manning, M., Marquis, M., Averyt, K., Tignor, M., Miller, H. L., & Chen, Z. (Eds.). (2007). *Climate Change 2007: The Physical Science Basis*. Cambridge University Press.

Stuvier, M, Quay, P. D., & Ostlund, H. G. (1983). Abyssal water C-14 distribution and the age of the world oceans. *Science, 219*, 849–851.

Stuiver, Minze, & Polach, H. A. (1977). Reporting of 14C Data. *Radiocarbon*, *19*(3), 355–363.

Takahashi, T., Broecker, W. S., & Bainbridge, A. E. (1981). The Alkalinity and Total Carbon Dioxide Concentration in the World Oceans. 16.

Teece, M. A., Fogel, M. L., Dollhopf, M. E., & Nealson, K. H. (1999). Isotopic fractionation associated with biosynthesis of fatty acids by a marine bacterium under oxic and anoxic conditions. *Organic Geochemistry*, *30*(12), 1571–1579. https://doi.org/10.1016/S0146-6380(99)00108-4

Trumbore, S. E., Sierra, C. A., & Hicks Pries, C. E. (2016). Radiocarbon Nomenclature, Theory, Models, and Interpretation: Measuring Age, Determining, Cycling Rates, and Tracing Source Pools. In *Radiocarbon and Climate Change*. Springer International Publishing. https://doi.org/10.1007/978-3-319-25643-6

Walker, B. D., Primeau, F. W., Beaupré, S. R., Guilderson, T. P., Druffel, E. R. M., & McCarthy, M. D. (2016). Linked changes in marine dissolved organic carbon molecular size and radiocarbon age. *Geophysical Research Letters*, *43*(19), 9. https://doi.org/10.1002/2016GL070359

Walker, B.D., Beaupré, S. R., Guilderson, T. P., Druffel, E. R. M., & McCarthy, M. D. (2011). Large-volume ultrafiltration for the study of radiocarbon signatures and size vs. Age relationships in marine dissolved organic matter. *Geochimica et Cosmochimica Acta*, *75*(18), 5187–5202. https://doi.org/10.1016/j.gca.2011.06.015

Walker, Brett D., Beaupré, S. R., Guilderson, T. P., McCarthy, M. D., & Druffel, E. R. M. (2016). Pacific carbon cycling constrained by organic matter size, age and composition relationships. *Nature Geoscience*, *9*(12), 888–891. https://doi.org/10.1038/ngeo2830

Wilkes, E. B., Lee, R. B. Y., McClelland, H. L. O., Rickaby, R. E. M., & Pearson, A. (2018). Carbon isotope ratios of coccolith–associated polysaccharides of Emiliania huxleyi as a function of growth rate and CO2 concentration. *Organic Geochemistry*, *119*, 1–10. https://doi.org/10.1016/j.orggeochem.2018.02.006

Williams, P. M., & Gordon, L. I. (1970). Carbon-13: Carbon-12 ratios in dissolved and particulate organic matter in the sea. *Deep Sea Research and Oceanographic Abstracts*, *17*, 19–27.

Williams, P. M., & Druffel, E. R. M. (1987). Radiocarbon in dissolved organic matter in the central North Pacific Ocean. *Letters to Nature*, *330*(6145), 246–248. https://doi.org/10.1038/330246a0

Zigah, P. K., McNichol, A. P., Xu, L., Johnson, C., Santinelli, C., Karl, D. M., & Repeta, D. J. (2017). Allochthonous sources and dynamic cycling of ocean dissolved organic carbon revealed by carbon isotopes: Carbon Isotopes of Marine DOC. *Geophysical Research Letters*, *44*, 2407–2415. https://doi.org/10.1002/2016GL071348

Zigah, P. K., Minor, E. C., Abdulla, H. A. N., Werne, J. P., & Hatcher, P. G. (2014). An investigation of size-fractionated organic matter from Lake Superior and a tributary stream using radiocarbon, stable isotopes and NMR. *Geochimica et Cosmochimica Acta*, *127*, 264–284. https://doi.org/10.1016/j.gca.2013.11.037

Chapter 2: Isotopic and optical heterogeneity of solid phase extracted marine dissolved organic carbon

This chapter was published in Marine Chemistry in 2020:

Lewis, C. B., Walker B.D.W, and Druffel E.R.M. 2020. "Isotopic and Optical Heterogeneity of Solid Phase Extracted Marine Dissolved Organic Carbon." *Marine Chemistry* 219 (February): 103752. https://doi.org/10.1016/j.marchem.2020.103752.

2.1 Abstract

Marine DOC is the ocean's largest exchangeable reservoir of organic carbon. The biogeochemical cycling of DOC plays an important role in ocean carbon storage on various timescales. This study examines how isotopic ($\Delta^{14}C$, $\delta^{13}C$) and optical (absorbance) properties of SPE-DOC change as a function of eluent volume (and hydrophobicity). These properties were measured in 28 SPE-DOC fractions incrementally eluted from Bond Elut PPL (styrene-divinylbenzene polymer) cartridges, totaling 32 mL of methanol. We show that the early eluted SPE-DOC has distinctly different $\Delta^{14}C$ and $\delta^{13}C$ values than those eluted later. This study reveals isotopic heterogeneity as a function of SPE-DOC elution volume. These results show a partitioning of two distinct sources of SPE-DOC during elution, indicating a gradual transition from "marine-like" DOC to "terrestrial-like" DOC along a hydrophobicity continuum.

2.2 Introduction

The marine DOC pool contains ~662 Pg of carbon (Hansell et al., 2009) and is comprised of thousands of individual molecules. Identifiable compound classes include carbohydrates, proteins, lipids, and black carbon (Coppola & Druffel, 2016; Dittmar & Paeng, 2009; Repeta, 2015; Ziolkowski & Druffel, 2010). Early radiocarbon ($\Delta^{14}C$) measurements revealed that the age of deep Pacific Ocean DOC is ~6000 ^{14}C years ($\Delta^{14}C$ = -525‰), indicating that bulk DOC is much older than DIC (2000 ^{14}C years, -240‰) (Williams and Druffel 1987). This implies that DOC survives multiple mixing cycles of the deep ocean. Understanding the processes responsible for this extended residence time of DOC is important for

our understanding of the oceanic carbon cycle. A large effort has been underway to characterize DOC on a molecular level, but large gaps remain in our understanding of the biogeochemical cycling of this complex carbon pool.

SPE is a common method for isolating DOC from seawater salts for further molecular and isotopic analysis. This technique sorbs the hydrophobic fraction of DOC onto a resin that is eluted in a concentrated aliquot of solvent, usually methanol. Bond Elut PPL (styrene-divinylbenzene polymer) SPE resins have been widely used by the marine DOC community for their ease of use and relatively high recoveries of DOC from seawater and freshwater (>40% and 60%, respectively; Dittmar et al. 2008).

SPE-DOC can be processed for $\delta^{13}C$ and $\Delta^{14}C$ analyses, which are powerful tools used to investigate the sources and cycling of DOC. The PPL method has been used to study changes in SPE-DOC $\Delta^{14}C$ with depth in the open ocean (Broek et al., 2017; Flerus et al., 2012; Zigah et al., 2017), and on a molecular level using FT-ICR-MS (Li et al., 2017). $\Delta^{14}C$ analysis paired with FT-ICR-MS of SPE-DOC extracted using PPL resins helped refine our understanding of how DOM degradation is linked to molecular formulae (Flerus et al., 2012; Lechtenfeld et al., 2014). DOC isolated using SPE is usually LMW DOC, and typically has either the same or lower $\delta^{13}C$ and $\Delta^{14}C$ values than bulk seawater (Broek et al., 2017; Coppola & Druffel, 2016; Druffel et al., 1992), indicating that PPL resins selectively isolate a specific fraction of older molecules. This result is echoed in CDOM and FDOM measurements that found less variability in SPE-DOM than bulk DOM (Wünsch et al., 2018). These studies provide evidence that SPE-DOC is different from bulk DOC.

Although PPL SPE-DOC extracts are used for isotopic analyses, there are little detailed carbon mass and isotopic blank assessments for seawater SPE-DOC protocols. A measured $\Delta^{14}C$ value represents the weighted-average $\Delta^{14}C$ value of all compounds in a sample, as well as that of the process-blank. Therefore, the mass and the isotopic value of the process-blank must be determined to accurately assess the true $\Delta^{14}C$ value of the sample. In addition, changes in seawater SPE-DOC isotopic and chemical composition during elution remain undetermined.

The first objective of this study was to optimize the PPL resin protocol (Dittmar et al., t) for maximum SPE-DOC recoveries for future compound specific radiocarbon analyses. Our second objective was to assess extraneous-carbon blanks in our SPE-DOC $\Delta^{14}C$ and $\delta^{13}C$ measurements. Extraneous carbon refers to the amount of carbon added to the sample from the resin and other processes, and must be quantified in order to correct for true environmental isotope values. Our third objective was to determine whether the isotopic and optical composition of SPE-DOC changes with increasing elution volume, and if so, how this impacts final $\Delta^{14}C$ and $\delta^{13}C$ measurements of SPE-DOC.

We present evidence that PPL resins elute marine-derived SPE-DOC first, followed by terrestrial SPE-DOC, based on changing stable isotopic ($\delta^{13}C$) and radiocarbon ($\Delta^{14}C$) signatures of SPE-DOC captured at different elution volumes. We also present a detailed blank assessment of PPL SPE-DOC using the applied background correction method (Santos et al. 2010).

2.3 Materials and methods

2.3.1 Sample collection

Seawater samples were collected from the Newport Beach Pier, CA (33° 36′ 21″ N, 117° 55′ 52″ W). We collected large volume samples (12.5 to 15 L) to match the requirements needed for compound specific radiocarbon analysis of dissolved black carbon. A flowchart to clarify sampling dates, volumes, and subsequent analyses is shown in Figure 4. On March 13, 2017, one 15 L sample (herein called sample 1) was collected for CDOM (chromophoric dissolved organic matter) absorbance analyses. On April 20, 2017, 30 L were collected: 5 L were allocated to one PPL resin for CDOM absorbance analyses (sample 2A), and two 12.5 L aliquots were allocated to two PPL resins for duplicate isotopic analyses (samples 2B and 2C). On August 23, 2017, 15 L were collected using one PPL cartridge for isotopic analyses (sample 3).

Seawater was collected from 0–1 m depth using bucket casts off the pier and filtered using Whatman GF/F filters (0.7 μM) into 1 gallon glass jugs. All glassware and filters were previously baked

at 540°C for 2 hours to eliminate organic carbon contamination. One-gallon samples were immediately acidified to 0.01 M with H_2SO_4 (ACS grade, Lot# 160128). Seawater was extracted using the PPL SPE method (Dittmar et al. 2008) on the day of collection.

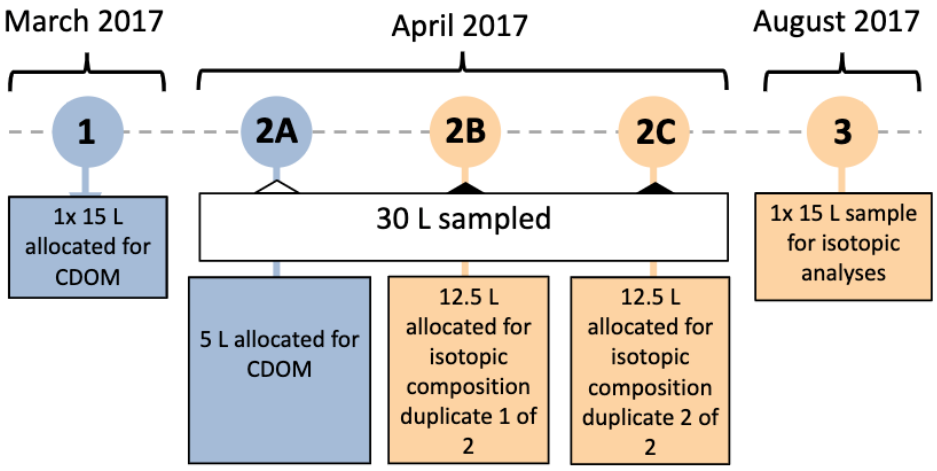

Figure 4. Flow chart describing all sequentially eluted SPE-DOC samples. One 15 L sample was collected in March 2017, eluted sequentially, and measured for CDOM absorbance to obtain a preliminary estimate for where absorbance drops to baseline. Thirty-two mL of methanol was required before absorbances returned to pure methanol absorbance. In April 2017, 30 L were collected. 5 L were allocated to one PPL resin for subsequent CDOM analysis, and the remaining 25 L were split between 2 PPL resins, each for isotopic analyses. Sample 2B was measured for $\Delta^{14}C$, and 2C was measured for $\Delta^{14}C$ and $\delta^{13}C$. 15 L were collected in August 2017 for extraction on one PPL cartridge and $\Delta^{14}C$ and $\delta^{13}C$ analyses.

2.3.2 Solid-phase extraction and elution of SPE-DOC

PPL cartridges (Bond Elut-PPL, 1 gm 6 mL, Part No: 12255002) were activated with methanol (LC-MS grade, CAS# 67-56-1) and rinsed with Milli-Q water (TOC <4 ppb) that had been acidified to 0.01 M with H_2SO_4 (ACS grade, Lot# 160128). The cartridges were loaded with acidified seawater samples at 40 mL/minute using acid-cleaned (10% HCl) Teflon tubing and a Masterflex peristaltic pump. Cartridges were then rinsed with 40 mL of 0.01 M H_2SO_4 and stored at 4°C for 18 hours. Before elutions, cartridges were dried for 30 minutes under UHP N_2. Typically, SPE-DOC is eluted with methanol in a single volume before further processing. For this study, SPE-DOC was eluted in many increments. The first set of samples was eluted in increments of 1 mL, measured by height in a cleaned spectrophotometry

cuvette. Sample 2A, 2B, 2C and 3 were also eluted incrementally, but the volume of each incremental sample was measured by weight difference. It is assumed that the density of methanol at 22.0°C is 0.792 g cm^{-3}. Sequential elutions were carried out until a total of 27-28 SPE-DOC fractions were obtained, for a total volume of 32 mL methanol. It is assumed that the eluted liquid is 100% methanol, containing no residual water from sample storage.

2.3.3 Spectrophotometric, manometric, and isotopic analyses of SPE-DOC

SPE-DOC from samples 1 and 2A were measured for CDOM absorbance at 325 nm and 443 nm on a Thermo Fisher G10S Spectrophotometer. The instrument was tared to a pure methanol baseline. SPE-DOC methanol extracts were homogenized in the cuvette using a baked glass pipet prior to each analysis.

SPE-DOC from samples 2B, 2C, and 3 were dried for 24 hours in a centrifugal evaporator equipped with a -60°C chiller trap. Cupric oxide and silver wire were added to quartz tubes containing the dried samples. Quartz tubes were flame-sealed under vacuum and combusted at 850°C for 2 hours. The resultant CO_2 gas was extracted on a vacuum line and purified cryogenically. The mass of CO_2 gas was quantified using a calibrated manometric pressure gauge in a known volume of the glass line. Assuming complete combustion, the mass of inorganic C in CO_2 is representative of the amount of organic C from the SPE-DOC sample. The CO_2 gas was then transferred to Pyrex tubes for sealed-tube zinc graphitization (Walker & Xu, 2018; Xu et al., 2007). For samples >45 μg C, an isotopically equilibrated split was taken for $\delta^{13}C$ measurement. Fractions yielding less than this total mass do not have an accompanying $\delta^{13}C$ measurement. Radiocarbon measurements were performed at the UC Irvine Keck Carbon Cycle Accelerator Mass Spectrometer Facility. Radiocarbon data are reported as $\Delta^{14}C$ (Stuiverr & Polach, 1977) for geochemical samples without known age. Stable isotopic ($\delta^{13}C$) measurements were performed on a Gas Bench II and Thermo Electron Delta Plus mass spectrometer, corrected using

calibrated isotopic gas standards (to NIST NBS-19) and are reported in standard permille (‰) notation relative to V-PDB (Vienna Pee-Dee Belemnite) scale.

2.3.4 Carbon mass and isotopic blank determinations and corrections

SPE-DOC $\Delta^{14}C$ measurementswere corrected for modern and dead carbon contamination using an indirect-blank assessment. The applied background correction method is described by (Santos et al., 2010). Tannic and salicylic acids (Sigma Aldrich, Lot # MKCD6313 and Lot # MKCC5914) were chosen as standard materials, because they both contain aromatic rings that have a high affinity for the PPL resin. Our tannic and salicylic acid standards were determined to have $\Delta^{14}C$ values of 9±2‰ and -859±1‰, respectively. Three masses of each standard, ranging from 30-700 μg C (See Table 4 for exact masses), were loaded onto PPL cartridges according to standard procedure and eluted with 6 mL of methanol (LC-MS grade, CAS# 67-56-1), in order to assess changes in carbon blank with increasing sample size. This process was repeated a second time with an elution volume of 32 mL, to assess changes in carbon blank with increased methanol volume. For clarity, Figure 10 describes this experimental procedure using a flow chart. Eluted samples were dried and prepared for isotopic measurements as described in Section 2.3.3. Blanks of 1.1 μg C/ mL methanol for the 0-6 mL elutions, and blanks of 0.1 μg C/mL methanol for 6-32 mL, were determined. A mass-balance was applied using the measured PPL resin $\Delta^{14}C$ value of -998±1‰ to blank-correct the sample $\Delta^{14}C$ values. Observed $\delta^{13}C$ values remain uncorrected, because resin C contributes <1% of the mass for these samples, and is negligible for mass-balance correction of $\delta^{13}C$ values.

2.4 Results

2.4.1 SPE-DOC concentrations

Figure 5a shows cumulative elution volume versus the blank corrected carbon mass of the SPE-DOC fractions. Distinct peaks in carbon mass appear at 1.6, 1.8 and 2.0 mL for samples 2B, 2C, and 3 respectively. Within the initial 2 mL elution, 60±1% of cumulative carbon by mass was recovered for samples 2B and 2C, and 16±1% was recovered for sample 3. Although sample 3 eluted more gradually, all samples reached 96±1% cumulative SPE-DOC by 6 mL eluted methanol. Extending the elution to 32 mL yielded 4.8±1.0% more SPE-DOC for all three samples, than if the elution was stopped at 6 mL. Duplicate samples 2B and 2C had [SPE-DOC] values of 26.3±2.0 μM and 28.6±2.0 μM, respectively. For sample 3, [SPE-DOC] was 33.7±2.0 μM. Concentrations were calculated by dividing the sum of blank-corrected carbon masses of all fractions in one profile by the volume of seawater extracted.

2.4.2 SPE-DOC absorbance

Raw absorbance data measured at 325 and 443 nm were converted to natural logarithm absorption coefficients following (Braslavsky, 2007) and were carbon normalized. Absorbances at 325 nm divided by 443 nm (E_3:E_4) are plotted in Figure 6 as a function of eluted methanol volume. The E_3:E_4 values for samples 1 and 2A are maximum at ~3 mL eluted methanol, then decrease to ~10 mL eluted methanol. After 10 mL eluted methanol, sample 1 E_3:E_4 values increase, while those for sample 2A remain lower than 2. We acknowledge that a degree of caution should be used with the interpretation of these CDOM data in context to previous work, because the volumes of extracted seawater differ between Sample 1 and 2A (See Figure 4), and the wavelengths measured are different than those recommended for spectral slope studies (275 to 295 nm) (Helms et al., 2008). Basic implications of the decreasing ratio of absorbance at 325 to 443 nm in context to previous absorbance studies and our isotopic measurements are presented in Section 2.8.

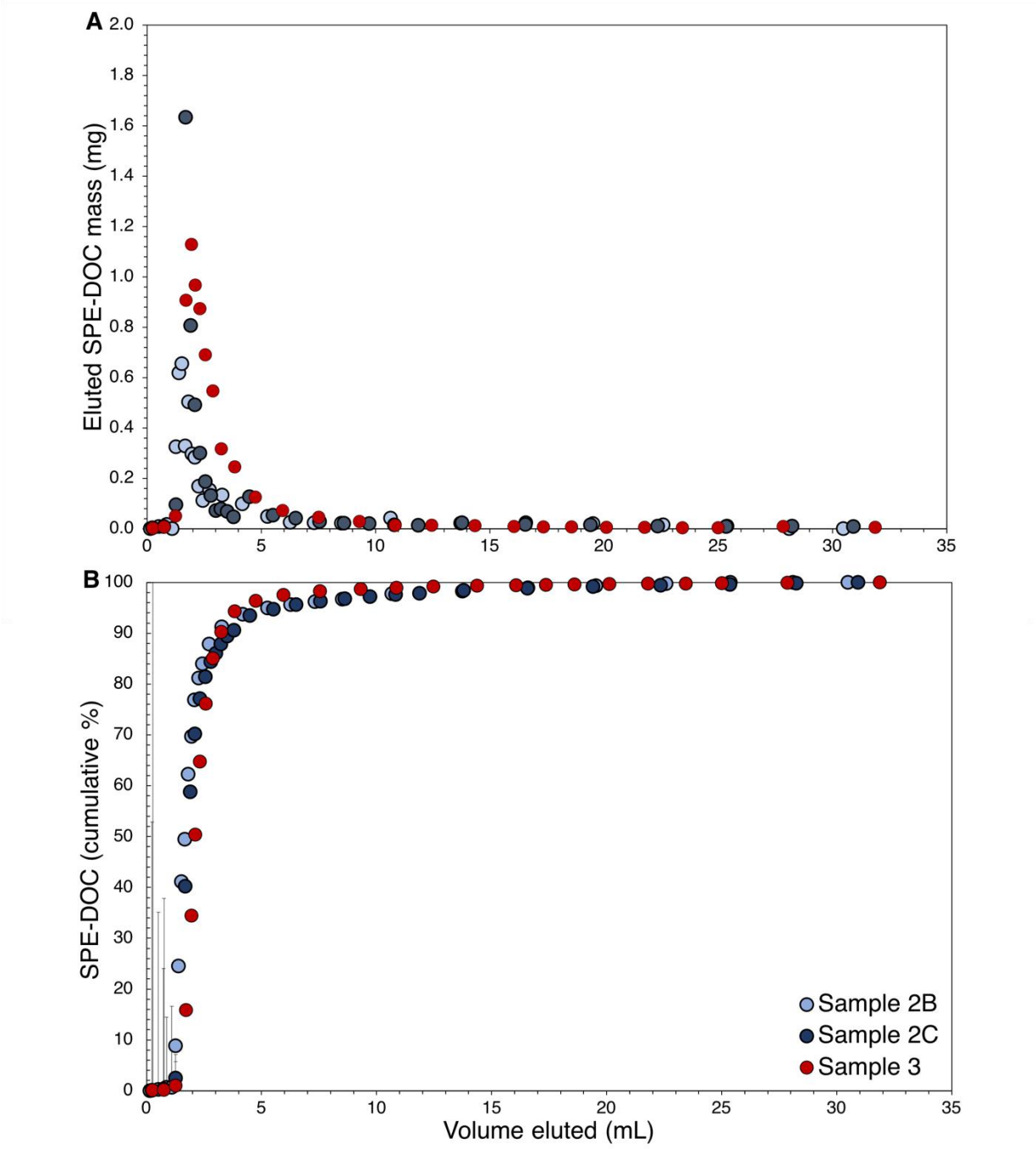

Figure 5. (a) Eluted SPE-DOC masses for samples 2B, 2C and 3 show peaks at 1.6-2.0 mL of eluted methanol. (b) The cumulative percent of isolated SPE-DOC eluted with increasing volume. Percent values were normalized using the total amount of SPE-DOC recovered for each sample.

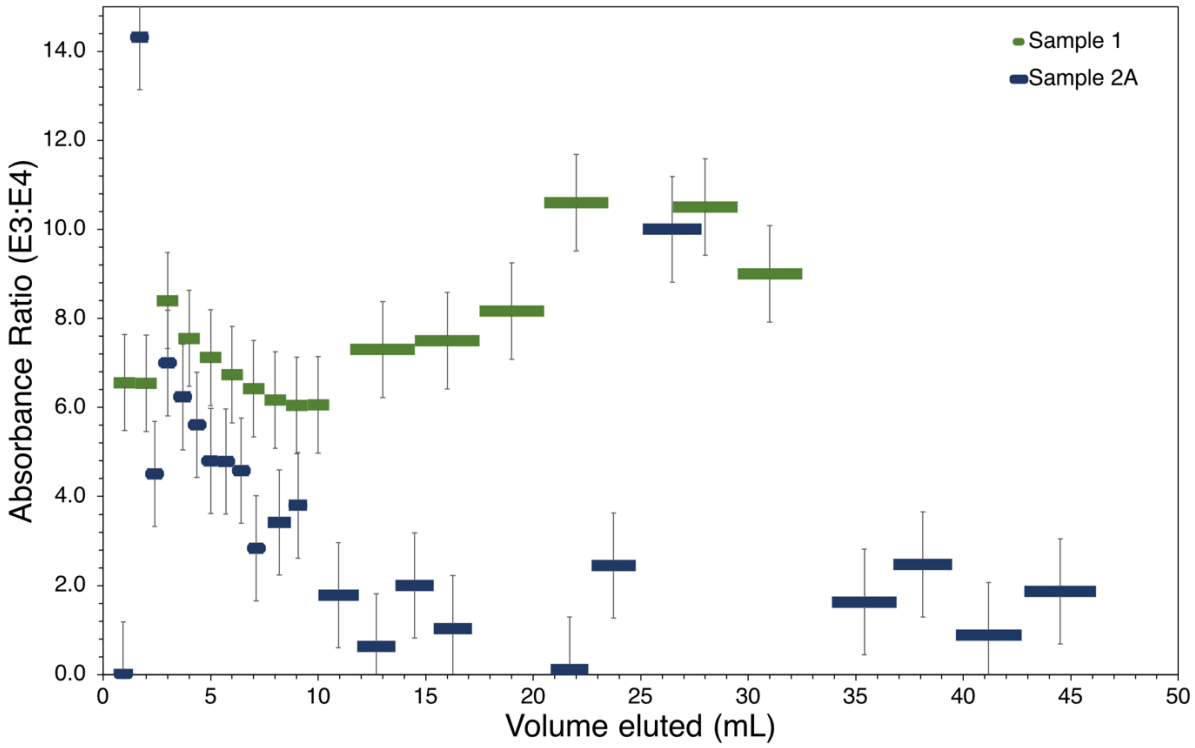

Figure 6. Ratio of CDOM absorbance at 325 and 443 nm (E_3:E_4) from sample 1 and sample 2A versus total volume eluted. From ~3-10 mL, both samples 1 and 2A have negative slopes, indicative of a relative increase in eluted CDOM that absorbs at longer wavelengths (443 nm) versus shorter wavelengths (325 nm). Horizontal bars indicate the integrated volume for each sample. Vertical bars represent standard error.

2.4.3 SPE-DOC $\Delta^{14}C$ values

Radiocarbon measurements of SPE-DOC from the sequential elutions for samples 2B, 2C and 3 are shown in Figure 7. There is variability in the $\Delta^{14}C$ values for all samples. Samples 2B and 2C have local minimum $\Delta^{14}C$ values of -251±5‰ and -221±5‰ between ~1.5-2 mL eluted methanol. As the elution continues, 2B and 2C have progressively higher $\Delta^{14}C$ values, rising to maxima of +253±9‰ and +386±23‰ at 5.8 and 8.1 mL, respectively. The similarities between the $\Delta^{14}C$ profiles of duplicate samples 2B and 2C indicates that our method is reproducible and robust. This pattern of early $\Delta^{14}C$ minimum values corresponding with peak [SPE-DOC] elution, is also found in sample 3. Sample 3 has a minimum of -302±4‰ at 2 mL, then values steadily increase to -123±31‰, and plateau between 5-12 mL

eluted methanol. The major difference between samples 2B and 2C versus sample 3 is the gradient of change between the local minimum at 2 mL and the progressive increase in $\Delta^{14}C$ value throughout the elution. Reasons for this are discussed in section 2.5.

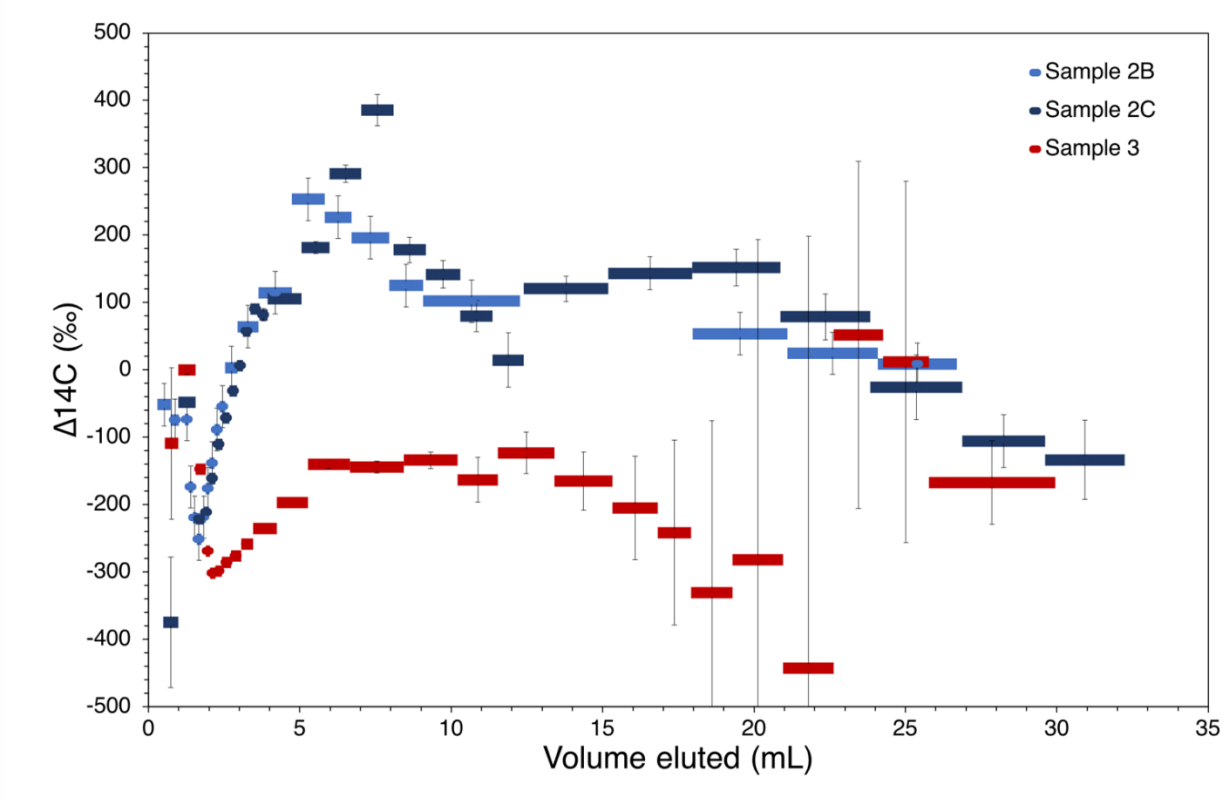

Figure 7. $\Delta^{14}C$ values of sequentially eluted fractions from samples 2B, 2C and 3 versus methanol volume eluted. Horizontal bars indicate the integrated volume of eluted methanol related to each sample, and measured $\Delta^{14}C$ value. Vertical bars represent the propagated uncertainty of our $\Delta^{14}C$ measurement including the contribution of extraneous carbon.

2.4.4 SPE-DOC $\delta^{13}C$ values

The $\delta^{13}C$ values of the sequential elutions for samples 2C and 3 are shown in Figure 8. SPE-DOC has high $\delta^{13}C$ values early in the elution, and lower values by 3.5 mL. Sample 2C decreases from a $\delta^{13}C$ value of -20.2‰ to -23.7‰ from 1.5 to 6 mL eluted methanol. Sample 3 decreases from -21.8‰ to -24.4‰

from 1.9 to 6.6 mL eluted methanol. Unfortunately, $\delta^{13}C$ could not be measured for SPE-DOC fractions containing less than 45 µg C, limiting this dataset to the early (high C mass) eluent fractions.

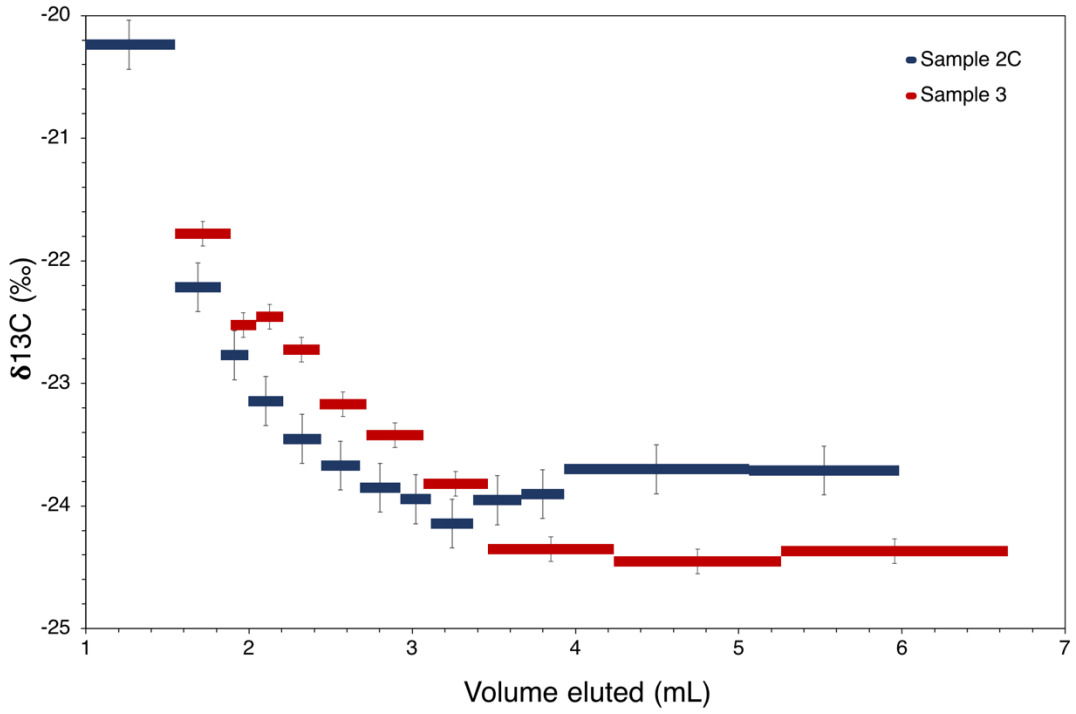

Figure 8: SPE-DOC $\delta^{13}C$ versus methanol volume eluted. Horizontal bars indicate the duration of eluted methanol related to each sample, and measured $\delta^{13}C$ value. Fractions less than 45 µg SPE-DOC (fractions <1 mL and > 7 mL) were not measured for $\delta^{13}C$. Vertical bars indicate the uncertainty of 0.2‰ for Sample 2C and 0.1‰ for Sample 3.

2.5. Discussion

Most SPE-DOC in our samples is contained within the first 2 mL of elution, whose $\Delta^{14}C$ and $\delta^{13}C$ values closely resemble those of phytoplankton-derived, open ocean DOC (Druffel et al. 1992; Williams and Gordon 1970). Over the next ~5 mL of eluted SPE-DOC, the $\delta^{13}C$ values are lower, similar to those of terrestrial C_3 plants (Williams and Gordon 1970), and $\Delta^{14}C$ values reach maximum values. Our $\Delta^{14}C$ and $\delta^{13}C$ datasets together imply that there is a compositional shift in the eluted SPE-DOC, from marine-derived to terrestrial-derived SPE-DOC.

Mid-elution $\Delta^{14}C$ values for samples 2B and 2C were greater than -50‰, which indicates the presence of bomb-^{14}C that was produced during the late 1950s and early 1960s (Nydal & Lövseth, 1983). During the equilibration of bomb-$^{14}CO_2$ between the atmosphere and surface ocean, DIC $\Delta^{14}C$ values in seawater rose to values no higher than +195‰ in the Pacific (Ostlund and Stuiver, 1980). Therefore, samples with $\Delta^{14}C$ values greater than +195‰, such as those > 6 mL in samples 2B and 2C, must contain terrestrially-derived organic matter that was produced after the early 1960s.

Stable carbon isotopic signatures, in this case, are the weaker source indicator because many factors can influence the $\delta^{13}C$ signature of organic matter. Terrestrial C_3 plants synthesize tissues depleted in ^{13}C relative to their C_4 counterparts (-23‰ to -27‰ versus -12‰ to -13‰, respectively), while marine phytoplankton have more positive values (-21‰) (Williams and Gordon 1970; Benner et al. 1987). For example, a value of -21‰ could indicate the presence of SPE-DOC that originated from phytoplankton, or a mixture of C_3 and C_4 plant organic matter. It is difficult to assign a source to SPE-DOC based only on $\delta^{13}C$. In this case, our $\Delta^{14}C$ data clearly show the presence of terrestrially-derived DOC where values are >+195‰, because these values could only have been produced on land. These values appear in the same elution volume as the low $\delta^{13}C$ values (Fig. 7 and 8).

PPL has been shown to preferentially sorb hydrophobic SPE-DOC that is lower molecular weight and typically older than bulk DOC (Broek et al., 2017; Coppola & Druffel, 2016; Druffel et al., 1992). Our data indicate PPL is actively partitioning the DOC during methanol elution according to a hydrophobicity continuum. Because hydrophobicity and aromaticity are linked, partitioning according to aromaticity may also be involved. Further experimental evidence of changes in aromaticity indices with increased elution volume and decreases in molecular polarity could be used to deconvolute these properties.

2.6. Implications for further work

One objective of this study was to optimize the PPL protocol for SPE-DOC isotopic analysis. We found that an extra 5% of SPE-DOC can be extracted from coastal seawater using increased elution volume. Another objective of this study was to assess changes in SPE-DOC isotopic composition with increased elution volume. The isotopic heterogeneity indicates gradients in composition and polarity of the SPE-DOC. This implies that SPE-DOC that elutes early is relatively polar, while SPE-DOC that elutes later is relatively non-polar, based on SPE-DOC affinity to the non-polar PPL resin.

This work could be expanded by integrating analyses capable of showing individual molecular group or aromaticity changes with increased eluted volume. More research is needed to show if these trends are applicable in other marine environments, such as estuaries and the open ocean. For example, FT-ICR-MS analyses of sequentially eluted SPE-DOC may shed light on the oxidation state of molecular groups in different parts of the hydrophobicity continuum. This technique could be used in open ocean studies of refractory DOM, allowing separation of SPE-DOM based on polarity before assessing where they fall in reference to the "island of stability" (Lechtenfeld et al., 2014). This approach may provide more information about the correlation between $\Delta^{14}C$ values, which is a measure of degradability, and molecular structure.

Sequential elutions such as those presented here may provide more detail about the diversity of isotopic signatures within a given SPE-DOC sample. In samples 2B and 2C, the distinctly terrestrial SPE-DOC signature (>+195‰) would have gone unnoticed had it not been eluted in discrete aliquots. Because the later elution samples were a much smaller mass-fraction of the total sample, the weighted-average SPE-DOC $\Delta^{14}C$ signature would have been lower and hidden this interesting piece of information. Sequential SPE-DOC elutions using this method could be used with other analyses to pair changing isotopic composition of each fraction to molecular level characterizations along a hydrophobicity continuum.

2.7. References

Beaupré, S. R. (2015). The Carbon Isotopic Composition of Marine DOC. In *Biogeochemistry of Marine Dissolved Organic Matter* (pp. 335–368). Elsevier. https://doi.org/10.1016/B978-0-12-405940-5.00006-6

Benner, R., Fogel, M. L., Sprague, E. K., & Hodson, R. E. (1987). Depletion of 13C in lignin and its implications for stable carbon isotope studies. *Nature*, *329*(6141), 708–710. https://doi.org/10.1038/329708a0

Braslavsky, S. E. (2007). Glossary of terms used in photochemistry, 3rd edition (IUPAC Recommendations 2006). *Pure and Applied Chemistry*, *79*(3), 293–465. https://doi.org/10.1351/pac200779030293

Broecker, W. S., & Peng, T. H. (1982). *Tracers in the Sea*.

Broek, T. A. B., Walker, B. D., Guilderson, T. P., & McCarthy, M. D. (2017). Coupled ultrafiltration and solid phase extraction approach for the targeted study of semi-labile high molecular weight and refractory low molecular weight dissolved organic matter. *Marine Chemistry*, *194*, 146–157. https://doi.org/10.1016/j.marchem.2017.06.007

Coppola, A. I., & Druffel, E. R. M. (2016). Cycling of black carbon in the ocean. *Geophysical Research Letters*, *43*(9), 4477–4482. https://doi.org/10.1002/2016GL068574

Dittmar, T., Koch, B., Hertkorn, N., & Kattner, G. (2008). A simple and efficient method for the solid-phase extraction of dissolved organic matter (SPE-DOM) from seawater. *Limnology and Oceanography: Methods*, *6*(6), 230–235.

Dittmar, T., & Paeng, J. (2009). A heat-induced molecular signature in marine dissolved organic matter. *Nature Geoscience*, *2*(3), 175–179. https://doi.org/10.1038/ngeo440

Druffel, E. R. M., Williams, P. M., Bauer, J. E., & Ertel, J. R. (1992). Cycling of Dissolved and Particulate Organic Matter in the Open Ocean. *Journal of Geophysical Research*, *97*(C10), 15,639-15,659.

Flerus, R., Lechtenfeld, O. J., Koch, B. P., McCallister, S. L., Schmitt-Kopplin, P., Benner, R., Kaiser, K., & Kattner, G. (2012). A molecular perspective on the ageing of marine dissolved organic matter. *Biogeosciences*, *9*(6), 1935–1955. https://doi.org/10.5194/bg-9-1935-2012

Hansell, D. A., Carlson, C. A., Repeta, D. J., & Schlitzer, R. (2009). Dissolved organic matter in the ocean: A controversy stimulates new insights. *Oceanography*, *22*(4), 202–211.

Helms, J. R., Stubbins, A., Ritchie, J. D., Minor, E. C., Kieber, D. J., & Mopper, K. (2008). Absorption spectral slopes and slope ratios as indicators of molecular weight, source, and photobleaching of chromophoric dissolved organic matter. *Limnology and Oceanography*, *53*(3), 955–969.

Lechtenfeld, O. J., Kattner, G., Flerus, R., McCallister, S. L., Schmitt-Kopplin, P., & Koch, B. P. (2014). Molecular transformation and degradation of refractory dissolved organic matter in the Atlantic and Southern Ocean. *Geochimica et Cosmochimica Acta*, *126*, 321–337. https://doi.org/10.1016/j.gca.2013.11.009

Li, Y., Harir, M., Uhl, J., Kanawati, B., Lucio, M., Smirnov, K. S., Koch, B. P., Schmitt-Kopplin, P., & Hertkorn, N. (2017). How representative are dissolved organic matter (DOM) extracts? A comprehensive study of sorbent selectivity for DOM isolation. *Water Research*, *116*, 316–323. https://doi.org/10.1016/j.watres.2017.03.038

Nydal, R., & Lövseth, K. (1983). Tracing bomb ^{14} C in the atmosphere 1962–1980. *Journal of Geophysical Research*, *88*(C6), 3621. https://doi.org/10.1029/JC088iC06p03621

Peuravuori, J., & Pihlaja, K. (1997). Molecular size distribution and spectroscopic properties of aquatic humic substances. *Analytica Chimica Acta*, *337*(2), 133–149.

Repeta, D. J. (2015). Chemical Characterization and Cycling of Dissolved Organic Matter. In *Biogeochemistry of Marine Dissolved Organic Matter* (pp. 21–63). Elsevier. https://doi.org/10.1016/B978-0-12-405940-5.00002-9

Santos, G. M., Southon, J. R., Drenzek, N. J., Ziolkowski, L. A., Druffel, E., Xu, X., Zhang, D., Trumbore, S., Eglinton, T. I., & Hughen, K. A. (2010). Blank Assessment for Ultra-Small Radiocarbon Samples: Chemical Extraction and Separation Versus AMS. *Radiocarbon*, *52*(03), 1322–1335. https://doi.org/10.1017/S0033822200046415

Stuiverr, M., & Polach, H. A. (1977). Reporting of 14C Data. *Radiocarbon*, *19*(3), 355–363.

Summers, R. S. (n.d.). Molecular Size Distribution and Spectrospcopic Characterization of Humic Substances. *The Science of the Total Environment*, *62*, 27–37.

Walker, B. D., & Xu, X. (2018). An improved method for the sealed-tube zinc graphitization of microgram carbon samples and 14C AMS measurement. *Nuclear Instruments and Methods in Physics Research Section B: Beam Interactions with Materials and Atoms*. https://doi.org/10.1016/j.nimb.2018.08.004

Williams, P. M., & Gordon, L. I. (1970). Carbon-13: Carbon-12 ratios in dissolved and particulate organic matter in the sea. *Deep Sea Research and Oceanographic Abstracts*, *17*, 19–27.

Williams, P. M., & Druffel, E. R. M. (1987). Radiocarbon in dissolved organic matter in the central North Pacific Ocean. *Letters to Nature*, *330*(6145), 246–248. https://doi.org/10.1038/330246a0

Wünsch, U. J., Geuer, J. K., Lechtenfeld, O. J., Koch, B. P., Murphy, K. R., & Stedmon, C. A. (2018). Quantifying the impact of solid-phase extraction on chromophoric dissolved organic matter composition. *Marine Chemistry*, *207*, 33–41. https://doi.org/10.1016/j.marchem.2018.08.010

Xu, X., Trumbore, S. E., Zheng, S., Southon, J. R., McDuffee, K. E., Luttgen, M., & Liu, J. C. (2007). Modifying a sealed tube zinc reduction method for preparation of AMS graphite targets: Reducing background and attaining high precision. *Nuclear Instruments and Methods in Physics Research Section B: Beam Interactions with Materials and Atoms*, *259*(1), 320–329. https://doi.org/10.1016/j.nimb.2007.01.175

Zigah, P. K., McNichol, A. P., Xu, L., Johnson, C., Santinelli, C., Karl, D. M., & Repeta, D. J. (2017). Allochthonous sources and dynamic cycling of ocean dissolved organic carbon revealed by carbon isotopes: Carbon Isotopes of Marine DOC. *Geophysical Research Letters*, *44*, 2407–2415. https://doi.org/10.1002/2016GL071348

Ziolkowski, L. A., & Druffel, E. R. M. (2010). Aged black carbon identified in marine dissolved organic carbon. *Geophysical Research Letters*, *37*(16), n/a-n/a. https://doi.org/10.1029/2010GL043963

2.8. Supporting Information for Chapter 2

2.8.1. SPE resin extraneous carbon assessment

SPE techniques are useful for concentrating organic matter out of seawater for biogeochemical analyses.SPE techniques must be assessed for extraneous carbon (C_{ex}) that may leach from the resin. C_{ex} contributes a discrete mass and isotopic composition that contributes to an observed value according to the following equation:

$$\Delta^{14}C_{observed} = (Fraction_{extraneous})(\Delta^{14}C_{extraneous}) + (Fraction_{environmental})(\Delta^{14}C_{environmental})$$

Assessing the mass and isotopic composition of C_{ex} allows this equation to be solved for $\Delta^{14}C_{environmental}$, a geochemical sample of unknown $\Delta^{14}C$. Direct and indirect approaches for assessing C_{ex} are described below.

2.8.1.1. Direct blanks

Direct blanks involve loading 15 L of acidified MilliQ water onto a 1 g PPL (Bond Elut-PPL, 1 gm 6 mL, Part No: 12255002) resin according to standard procedures (Dittmar et al., 2008), eluting sequentially, and measuring the mass and isotopic composition of the carbon that was leached. 15 L of MilliQ were acidified to 0.01 M with H_2SO_4 (ACS grade, Lot# 160128). This volume was pumped onto the PPL resin using acid-cleaned (10% HCl) Masterflex silicone tubing at 40 mL/minute. After loading, the PPL resin was dried for 30 minutes under a UHP N_2 and eluted sequentially using methanol (LC-MS grade, CAS# 67-56-1) into 5" quartz tubes. Volumes of each fraction were determined by taking the difference of the weight of the empty and full elution vial, assuming the density of methanol at 22.0°C is 0.792 g. Samples were flame sealed under vacuum with cupric oxide and silver wire, combusted at 850°C, and measured for C mass using vacuum line manometry.

As shown in Figure 9and Table 3, the eluted C mass quickly drops from 7.7 μg C/mL in 0-1.25 mL methanol eluted to 0.5 μg/mL at 6 mL methanol eluted. An important caveat of this direct blank

assessment is the presence of organic matter in MilliQ. Our lab MilliQ contains 3 ppb TOC, meaning in 15 L there is ~150 μg. In 22 mL methanol eluted, 53.7 μg C were cumulatively eluted, meaning a 35% recovery of MilliQ TOC. Indirect blank assessments discussed below are a more accurate assessment of C_{ex}.

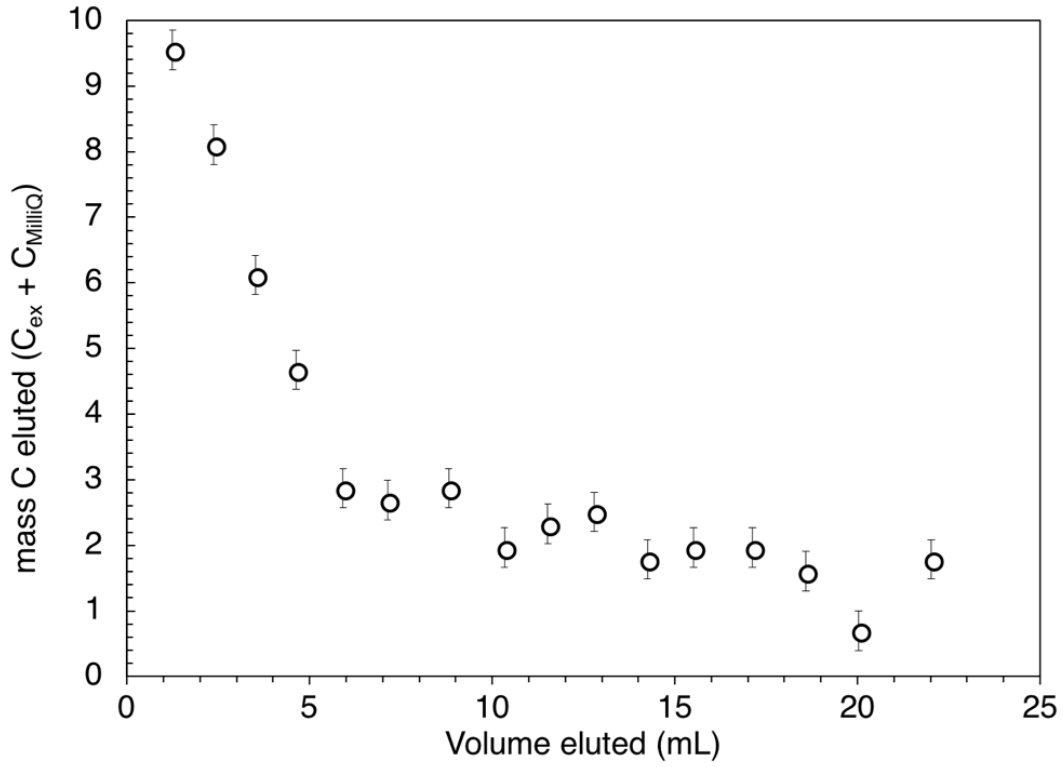

Figure 9: Mass of extraneous carbon (C_{ex}) from the PPL resin and MilliQ water plotted versus volume of methanol eluted. C_{ex} mass decreases over time; indicating an initial leaching of C_{ex} that may be dissolved in methanol.

Table 3 Mass of C_{ex} eluted per mL methanol in direct blank assessment.

Elution Fraction	Cumulative Elution Volume (mL)	C_{ex} Mass eluted (mg)	[C_{ex}] mg C/mL
1	1.2	9.6	7.7
2	2.4	8.1	3.4
3	3.5	6.1	1.7
4	4.6	4.7	1
5	5.9	2.9	0.5
6	7.1	2.7	0.4
7	8.8	2.9	0.3
8	10.3	2	0.2
9	11.5	2.3	0.2
10	12.8	2.5	0.2
11	14.2	1.8	0.1
12	15.5	2	0.1
13	17.1	2	0.1
14	18.6	1.6	0.1
15	20	0.7	0
16	22	1.8	0.1

2.8.1.2 Indirect-blanks

Indirect process blanks assess the difference between the consensus $\Delta^{14}C$ value of a standard and the $\Delta^{14}C$ of that standard after processing. If there is no C_{ex} present, the $\Delta^{14}C$ value after processing will be equal to the consensus value. More C_{ex} will yield more deviation from the consensus value. Tannic acid and salicylic acid were chosen as indirect standards because they contain aromatic rings and have quite different $\Delta^{14}C$ values; the consensus value of tannic acid is 9±2‰, and that for salicylic acid is -859±1‰. PPL resins used in this study are polystyrene divinyl-benzene resins with an isotopic signature of -998±1‰.

Both tannic and salicylic acid were evaluated for C_{ex} in a 3-part size-series for elutions of ~6 mL and ~32 mL each, yielding a total of 12 elutions. For clarity, Figure 10 outlines this experimental procedure in a flow chart. Stock solutions of tannic and salicylic acid were created, and pipetted by volume using an Eppendorf pipette with a cleaned and baked glass-pipette tip. Six mL of acidified MilliQ water were added, and each standard was loaded onto an individual PPL resin. Elutions and manometric analyses were performed as described in section 2.3.2 and 2.3.3.

Using the applied background correction described by (Santos et al. 2010) and our size-series ranging from 30 to 700 μg of standard, C_{ex} was determined to be 6.5±3 μg C for 6 mL elutions, and 9.8±4 μg C for 32 mL elutions. Assuming the following equation is true:

$$C_{ex}\text{total (32 mL)} - C_{ex}\text{initial (6 mL)} = C_{ex}\text{ (6 to 32 mL)}$$

The initial 6 mL C_{ex} value 6.5±3 μg C, normalized by volume yields 1.1 μg C_{ex} / mL. C_{ex} for samples between 6-32 mL methanol was determined to be 9.8 – 6.5 = 3.3±5 ug C. Normalized by 26 mL, this yields 0.1 μg C_{ex} / mL. Environmental samples in the main text were corrected for C_{ex} contribution of $\Delta^{14}C$ = -998±1 using a mass-balance normalized by their volume. The contribution of C_{ex} relative to sample C is very small, typically <0.1% for early eluted samples, and increasing towards later eluted samples because C_{ex} contribution is held constant while total sample size decreased. Radiocarbon ($\Delta^{14}C$) values for sample 2A, 2B, and 3 before and after correction are overlaid in Figure 11..

After C_{ex} correction, weighted average $\Delta^{14}C$ values of different elution volumes can be compared, shown in Table 5(b) . Although modern SPE-DOC elutes post-6 mL, the weighted average values for higher elution volumes remain close to the 6 mL $\Delta^{14}C$ value because the majority of SPE-DOC (>90%) mass elutes between 0-6 mL.

2.8.2 CDOM measurements in context

The decrease in the 325 to 443 nm (E_3:E_4) absorbance ratio for sample 2A is noteworthy in context with the $\Delta^{14}C$ and $\delta^{13}C$ measurements. *Direct* comparison to CDOM absorbance data in previous publications cannot be made, because we measured absorbance at wavelengths 325 and 443nm, while shorter wavelengths (275 to 295 nm) were used in earlier studies (Helms et al., 2008). However, previous work citing both shorter (250 to 365 nm) and longer (465 to 665 nm) wavelengths found decreasing E_2:E_3 and E_4:E_6 ratios correlated with increased molecular size and humification (Peuravuori and Pihlaja 1997; Summers, 1987.; Helms et al. 2008). Our decreasing ratio of 325 to 443 nm absorbances is concabeurrent with decreasing $\delta^{13}C$ and increasing $\Delta^{14}C$ signatures, which imply a compositional shift during PPL elutions.

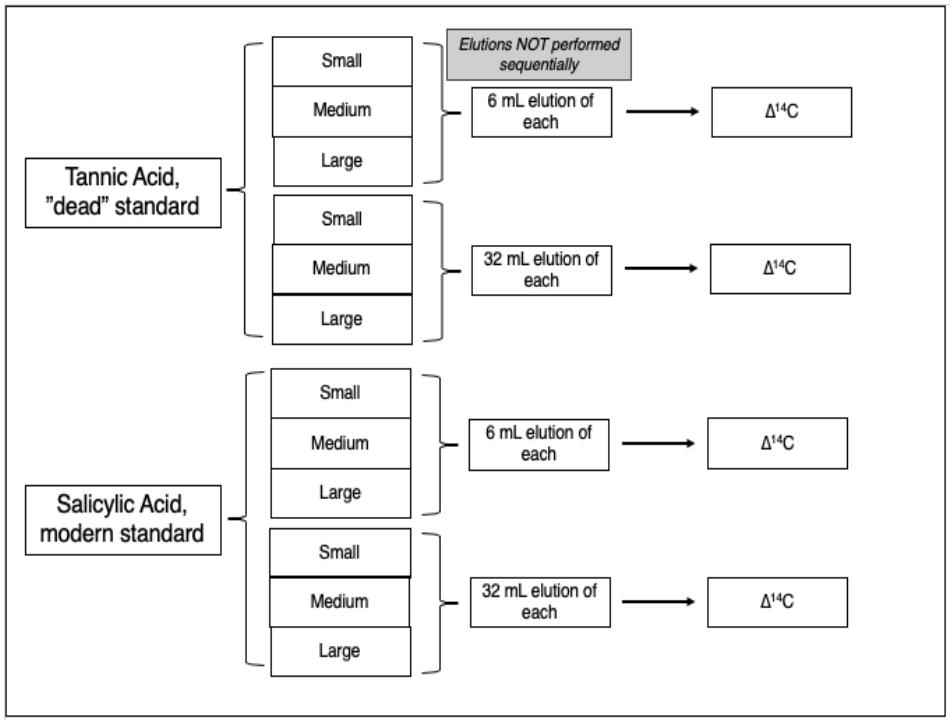

Figure 10: Flow chart depicting the indirect-blank assessment layout. For both modern and dead standards, 6 mL and 32 mL elutions were performed on a size-series of the loaded standard compounds. This yields 12 total elutions used to assess the modern and dead C_{ex} contribution from PPL resins.

Table 4. Data from indirect assessment of C_{ex} mass.

UCID	Standard	Elution volume	µg C added	PPL % recovery	Raw $\Delta^{14}C$ (‰)	±
21477	Tannic	6	50	91	-94	22
21478	Tannic	6	90.3	84	-53	13
21479	Tannic	6	699.4	92	2	2
21480	Salicylic	6	41.5	16	-1000	-585
21481	Salicylic	6	123.5	28	-893	48
21482	Salicylic	6	700	53	-859	2
21483	Tannic	32	50	91	-138	19
21484	Tannic	32	90.3	60	-136	16
21485	Tannic	32	699.4	94	-7	2
21486	Salicylic	32	35.2	37	-764	113
21487	Salicylic	32	123.5	37	-880	35
21488	Salicylic	32	700	66	-860	2

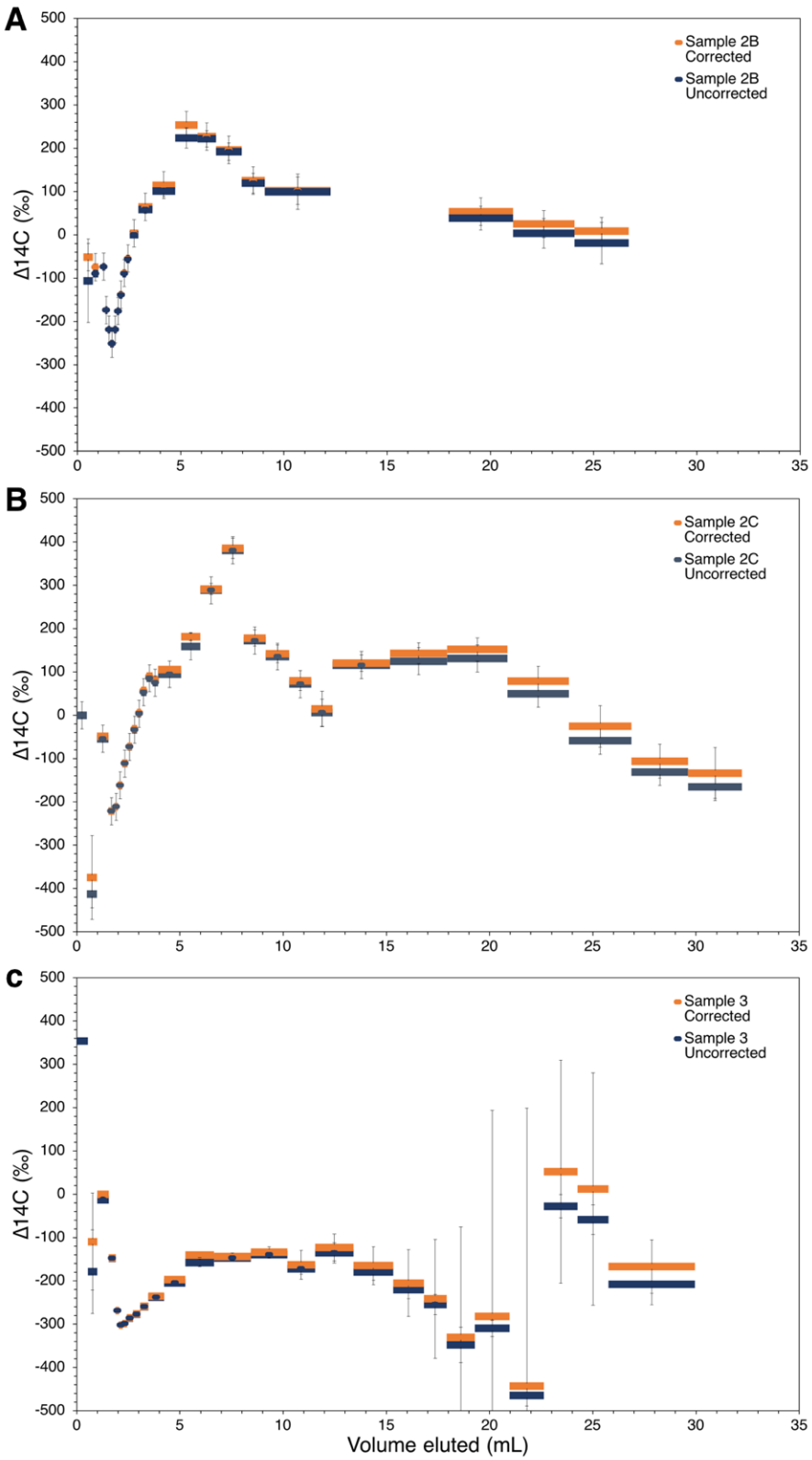

Figure 11: Overlaid plots of raw (blue bars) and corrected (orange bars) $\Delta^{14}C$ profiles for each of the three elution profiles. A, B, and C refer to sample 2A, 2B, and 3 respectively.

Table 5. (a) The cumulative percent of SPE-DOC mass eluted relative to total at different elution points. (b) Weighted average SPE-DOC $\Delta^{14}C$ values for different total elutions volumes. Although more modern SPE-DOC elutes later, the weighted average remains close to the 6 mL value because >94% of SPE-DOC mass elutes in that section.

(a)

UCID	~6 mL	~10 mL	~20 mL	~32 mL
Sample 2B	94.9	96.7	99.3	100
Sample 2C	94.6	97.2	99.1	100
Sample 3	97.5	98.7	99.7	100

(b)

UCID	~6 mL	~10 mL	~20 mL	~32 mL
Sample 2B	-139±6	-136±6	-134±6	-134±6
Sample 2C	-145±9	-138±10	-136±11	-136±12
Sample 3	-247±5	-250±5	-252±6	-252±6

Table 6. Tables (a), (b), and (c) show datasets 2B, 2C, and 3, respectively. Cells with n/a represent where that parameter was not applicable, and cells with n.m. represent where a parameter was not measured. Cells with "lost" represent data lost during AMS measurement.

(a)

Sample Set	UCID	UCI AMS#	Fraction #	Total Volume Eluted	corrected carbon mass (ug)	corrected $\Delta^{14}C$ (‰)	±	δ13C (‰)	±
2B	20910	n/a	1	0.3	lost	lost	n/a	n.m.	n.m.
2B	20911	189457	2	0.7	8.1	-52	55	n.m.	n.m.
2B	20912	189458	3	1.0	17.0	-75	19	n.m.	n.m.
2B	20913	n/a	4	1.2	lost	lost		n.m.	n.m.
2B	20914	189459	5	1.3	324.5	-74	2	n.m.	n.m.
2B	20915	189460	6	1.5	619.0	-174	3	n.m.	n.m.
2B	20916	189461	7	1.6	655.6	-219	2	n.m.	n.m.
2B	20917	189462	8	1.7	329.0	-251	2	n.m.	n.m.
2B	20918	189463	9	1.9	503.2	-219	2	n.m.	n.m.
2B	20919	189464	10	2.0	295.9	-176	3	n.m.	n.m.
2B	20920	189465	11	2.2	282.8	-138	3	n.m.	n.m.
2B	20921	189466	12	2.4	168.2	-89	3	n.m.	n.m.
2B	20922	189467	13	2.5	112.1	-55	3	n.m.	n.m.
2B	20923	189468	14	2.9	152.8	3	3	n.m.	n.m.
2B	20924	189469	15	3.6	133.1	64	3	n.m.	n.m.
2B	20925	189470	16	4.7	98.1	115	4	n.m.	n.m.
2B	20926	189471	17	5.8	48.5	253	9	n.m.	n.m.
2B	20927	189472	18	6.7	25.8	227	19	n.m.	n.m.
2B	20928	189473	19	7.9	23.7	196	11	n.m.	n.m.
2B	20929	189474	20	9.1	21.5	125	14	n.m.	n.m.
2B	20930	189475	21	12.3	40.9	102	8	n.m.	n.m.
2B	20931	n/a	22	15.2	21.3	lost	n/a	n.m.	n.m.
2B	20932	n/a	23	18.0	23.5	lost	n/a	n.m.	n.m.
2B	20933	189476	24	21.1	19.2	54	16	n.m.	n.m.
2B	20934	189477	25	24.1	14.8	25	21	n.m.	n.m.
2B	20935	189478	26	26.7	10.5	8	34	n.m.	n.m.
2B	20936	n/a	27	29.5	lost	lost	n/a	n.m.	n.m.
2B	20937	n/a	28	31.5	lost	lost	n/a	n.m.	n.m.

(b)

Sample Set	UCID	UCI AMS#	Fraction #	Total Volume Eluted	corrected carbon mass (ug)	corrected $\Delta^{14}C$ (‰)	±	δ13C (‰)	±
2C	21049	201959	3	1.5	94.6	-48	3	-20.2	0.2
2C	21050	201960	4	1.8	1633.9	-221	2	-22.2	0.2
2C	21051	201961	5	2.0	807.2	-211	1	-22.8	0.2
2C	21052	201962	6	2.2	491.1	-161	1	-23.1	0.2
2C	21053	201963	7	2.4	300.5	-111	2	-23.5	0.2
2C	21054	201964	8	2.7	185.9	-72	3	-23.7	0.2
2C	21055	201965	9	2.9	131.8	-32	3	-23.9	0.2
2C	21056	201966	10	3.1	71.2	7	5	-23.9	0.2
2C	21057	201967	11	3.4	77.6	57	4	-24.1	0.2
2C	21058	201968	12	3.7	68.9	91	5	-24.0	0.2
2C	21059	201969	13	3.9	47.3	82	9	-23.9	0.2
2C	21060	201970	14	5.1	126.3	105	4	-23.7	0.2
2C	21061	201971	15	6.0	53.1	181	9	-23.7	0.2
2C	21062	201972	16	7.0	41.0	291	13	n.m.	n.m.
2C	21063	201973	17	8.1	28.0	386	23	n.m.	n.m.
2C	21064	201974	18	9.2	21.5	178	19	n.m.	n.m.
2C	21065	201975	19	10.3	19.4	142	20	n.m.	n.m.
2C	21066	201976	20	11.4	15.0	80	23	n.m.	n.m.
2C	21067	201977	21	12.4	12.9	15	41	n.m.	n.m.
2C	21068	201978	22	15.2	23.7	121	19	n.m.	n.m.
2C	21069	201979	23	17.9	17.0	143	24	n.m.	n.m.
2C	21070	201980	24	20.9	14.9	152	27	n.m.	n.m.
2C	21071	201981	25	23.8	10.5	79	34	n.m.	n.m.
2C	21072	201982	26	26.9	8.4	-26	48	n.m.	n.m.
2C	21073	201983	27	29.6	10.5	-106	39	n.m.	n.m.
2C	21074	201984	28	32.2	8.3	-134	59	n.m.	n.m.

(c)

Sample Set	UCID	UCI AMS#	Fraction #	Total Volume Eluted	corrected carbon mass (ug)	corrected $\Delta^{14}C$ (‰)	±	δ13C (‰)	±
3	21233	197504	3	1.5	48.8	0	6	n.m.	n.m.
3	21234	197505	4	1.9	905.9	-148	2	-21.8	0.1
3	21235	197506	5	2.0	1127.3	-269	2	-22.5	0.1
3	21236	197507	6	2.2	966.2	-302	2	-22.5	0.1
3	21237	197508	7	2.4	871.7	-298	1	-22.7	0.1
3	21238	197509	8	2.7	689.1	-286	1	-23.2	0.1
3	21239	197510	9	3.1	545.1	-277	2	-23.4	0.1
3	21240	197511	10	3.5	315.3	-259	2	-23.8	0.1
3	21241	197512	11	4.2	244.0	-236	3	-24.4	0.1
3	21242	197513	12	5.3	123.4	-197	2	-24.5	0.1
3	21243	197514	13	6.6	71.5	-140	6	-24.4	0.1
3	21244	197515	14	8.4	44.9	-144	9	n.m.	n.m.
3	21245	197516	15	10.2	27.7	-134	13	n.m.	n.m.
3	21246	197517	16	11.5	12.8	-163	33	n.m.	n.m.
3	21247	197518	17	13.4	12.7	-123	31	n.m.	n.m.
3	21248	197519	18	15.3	10.5	-165	43	n.m.	n.m.
3	21249	197520	19	16.8	7.4	-205	77	n.m.	n.m.
3	21250	197521	20	17.9	6.3	-242	137	n.m.	n.m.
3	21251	197522	21	19.3	5.2	-331	255	n.m.	n.m.
3	21252	197523	22	21.0	4.1	-282	476	n.m.	n.m.
3	21253	197524	23	22.6	4.1	-443	641	n.m.	n.m.
3	21254	197525	24	24.3	2.0	52	257	n.m.	n.m.
3	21255	197526	25	25.8	2.0	12	268	n.m.	n.m.
3	21256	197527	26	30.0	8.2	-167	62	n.m.	n.m.
3	21257	197528	27	33.3	3.9	lost	n/a	n.m.	n.m.

2.8.3 Supporting information references

Helms, J. R., Stubbins, A., Ritchie, J. D., Minor, E. C., Kieber, D. J., & Mopper, K. (2008). Absorption spectral slopes and slope ratios as indicators of molecular weight, source, and photobleaching of chromophoric dissolved organic matter. *Limnology and Oceanography*, *53*(3), 955–969.

Peuravuori, J., & Pihlaja, K. (1997). Molecular size distribution and spectroscopic properties of aquatic humic substances. *Analytica Chimica Acta*, *337*(2), 133–149.

Santos, G. M., Southon, J. R., Drenzek, N. J., Ziolkowski, L. A., Druffel, E., Xu, X., Zhang, D., Trumbore, S., Eglinton, T. I., & Hughen, K. A. (2010). Blank Assessment for Ultra-Small Radiocarbon Samples: Chemical Extraction and Separation Versus AMS. *Radiocarbon*, *52*(03), 1322–1335. https://doi.org/10.1017/S0033822200046415

Summers, R. S., Cornel, P. K., & Roberts, P. V. (1987). Molecular Size Distribution and Spectrospcopic Characterization of Humic Substances. *The Science of the Total Environment*, *62*, 27–37.

Chapter 3: New radiocarbon constraints on the global cycling of solid-phase extractable dissolved organic carbon

3.1. Abstract

DOC $\Delta^{14}C$ measurements in the deep ocean suggest it can be >6500 ^{14}C years old. The mechanisms that mediate this residence time remain unconstrained. SPE is a widely used technique that isolates hydrophobic, LMW DOC that is typically older. We present SPE-DOC concentrations and $\Delta^{14}C$ values for three GO-SHIP Repeat Hydrography transects, spanning the Pacific and Indian Oceans. Comparisons of SPE-DOC with total DOC $\Delta^{14}C$ values are used with an isotopic mass-balance to estimate the size of the RDOC reservoir and changes in relative abundance in the global ocean. Estimated RDOC abundance is similar across the deep Pacific and Indian Oceans (average = 88±1%, 33±2 μM), whereas surface RDOC varies as a function of total DOC. Our results fill in spatial SPE-DOC $\Delta^{14}C$ sampling gaps for the global ocean, and our mass-balance RDOC estimates are consistent with previous observations of a "two-pool" model of DOC cycling.

3.2. Introduction

The ocean contains ~662 Pg of dissolved organic carbon (DOC) (Hansell et al., 2009); the largest exchangeable reservoir of organic carbon in the ocean (Hedges, 1992). However, the mechanisms that mediate DOC cycling are still areas of ongoing research. $\Delta^{14}C$ measurements are key tools used to investigate carbon cycling (McNichol & Aluwihare, 2007), including DOC. The first DOC $\Delta^{14}C$ depth profiles showed DOC is 6000 ^{14}C years old in the deep ocean (Williams & Druffel, 1987). This is much older than DIC (2200 ^{14}C years) from which DOC is photosyntheized and implies a large amount of RDOC is resistant to biological degradation.

Measurements of total [DOC] and DOC $\Delta^{14}C$ have been made in the North Pacific, South Pacific, Southern Ocean, Atlantic Ocean, and Indian Ocean (Bercovici et al., 2018; Druffel & Griffin, 2015; Druffel et al., 2019; Druffel & Bauer, 2000; Williams & Druffel, 1987). Measurements repeatedly show

high concentrations and $\Delta^{14}C$ values in the surface ocean, and lower values below 1000m. These findings led to the "two-pool" model, that postulates the existence of a homogeneously old pool of RDOC in the deep ocean, and a surface pool containing a 1:1 mixture of RDOC and recently produced, labile DOC (Williams & Druffel, 1987). The "two-pool" model has remained a simple, effective representation of the net system. However, it does not consider the various reactivities of individual molecular classes that also require characterization (Beaupré, 2015).

Ultrafiltration (UF) is commonly used to isolate HWM DOC, while SPE is used to isolate hydrophobic DOC that is LMW and typically older. These techniques have yielded a wealth of information about different fractions of DOC (Aluwihare et al., 2002; Broek et al., 2017; Coppola & Druffel, 2016; Druffel et al., 1992; Hertkorn et al., 2013; Lechtenfeld et al., 2014; McNichol & Aluwihare, 2007; Medeiros et al., 2015; Repeta & Aluwihare, 2006; Santschi et al., 1998; Ziolkowski & Druffel, 2010) and demonstrated a strong relationship between apparent size and radiocarbon age (Guo et al., 1996; Loh et al., 2004; Walker et al., 2016(a); Walker et al., 2016(b); Walker et al., 2011). SPE-DOC $\Delta^{14}C$ has been characterized at Station Aloha, in the North Pacific Ocean, the Atlantic, and Southern Oceans (Bercovici et al., 2018; Broek et al., 2017, 2020; Hertkorn et al., 2013; Lechtenfeld et al., 2014; Zigah et al., 2017). SPE-DOC has been shown to overlap significantly with RDOC. It contains CRAM (Hertkorn et al., 2013), and groups of "stable" DOC molecules with low $\Delta^{14}C$ and lower H/C and O/C ratios than labile molecules (Broek et al., 2017, 2020; Coppola & Druffel, 2016; Lechtenfeld et al., 2014; Zigah et al., 2017). This implies SPE-DOC contains unreactive LMW DOC (according to the size-reactivity model). RDOC has also been classified as DOC in the deep ocean where there is no vertical concentration gradient (>1000 m and <42 μM) (Hansell, 2013). Although it is a simplification, for the purposes of this study, we assume SPE-DOC is RDOC.

Estimates of RDOC production in the global ocean ranges by orders of magnitude (Benner & Herndl, 2011; Brophy & Carlson, 1989; Hansell, 2013; Walker et al., 2016) and few global concentration estimates exist. DOC concentration gradients were used to estimate that 95% of all DOC is RDOC

(Hansell 2013). Continued efforts to constrain cycling of RDOC in more detail is important for our understanding of how the ocean will respond to changes in the carbon cycle.

This work presents a dataset of SPE-DOC $\Delta^{14}C$ signatures from three GO-SHIP Repeat Hydrography cruises; two in the Pacific Ocean spanning >120° of combined latitude and several different ocean biomes (Moreno et al., 2020), and one cruise in western Indian Ocean. We use SPE-DOC and total DOC $\Delta^{14}C$ from the same cruises and construct a mass-balance model to estimate RDOC abundance in different ocean regions. The unprecedented span of our dataset allows us to test new meridional constrains on the two-pool model.

3.3. Methods

3.3.1 Sample collection

Seawater samples were collected aboard GO-SHIP Repeat Hydrography cruises P16N (2015), P18 (2016/17), and IO7N (2018) aboard the NOAAS Ronald H. Brown (see Figure 12). All samples were collected using Bullister-type Niskin bottles through silicone tubing (soaked in 10% hydrochloric acid) into 1-gallon, pre-baked glass bottles (540°C for 2 hours) and acidified to pH 2 with concentrated sulfuric acid (ACS grade, Lot# 160128). Seawater from <200 m depth was filtered using a Whatman GF/F 0.7 μm filter. Due to water budget and sample volume limitations, large volumes of depth-integrated seawater were sampled for SPE-DOC in two depth ranges; surface water (0-200m) and deep water (2000-4000m). Table 8 shows sample locations, volumes, sampling depth ranges, weighted average depths, [SPE-DOC], and radiocarbon ($\Delta^{14}C$) measurements. Duplicate samples were collected on P18 station 168 (50°S) in surface water, and from station 77 (7°S) in deep water. Post collection, P16N seawater samples were frozen at sea and shipped back to the laboratory at UC Irvine for future analyses, while the P18 and IO7N water samples were processed at sea, as described in the next section.

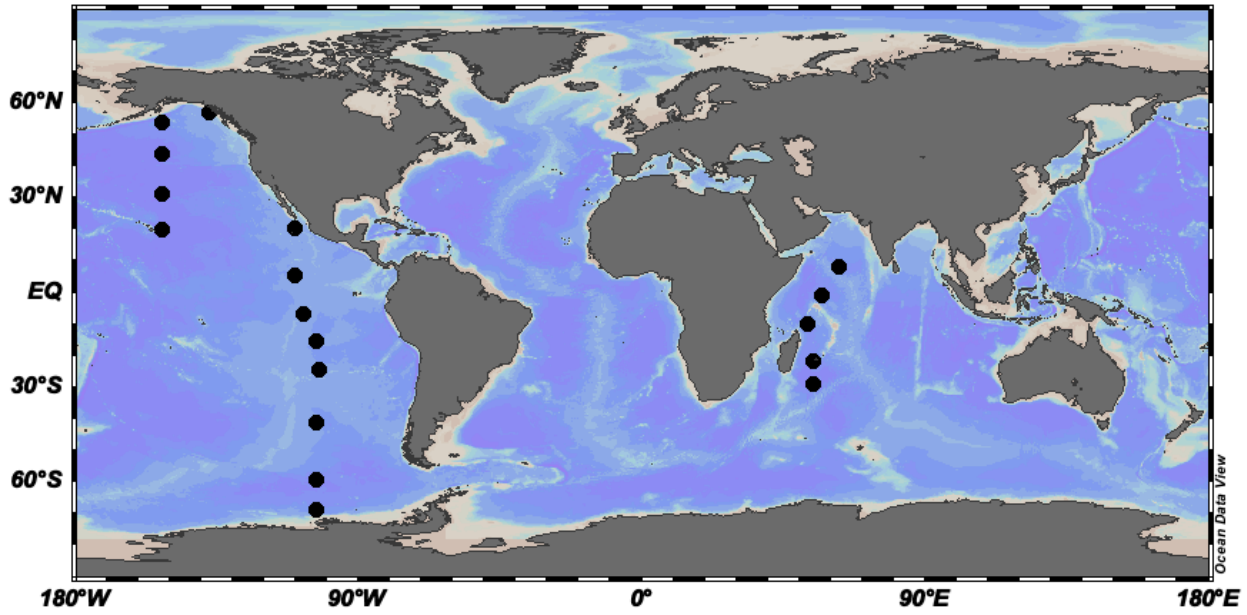

Figure 12. SPE-DOC sampling stations along three GO-SHIP Repeat Hydrography cruise transects P16N (2015) in the North Central Pacific Ocean , P18 (2016/2017) in the eastern Pacific Ocean, and IO7N (2018) in the Indian Ocean are depicted.

3.3.2 Solid-phase extraction, elution, and radiocarbon analysis of SPE-DOC

For seawater samples from P18 and IO7N, SPE was performed at sea using PPL cartridges (Bond Elut-PPL, 1 gm 6 mL, Part No. 12255002) according to (Dittmar et al., 2008) and stored in the dark at 4°C until extraction at UC Irvine.

Seawater samples from the P16N cruise were processed after four years of freezing, which produced crystalline precipitate in the thawed sample similar to a previous study (Beaupré & Druffel, 2009). Seawater was thawed in a hot water bath and shaken vigorously until the precipitate was no longer visible. Samples were then acidified to pH 2 with sulfuric acid (ACS grade, Lot# 160128) and extracted onto PPL cartridges as described above.

Before elution, PPL cartridges were dried under a steady stream of ultra high purity N2(g) for 30 minutes to remove residual MilliQ water (3 ppb DOC). SPE-DOC was eluted with LC/MS grade methanol following established methods (Dittmar et al. 2008). However the elution volume of methanol was increased to 32 mL following results in a recent study (Lewis et al., 2020). SPE-DOC was eluted into

pre-weighed and pre-combusted (540°C/2h) 50 mL round-bottom centrifuge vials (VWR product #89091-460), and weighed after elution to determine the exact volume. Vials were stored at -20°C until further processing.

Aliquots of the total SPE-DOC extract were taken for measurements of [SPE-DOC] and $\Delta^{14}C$. First, SPE-DOC extracts were homogenized with a baked glass Pasteur pipette and ~1 mL was removed and transferred to 10 cm long, 6mm OD quartz vials that had been pre-baked and pre-weighed. The exact volume of SPE-DOC aliquots was determined by mass-difference. Splits were dried in a centrifugal evaporator with a -60°C chiller trap (Savant SpeedVac SC200) for a minimum of 12 hours. Pre-baked cupric oxide and silver wire were added, and the outside of these quartz tubes were cleaned with acetone, dried, and placed inside larger 9mm diameter, 20 cm long quartz vial. These 'double tube' samples were sealed under vacuum and combusted at 850°C for two hours. The process-blank of the double tube process was measured for mass and $\Delta^{14}C$ via secondary standards and the indirect method (Santos et al., 2007) and subtracted from sample values. Sample CO_2 was extracted cryogenically on a vacuum line and quantified manometrically. Using the volume of SPE methanol extract and the carbon mass from each split, the concentration was calculated as [SPE-DOC] in μmol L^{-1} (μM). [SPE-DOC] divided by concentration of total organic carbon measured by UV-oxidation (total [DOC]), reported in (Druffel et al., 2019; Druffel et al., 2021), is the "percent recovery". Purified CO2 was converted to graphite on an iron catalyst at 550°C for $\Delta^{14}C$ analysis following the sealed tube Zn method (Walker & Xu, 2018; Xu et al., 2007). Radiocarbon measurements were performed at the UC Irvine Keck Carbon Cycle Accelerator Mass Spectrometry Facility. Data is reported as fraction modern (FM) and $\Delta^{14}C$ (Table 8) for geochemical samples without known age (Stuiver & Polach, 1977).

Radiocarbon ($\Delta^{14}C$) and [SPE-DOC] measurements were corrected for the presence of extraneous carbon (Cex) from the PPL SPE resin following (Lewis et al., 2020).

3.4. Results

3.4.1 SPE-DOC concentrations and percent recoveries

[SPE-DOC] are shown in Figure 14(a) and (b) for the surface and deep ocean, respectively. Surface [SPE-DOC] measurements from P18 are lowest at 69°S (14.8±0.8 μM), and increase slightly in the Southern Ocean (duplicate samples at 50°S: 22.2±1.2 μM and 19.1±1.0 μM). Lower values are found in at 40°S, and increase northward before peaking at the northern edge of the Southern Hemisphere subtropical gyre (29.2±0.4 μM at 15°S). [SPE-DOC] decreases across the equatorial region until 20°N. In P16N data, the highest concentration of 38.6±2.5 μM at 30°N and lowest concentration of 25.7±0.2 μM at 53°N. In the Indian Ocean, surface [SPE-DOC] is highest at the southernmost station (34.2±1.8 μM at 29.5°S).

P18 deep ocean (Figure 14(b)) [SPE-DOC] averaged 17.7±3.0 μM. A clear gradient exists in deep ocean [SPE-DOC] between the highest concentrations in the Southern Ocean (22.8±1.3 μM at 69°S) and the lowest concentrations in the subtropics (12.3±1.0 μM at 24°S). Deep ocean P16N measurements are significantly offset from P18 and IO7N data. The highest concentration is found in the lone Southern Hemisphere station (46.0±2.8 μM at 15.5°S). Concentrations are lower, and equal within error at higher latitudes in the North Pacific Ocean (33.4±2 μM). Reasons for elevated [SPE-DOC] in deep P16N water is discussed below. Deep ocean [SPE-DOC] in the Indian Ocean showed robust consistency from 30°S to 17°N, ranging 17.6±0.9 μM to 19.3±1.0 μM.

Average SPE-DOC recoveries from each cruise transect are shown in Figure 13. P18 and IO7N average SPE-DOC recoveries range between 46±3% and 51±10%. These recoveries are consistent with previous similar measurements of SPE-DOC (Broek et al., 2017; Dittmar et al., 2008; Lewis et al., 2020). P16N deep ocean recovery is a clear outlier, averaging 91±15% recovery (n = 6). Incomplete drydown of methanol could have increased [SPE-DOC] but this would also have led to a notable decrease in $\Delta^{14}C$ (methanol has a fossil $\Delta^{14}C$ signature of -1000‰). P16N deep samples average concentrations 15 μM

higher than deep samples from P18 and IO7N. If this excess 15 µM is from methanol contamination, and it assumed that P16N [SPE-DOC] and $\Delta^{14}C$ values should be similar to P18 and IO7N, this would cause P16N $\Delta^{14}C$ to decrease to -760‰. On the contrary, the P16N $\Delta^{14}C$ is significantly higher (younger) than P18 $\Delta^{14}C$ (discussed further in Section 3.5.1). Therefore, methanol contamination is unlikely the source of high SPE-DOC recoveries. Unlike P18 and IO7N samples, P16N seawater was frozen prior to solid-phase extraction. Deep samples required vigorous shaking to remove crystalline precipitate (described in Section 3.2); however, the mechanism through which this process would increase [SPE-DOC] remains unknown.

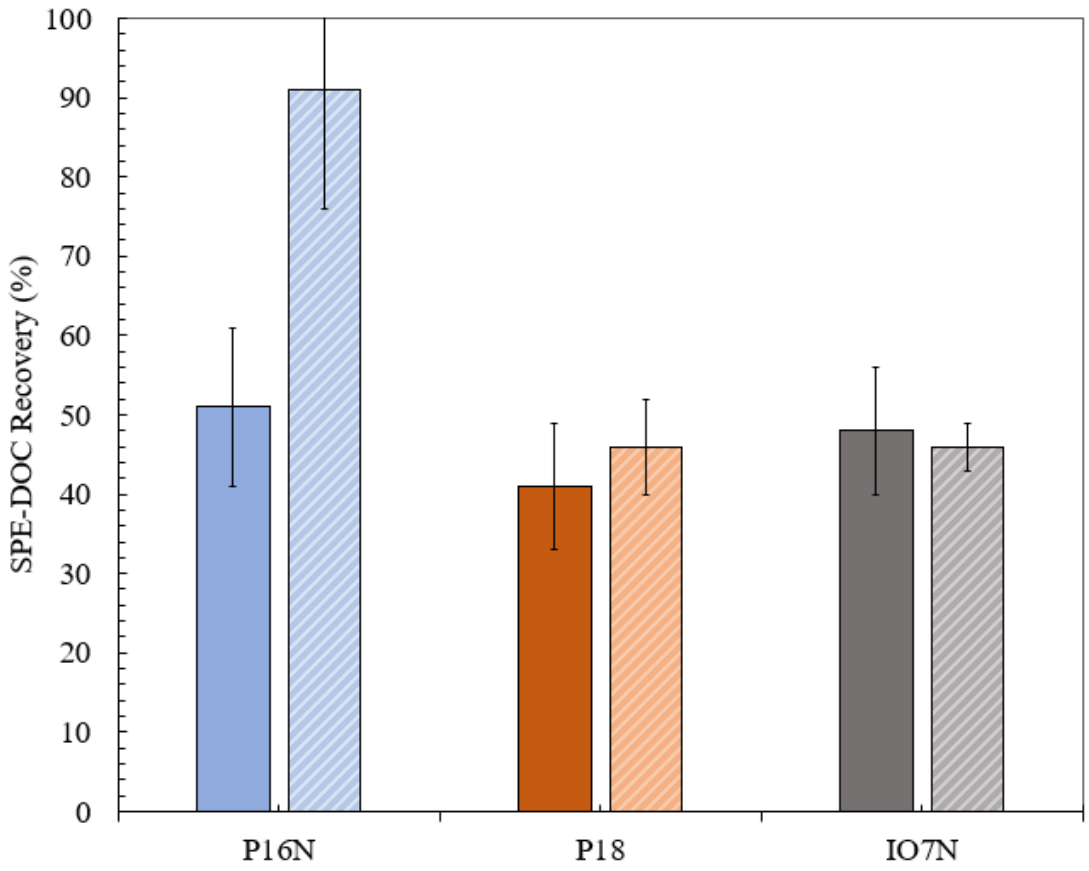

Figure 13. SPE-DOC recoveries from three GO-SHIP cruises expressed as percent of total DOC. Deep ocean datasets are in striped boxes, while surface ocean datasets are in solid colored boxes. The P16N deep ocean dataset is a clear outlier, and reasons for this is discussed in Section 3.4.1.

3.4.2 SPE-DOC $\Delta^{14}C$ results

SPE-DOC radiocarbon values ($\Delta^{14}C$) of surface and deep samples are shown in Figure 14(c) and (d), respectively. Deep ocean $\Delta^{14}C$ values (Figure 14(d)) from P16N and P18 average -513±22‰ (n=7) and -565±37‰ (n=10), respectively. The highest $\Delta^{14}C$ values from P18 found in the Southern Ocean (-513±15‰) are similar to those in the North Pacific from P16N (-520±32‰ to -483±39‰). Very low deep ocean $\Delta^{14}C$ values are -627±90‰ and -619±47‰ at 15°S and 20°N, respectively. Reason for this are discussed further in Section 3.5.1. Deep ocean $\Delta^{14}C$ values in the Indian Ocean are remarkably constant, ranging between -515±6‰ and -499±5‰ (average = –507±7‰ (n=5)).

Surface Pacific Ocean SPE-DOC $\Delta^{14}C$ values (Figure 14(c)) are much more variable than the deep values. The two lowest surface ocean SPE-DOC $\Delta^{14}C$ values are found at 69°S (-542±16‰) and 20°N (-543±57‰). Values increase from the Southern Ocean into the Southern Hemisphere subtropical gyre, up to -288±11‰ at 24°S. At 20°N, a very low $\Delta^{14}C$ signature is found in the coastal upwelling zone (-543±57‰) (see Section 3.5.1). North Pacific surface SPE-DOC $\Delta^{14}C$ are variable compared to the South Pacific Ocean. In the Indian Ocean, values are lowest near the equator (-389±10‰ at 2°S) and increase toward higher latitudes (-354±8‰ and -341±9‰ at 22.5°S and 17°N, respectively.)

Table 7. Data regarding SPE-DOC sampling (stations, depth ranges, and weighted average depths), and manometric measurement of SPE-DOC ([SPE-DOC], total [DOC] from the closest available depth, and calculated PPL % recoveries).

UCI AMS #	UCID	GO-SHIP Cruise	Depth	Latitude (°N)	Longitude (°E)	Station	Sample Depth Range	Weighted Average Depth	±	[SPE-DOC] µM	±	DOC sampling depth	[DOC] from closest depth	PPL % Recovery	±
231004	22728	P16	Surface	-14	-151	5 to 6	90 - 150 m	120	1	35.0	1.9	100	83.9	41.7	1.9
231005	22729	P16	Surface	20	-152	106 to 107	15 - 75 m	37	1	33.2	1.7	26	74.9	44.4	1.7
X	22730	P16	Surface	53	-152	128	25 - 150 m	88	1	38.6	2.5	81	52.7	73.2	2.5
231006	22799	P16	Surface	43	-152	154	67 - 200 m	123	1	26.4	1.4	151	53.2	49.7	1.4
231007	22800a*	P16	Surface	53	-152	174	117 m	117	1	25.8	1.3	133	49.7	52.0	1.3
231008	22800b*	P16	Surface	53	-152	174	117 m	117	1	25.8	1.3	133	49.7	51.9	1.3
231009	22800c*	P16	Surface	53	-152	174	117 m	117	1	25.5	1.3	133	49.7	51.3	1.3
231010	22731	P16	Surface	57	-137	204	20 m	20	1	30.5	1.6	20	66.9	45.5	1.6
231011	22732	P16	Deep	-16	-151	3 to 4	2133 - 2667 m	2667	1	46.0	2.8	2799	39.0	118.0	2.8
231012	22733	P16	Deep	20	-152	105 to 106	2000 - 2533 m	2400	1	35.2	3.1	2401	37.1	95.0	3.1
231013	22734	P16	Deep	30	-152	128	2500 - 4000 m	2500	1	35.3	2.8	2334	38.5	91.8	2.1
231014	22734b*	P16	Deep	30	-152	128	2500 - 4000 m	2500	1	30.0	2.1	2334	38.5	78.0	2.1
231015	22735	P16	Deep	43	-152	154	2667 - 4133 m	2900	1	33.7	2.9	2400	39.9	84.4	2.9
231016	22736	P16	Deep	57	-137	205	2200	2200	1	31.8	2.5	2200	41.0	77.6	2.5
217540	22063*	P18	Surface	20	-110	10	90 - 191m	140	1	22.2	1.3	145	53.2	41.6	1.3
217541	22064*	P18	Surface	20	-110	10	91 - 191m	140	1	22.0	1.3	145	53.2	41.3	1.3
209388	21915	P18	Surface	5	-110	38	4 - 169 m	100	1	24.6	1.2	60	73.0	33.7	1.2
217548	21976	P18	Surface	-7	-108	77	3 - 91 m	28	1	26.7	1.4	4	63.9	41.8	1.4
217544	22069*	P18	Surface	-15	-103	98	3 - 106 m	40	1	29.5	1.6	60	63.5	46.4	1.6
217555	22070*	P18	Surface	-15	-103	98	3 - 106 m	40	1	28.9	1.5	60	63.5	45.5	1.5
217535	21969	P18	Surface	-24	-103	116	4 - 170 m	65	1	20.5	1.0	61	70.8	28.9	1.0
217538	21983	P18	Surface	-40	-103	150	4 - 195 m	65	1	15.9	0.8	70	54.9	29.0	0.8
217550	22122**	P18	Surface	-50	-103	168	3 - 200 m	16	1	22.2	1.2	4	46.6	47.6	1.2
217551	22123**	P18	Surface	-50	-103	168	3 - 200 m	118	1	19.1	1.0	4	n.m.	n.m.	1.0
217553	22125	P18	Surface	-60	-103	186	3 - 220 m	87	1	21.0	1.1	83	37.1	56.7	1.1
217555	22127	P18	Surface	-69	-103	205	2 - 125 m	135	1	14.8	0.8	176	39.3	37.7	0.8
217542	22066*	P18	Deep	20	-110	10	1999 - 3159 m	2532	1	18.0	1.0	2541	42.0	42.8	1.0
217543	22067***	P18	Deep	0	-110	10	1999 - 3159 m	2532	1	24.1	1.3				
209389	21916	P18	Deep	5	-110	38	2361 - 3670 m	3358	1	19.4	1.0	3299	40.0	48.4	1.0
217549	22077**	P18	Deep	-7	-108	77	2005 - 3281 m	3038	1	16.3	0.9	2940	37.5	43.4	0.9
217537	21980**	P18	Deep	-7	-108	77	2005 - 3281 m	2465	1	15.8	0.8	2500	33.9	46.7	0.8
217546	22072*	P18	Deep	-15	-103	98	2474 - 3850 m	3203	1	16.0	0.9	3199	38.9	41.0	0.9
217547	22073*	P18	Deep	-15	-103	98	2474 - 3850 m	3203	1	17.0	1.0	3199	38.9	43.8	1.0
217536	21971	P18	Deep	-24	-103	116	2060 - 3279 m	2904	1	12.3	0.6	2775	32.2	38.3	0.6
217539	21985	P18	Deep	-40	-103	150	2160 - 3639 m	2885	1	15.5	0.8	n.m.	34.0	45.6	0.8
217552	22124	P18	Deep	-50	-103	168	2199 - 3863 m	3006	1	20.2	1.0	2996	40.7	49.5	1.0
217554	22126	P18	Deep	-60	-103	186	2120 - 3899 m	2754	1	20.2	1.0	2701	37.7	53.6	1.0
217556	22128	P18	Deep	-69	-103	205	2830 - 4090 m	2481	1	22.8	1.2	2475	39.0	58.4	1.2
X	22716***	IO7	Surface	-30	55	2	4 - 214 m	120	1	34.2	1.8	139	54.9	62.2	1.8
230993	22717	IO7	Surface	-23	55	22	3 - 211 m	141	1	27.1	1.4	111	64.2	42.2	1.4
230994	22718	IO7	Surface	-11	53	46	3 - 201 m	125	1	23.8	1.3	122	51.4	46.4	1.3
230995	22718*	IO7	Surface	-11	53	46	3 - 201 m	125	1	22.4	1.2	122	51.4	43.6	1.2
230996	22719	IO7	Surface	-2	57	71	3 - 217 m	130	1	25.3	1.3	183	48.0	52.7	1.3
230997	22720	IO7	Surface	8	63	96	56 - 201 m	128	1	24.7	1.3	100	59.9	41.3	1.3
230998	22721	IO7	Surface	17	69	119	93 - 198 m	149	1	25.5	1.3	n.m.	n.m.	n.m.	
230999	22722	IO7	Deep	-30	55	2	2477 - 3977 m	3420	1	19.3	1.0	3225	38.1	50.5	1.0
231000	22723	IO7	Deep	-23	55	22	2477 - 4023 m	3292	1	18.6	1.0	3226	40.8	45.5	1.0
231001	22724	IO7	Deep	-11	53	46	2701 - 4200 m	3361	1	17.6	0.9	3525	39.9	44.1	0.9
X	22725	IO7	Deep	-2	57	71	2800 - 4000 m	3481	1	18.8	1.0	3501	39.7	47.3	1.0
231002	22726	IO7	Deep	8	63	96	2900 - 4100 m	3597	1	17.9	0.9	3300	40.7	43.9	0.9
231003	22727	IO7	Deep	17	69	119	2200 - 3610 m	2741	1	19.1	1.0	n.m.	n.m.	n.m.	

Table 8. SPE-DOC $\Delta^{14}C$ and $\delta^{13}C$ data, as well as total DOC isotope measurements used to calculate non-retained $\Delta^{14}C$ for the mass balance model presented in Section 3.5.2.1.

UCI AMS #	UCID	GO-SHIP Cruise	Depth	Latitude (°N)	Longitude (°E)	Station	Fraction Modern	±	Corrected SPE-DOC $\Delta^{14}C$ (‰)	±	DOC $\Delta^{14}C$ (‰) from Closest Depth	±	Non-retained DOC $\Delta^{14}C$ (‰)	±	Corrected SPE-DOC $\delta^{13}C$ (‰)	±
231004	22728	P16	Surface	-14.4	-150.6	5 to 6	0.689	0.010	-316.3	10.2	-260.0	2.1	-219.8	7.0	-22.7	0.2
231005	22729	P16	Surface	19.5	-152.0	106 to 107	0.754	0.007	-251.9	6.9	-212.9	2.2	-181.8	5.6	-22.7	0.2
X	22730	P16	Surface	53.0	-152.0	128	n.m.	n.m.	n.m.	n.m.	n/a	n/a	n/a	n/a	-22.5	0.2
231006	22799	P16	Surface	43.0	-152.0	154	0.651	0.005	-354.1	5.1	-356.4	2.0	-358.7	9.6	-22.4	0.2
231007	22800a*	P16	Surface	53.0	-152.0	174	0.583	0.006	-421.5	5.6	-402.5	2.0	-381.9	10.4	-22.5	0.0
231008	22800b*	P16	Surface	53.0	-152.0	174	0.583	0.009	-421.9	9.0						
231009	22800c*	P16	Surface	53.0	-152.0	174	0.585	0.007	-419.2	6.8						
231010	22731	P16	Surface	56.5	-137.3	204	0.705	0.007	-301.0	7.0	-275.9	1.6	-254.9	7.4	-22.7	0.2
231011	22732	P16	Deep	-15.5	-150.6	3 to 4	0.462	0.055	-541.7	54.9	n/a	n/a	n/a	n/a	-22.4	0.2
231012	22733	P16	Deep	19.5	-152.0	105 to 106	0.522	0.039	-482.9	38.9	n/a	n/a	n/a	n/a	-22.5	0.2
231013	22734	P16	Deep	30.0	-152.0	128	0.502	0.032	-502.4	32.3	n/a	n/a	n/a	n/a	-23.0	0.2
231014	22734b*	P16	Deep	30.0	-152.0	128	0.466	0.028	-537.7	28.2	n/a	n/a	n/a	n/a	-22.6	0.2
231015	22735	P16	Deep	43.0	-152.0	154	0.500	0.040	-504.4	39.9	n/a	n/a	n/a	n/a		
231016	22736	P16	Deep	56.7	-137.3	205	0.493	0.032	-511.0	32.4	n/a	n/a	n/a	n/a		
217540	22063*	P18	Surface	20.0	-110.0	10	0.453	0.057	-549.8	56.6	-332.4	1.8	-182.0	4.1	-23.4	0.1
217541	22064*	P18	Surface	20.0	-110.0	10	0.466	0.056	-537.0	55.5						
209388	21915	P18	Surface	5.0	-110.0	38	0.668	0.004	-336.4	4.5	-213.0	2.0	-150.3	2.8	-23.0	0.2
217548	21976	P18	Surface	-7.0	-107.5	77	0.630	0.028	-373.8	28.3	-267.7	1.9	-191.4	4.6	-23.0	0.2
217544	22069*	P18	Surface	-15.0	-103.0	98	0.601	0.031	-403.0	31.4	-227.5	4.5	-109.0	3.2	-23.0	0.2
217555	22070*	P18	Surface	-15.0	-103.0	98	0.679	0.016	-325.2	16.0						
217535	21969	P18	Surface	-24.0	-103.0	116	0.716	0.011	-287.8	10.7	-249.0	3.6	-233.2	3.4	-22.5	0.2
217538	21983	P18	Surface	-40.0	-103.0	150	0.613	0.020	-390.6	19.8	-312.6	1.7	-280.8	3.2	-22.6	0.2
217550	22122**	P18	Surface	-50.0	-103.0	168	0.600	0.021	-403.1	21.2	-355.0	3.6	-311.3	7.0	-23.0	0.2
217551	22123**	P18	Surface	-50.0	-103.0	168	0.574	0.028	-429.3	28.2					-23.1	0.2
217553	22125	P18	Surface	-60.0	-103.0	186	0.530	0.022	-473.1	21.6	-402.2	1.5	-309.5	7.9	-23.0	0.2
217555	22127	P18	Surface	-69.0	-103.0	205	0.472	0.028	-542.1	15.9	-469.3	1.3	-425.2	5.4	-22.4	0.2
217542	22066*	P18	Deep	20.0	-110.0	10	0.383	0.047	-619.1	46.9	-533.9	1.3	-470.2	8.4	-23.1	0.2
217543	22067***	P18	Deep	0.0	-110.0	10									-22.8	0.2
209389	21916	P18	Deep	5.0	-110.0	38	0.454	0.003	-549.0	2.7					-23.9	0.2
217549	22077**	P18	Deep	-7.0	-107.5	77	0.427	0.040	-575.9	39.5					-22.3	0.2
217537	21980**	P18	Deep	-7.0	-107.5	77	0.429	0.016	-573.6	16.4	-522.9	1.3	-478.4	7.1	-23.2	0.2
217546	22072*	P18	Deep	-15.0	-103.0	98	0.402	0.044	-600.9	44.3	-541.1	3.7	-481.0	7.4		
217547	22073*	P18	Deep	-15.0	-103.0	98	0.349	0.081	-653.1	81.0					-22.3	0.2
217536	21971	P18	Deep	-24.0	-103.0	116	0.428	0.016	-574.8	16.0	-542.8	3.4	-522.9	5.3	-22.2	0.2
217539	21985	P18	Deep	-40.0	-103.0	150	0.448	0.024	-554.8	23.9					-22.5	0.2
217552	22124	P18	Deep	-50.0	-103.0	168	0.482	0.015	-521.3	15.2	-536.6	2.9	-551.6	11.3	-22.5	0.2
217554	22126	P18	Deep	-60.0	-103.0	186	0.490	0.015	-513.7	15.1	-473.2	1.3	-426.5	9.5	-22.5	0.2
217556	22128	P18	Deep	-69.0	-103.0	205	0.460	0.016	-542.6	15.9	-483.1	1.3	-399.7	11.2	-23.1	0.2
X	22716***	IO7	Surface	-29.5	54.5	2									-22.3	0.2
230993	22717	IO7	Surface	-22.5	54.5	22	0.652	0.008	-353.7	8.3	-324.4	2.7	-303.0	7.4	-22.8	0.1
230994	22718	IO7	Surface	-10.8	53.2	46	0.637	0.009	-368.4	9.1	-338.6	3.2	-312.8	7.3		
230995	22718*	IO7	Surface	-10.8	53.2	46	0.632	0.006	-372.8	5.6					-22.3	0.2
230996	22719	IO7	Surface	-1.7	57.2	71	0.616	0.010	-389.0	10.3	-368.5	2.9	-345.7	9.7	-22.4	0.2
230997	22720	IO7	Surface	7.6	62.5	96	0.665	0.009	-340.4	8.8	-291.3	2.2	-256.8	5.7	-21.9	0.2
230998	22721	IO7	Surface	17.0	68.5	119	0.664	0.009	-341.4	9.3						
230999	22722	IO7	Deep	-29.5	54.5	2	0.504	0.007	-500.1	6.6	-496.9	2.2	-493.6	9.9	-22.1	0.2
231000	22723	IO7	Deep	-22.5	54.5	22	0.495	0.007	-509.2	7.0	-496.9	2.4	-486.6	8.5	-22.6	0.2
231001	22724	IO7	Deep	-10.8	53.2	46	0.493	0.007	-511.0	6.7	-505.2	3.7	-500.6	8.1	-22.4	0.2
X	22725	IO7	Deep	-1.7	57.2	71									-22.7	0.2
231002	22726	IO7	Deep	7.6	62.5	96	0.489	0.006	-514.7	6.2	-498.5	3.3	-485.8	7.9	-22.6	0.2
231003	22727	IO7	Deep	17.0	68.5	119	0.505	0.005	-499.3	5.4					-22.6	0.2

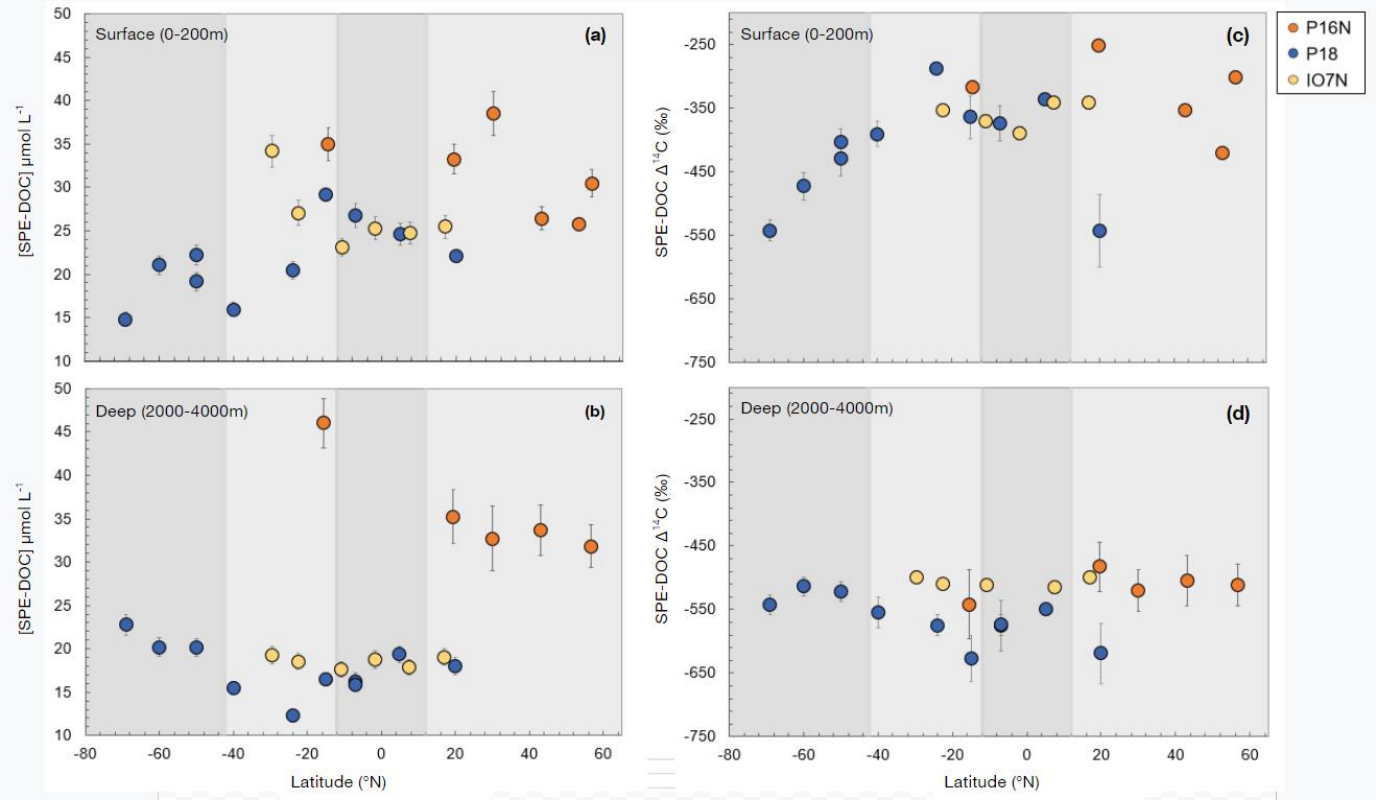

Figure 14. Panels (a) and (b) show [SPE-DOC] in the surface and deep ocean, respectively. Panels (c) and (d) show $\Delta^{14}C$ (‰) for the surface and deep ocean, respectively. All error bars represent the propagated error of the measurements, including corrections for blank carbon (C_{ex}). *The segmentation of the plot into four different color regions indicate where data has been 'binned' together for analysis of RDOC changes with latitude (Section 5). This only applies to P16N, and P18. All IO7N data has been grouped together in our model. See Section 3.5.2.1 for more information.

3.5. Discussion

3.5.1 Interpretations of regional SPE-DOC $\Delta^{14}C$ trends

3.5.1.1 The Southern Ocean

Observed [SPE-DOC] and $\Delta^{14}C$ values in surface and deep water become increasing similar from the mid-latitudes toward the Southern Ocean (Figure 14(c) and (d) and highlighted in Figure 15). At 69°S, surface and deep SPE-DOC $\Delta^{14}C$ values are indistinguishable within error, yet deep [SPE-DOC] is higher than the surface due to high SPE-DOC recoveries (58±1% at depth versus 38±1% at surface). Elevated deep water [SPE-DOC] may be due to increases in hydrophobic organic matter that sorb onto SPE resins, such as aromatic molecules or CRAM-like compounds. However, detailed molecular characterizations of our SPE-DOC would be required to confirm this. The general trend toward uniform values of [SPE-DOC] and $\Delta^{14}C$ in the Southern Ocean is likely due to the enhanced vertical mixing in this region. Low surface SPE-DOC $\Delta^{14}C$ values may also be influenced by DOC production via primary producers using low $\Delta^{14}C$ DIC from upwelling of CDW (Druffel & Bauer, 2000; Follett et al., 2014). Similar patterns of relatively low surface concentrations and water column homogeneity in the Southern Ocean are reflected in total DOC measurements (Bercovici et al., 2018; Druffel & Bauer, 2000; Hansell et al., 2009; Ogawa et al., 1999).

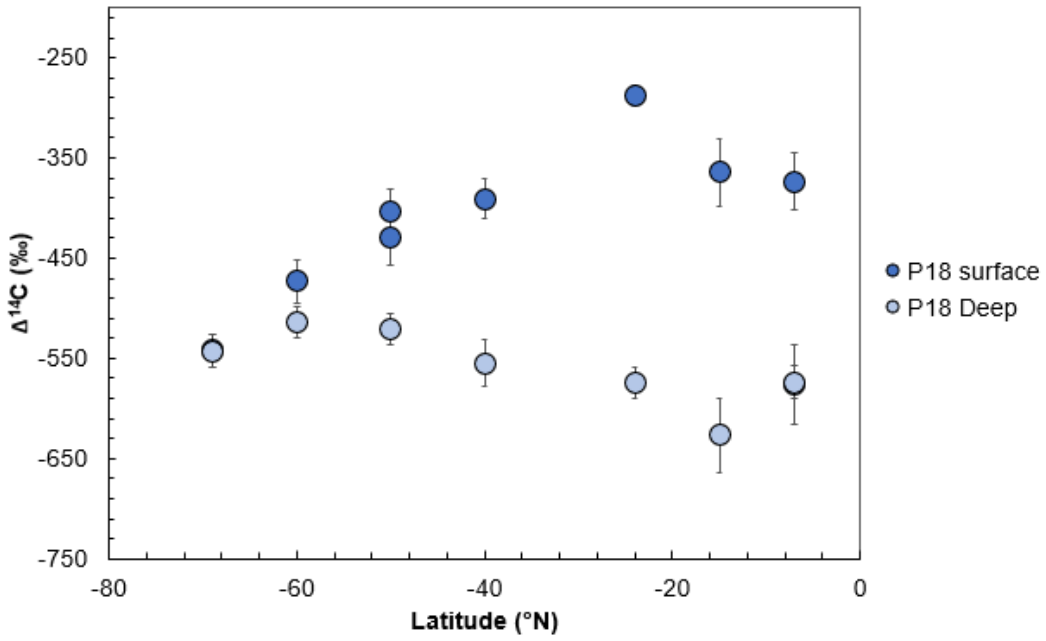

Figure 15. $\Delta^{14}C$ values in the surface and deep Southern Ocean become increasingly similar towards the most Southernly latitudes. This is likely due to strong mixing and the lack of pycnocline in this region.

3.5.1.2 The Pacific Ocean

Our highest surface [SPE-DOC] and $\Delta^{14}C$ values in the Pacific Ocean are found in the subtropical gyres. These regions are dominated by converging water masses and downwelling, which allows DOC (Hansell et al., 2009) and SPE-DOC to accumulate. This effect causes measurements from P16N and P18 to overlap at 15°S. Despite their differences in longitude, both samples are in the Southern Hemisphere subtropical gyre and have similar $\Delta^{14}C$ values (-316±10‰ and -364±34‰, respectively). At 20°N, there is another overlapping set of datapoints from P16N and P18. At 20°N, P16N is in the subtropical gyre (20°N, 150°W) and SPE-DOC has a high $\Delta^{14}C$ signature (-252±7‰). Its counterpart from P18 (20°N, 110°W) is in the upwelling region along the western coastline of North America (Fiedler & Talley, 2006) and has a very low $\Delta^{14}C$ similar to the Southern Ocean (-543±57‰).

A two-tailed student's t-test (DF = 14, t = 3.5, p = 0.01) reveals that the P16N deep SPE-DOC $\Delta^{14}C$ dataset is significantly younger than the P18 dataset. This is still the case when the two lowest values are removed (significant remains without outliers). Deep P18 $\Delta^{14}C$ values may be lower (older)

than deep P16N values because Pacific Deep Water (PDW) flows southward at our sampling depth (2900m), despite net northward meridional transport of Antarctic Bottom Water and Circumpolar Deep Water at the bottom of the Pacific Ocean (Talley, 2013). This is also shown by low [SPE-DOC] (12.3±0.6 μM) and the lowest $\Delta^{14}C$ value in reported in an SPE-DOC extract (-627±44‰) in PDW at 24°S.

3.5.1.3 The Indian Ocean

Deep water [SPE-DOC] in the Indian Ocean showed robust consistency in from 30°S to 17°N, ranging only slightly from 17.6±0.9 μM to 19.3±1.0 μM. (Bercovici et al., 2018) found similar homogeneity in total [DOC] in the South Indian Ocean. However, we note these two datasets do not overlap in latitude. Bercovici and co-workers (2018) attributed this trend to the mixing of North Atlantic Deep Water (NADW) and CDW which dampens signatures of freshly produced DOC. Our southernmost station is on the northern edge of the South Indian Ocean Gyre, likely leading to high [SPE-DOC] due to the accumulation of young DOC in subtropical gyres, similar to the Pacific Ocean. A t-test (DF = 19, t = 3.7, p = 0.01) shows that the deep Indian Ocean $\Delta^{14}C$ dataset is significantly younger than the deep Pacific Ocean $\Delta^{14}C$ dataset (P16N and P18 combined).

3.5.2 Meridional and basin estimates of $RDOC_{total}$

3.5.2.1 Developing a mass-balance framework

Total [DOC] and DOC $\Delta^{14}C$ were also measured on P16N, P18, and IO7N at higher vertical resolution of 14 depths per station (Druffel et al. 2019; Druffel et al., 2021; Druffel, unpublished data). SPE-DOC is compared directly to DOC $\Delta^{14}C$ at the closest available measurement. Selected DOC sampling depths and $\Delta^{14}C$ values used for this comparison are reported in Table 8. In the Indian Ocean, although each individual SPE-DOC $\Delta^{14}C$ value is lower than corresponding total DOC $\Delta^{14}C$ value in the surface and deep ocean, the datasets are not significantly different. In the Pacific Ocean (combining P16N and P18 datasets), SPE-DOC $\Delta^{14}C$ is significantly lower than total DOC $\Delta^{14}C$ in the surface, but not at

depth (surface: DF = 35, t = 3.0, critical-value = 2.04, p = 0.01; deep: DF = 26, t = 1.1, critical value = 2.06, p = 0.01). This is one indication of the presence of fresh, labile HMW DOC with high $\Delta^{14}C$ values superimposed on RDOC at the surface.

Using a mass-balance between SPE-DOC $\Delta^{14}C$ and the closest sampled total DOC $\Delta^{14}C$, the $\Delta^{14}C$ value of non-retained DOC can be calculated ($\Delta^{14}C_{nonretained}$) (Eqn 1, below), similar to (Broek et al., 2020) (Table 8 lists all calculated non-retained DOC $\Delta^{14}C$ values).

$$(\mathbf{1}) \quad \Delta^{14}C_{nonretained} = \frac{\Delta^{14}C_{totalDOC} - (\Delta^{14}C_{SPEDOC} * Fraction_{SPE-DOC})}{(1 - Fraction_{SPE-DOC})}$$

Since $\Delta^{14}C_{SPEDOC}$ is always lower than $\Delta^{14}C_{totalDOC}$, $\Delta^{14}C_{nonretained}$ values are always higher than $\Delta^{14}C_{totalDOC}$. Despite this, $\Delta^{14}C_{nonretained}$ are still much lower than surface DIC $\Delta^{14}C$, from which new DOC is produced. The offsets between these measured and derived data are shown for the surface P18 dataset in Figure 16. DIC $\Delta^{14}C$ values used in this comparison are shown in Table 9. This indicates a predominance of RDOC within the non-retained DOC fraction. The amount of RDOC within the non-retained DOC an be estimated using a second mass-balance calculation (Equation 2).

Table 9. DIC $\Delta^{14}C$ values used for comparison and the mass-balance model presented in Section 3.5.1.2.

Latitude	Surface Ocean	Reference
50°S to 70°S, Southern Ocean	-90±35‰	GO-SHIP IO8, 2016
15°S to 40°S, South Pacific	54±22‰	(Murata et al., 2007)
7°S to 20°N, Equatorial Pacific	41±6‰	(Druffel-Rodriguez et al. 2012)
20°N to 56°N, North Pacific	-2±30‰	GO-SHIP P16, 2016
Indian Ocean	50±20‰	(Key et al., 2004)
Atlantic Ocean	50±4‰	(Druffel et al., 2008)
Latitude	**Deep Ocean**	**Reference**
50°S to 70°S, Southern Ocean	-160±15‰	(Key et al., 2004)
15°S to 40°S, South Pacific	-200±15‰	(Key et al., 2004)
7°S to 20°N, Equatorial Pacific	-200±15‰	(Key et al., 2004)
20°N to 56°N, North Pacific	-243±15‰	(Druffel et al., 2008)
Indian Ocean	-175±15‰	(Key et al., 2004)
Atlantic Ocean	-70±4‰	(Druffel et al., 2008)

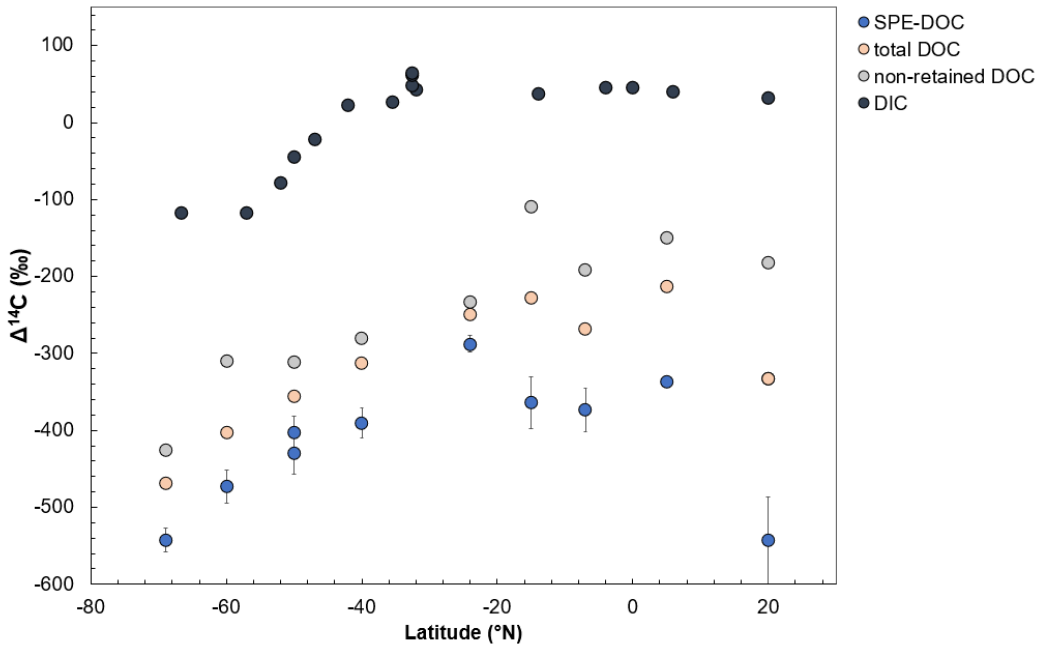

Figure 16. P18 surface SPE-DOC, total DOC, and non-retained DOC $\Delta^{14}C$ values, with separately measured DIC value overlaid. SPE-DOC is lower than total DOC $\Delta^{14}C$, because it contains LMW DOC that is typically more refractory. The non-retained DOC $\Delta^{14}C$ values are higher than total DOC $\Delta^{14}C$. The large gap that exists between non-retained DOC $\Delta^{14}C$ and DIC $\Delta^{14}C$ in the surface ocean indicates that a large proportion of DOC with low $\Delta^{14}C$ remains within the non-retained portion.

(2) $\Delta^{14}C_{\text{nonretained}} = \left(\Delta^{14}C_{\text{refractory-endmember}} * \mathbf{x}\right) + \left(\Delta^{14}C_{\text{labile-endmember}} * (1 - x)\right)$

Here, it is assumed that: 1) SPE-DOC is completely refractory and 2) that $\Delta^{14}C_{\text{non-retained}}$ comes from a two-component mixture of a refractory -endmember (with relative abundance ('x') and radiocarbon signature $\Delta^{14}C_{\text{refractory-endmember.}}$) and a labile component (with relative abundance ('1-x') and radiocarbon signature $\Delta^{14}C_{\text{labile-end-member}}$ represented by surface ocean DIC $\Delta^{14}C$).

By assuming that the proportions of each of these end-members add up to 1, a system of equations can be re-arranged to solve for the relative abundance of the refractory component 'x' (Equation 3; For the full algebraic derivation see Section 3.8). Finally, the total abundance of RDOC (sum of SPE-DOC and RDOC in non-retained fraction: hereby defined as $RDOC_{total}$) is calculated using Equation 4.

(3)

$$\%\ \text{RDOC in nonretained portion} = \mathbf{x} = \frac{\Delta^{14}C_{\text{non-retained}} - \Delta^{14}C_{\text{labile-endmember}}}{\Delta^{14}C_{\text{refractory endmember}} - \Delta^{14}C_{\text{labile-endmember}}}$$

(4) $RDOC_{\text{total}} = \text{Fraction}_{\text{SPE-DOC}} + \left(x * \left(1 - \text{Fraction}_{\text{SPE-DOC}}\right)\right)$

This calculation is made for different ocean regions by binning our SPE-DOC and total DOC data into meridional zones, and averaging the data within each zone (Southern Ocean: 70°S to 45°S, South Pacific Ocean: 45°S to 10°S, Equatorial Pacific: 10°S to 15°N, North Pacific Ocean: 15°N to 56°N, (depicted by background gradations in Figure 14). The Indian Ocean is binned using the average of all data from IO7N, and is *not* broken up by latitude. Note, deep North Pacific data was removed due to anomalously high [SPE-DOC] resulting in an estimate only at the surface. Low data from P18 Stn 10 (20°N) was removed from North Pacific surface bin because, instead of the meridian, its proximity to the coastline was the primary control on $\Delta^{14}C$ values, this may have skewed the estimate. An estimate of deep

Atlantic Ocean $RDOC_{total}$ is made by comparing deep SPE-DOC $\Delta^{14}C$ from (Flerus et al., 2012) (-464‰) to total DOC $\Delta^{14}C$ data from (Druffel et al., 2016) where the transects intersect (A16N Station 66 (32°N) and A10 Station 35 (30°S) (data points are averaged).

It is important to note that the accuracy of these calculations are dependent upon selecting appropriate labile and refractory end-member $\Delta^{14}C$ values. We select surface DIC $\Delta^{14}C$ values for labile end-members because freshly produced DOM in the surface ocean will reflect these DIC $\Delta^{14}C$ values (Table 9). Selecting the most appropriate end-member for refractory RDOC is important because the non-retained portion can only be observed indirectly, and the $\Delta^{14}C$ value can come from different mixtures. The lower the value of $\Delta^{14}C_{refractory\ endmember}$ the lower the resulting $RDOC_{total}$ (and the higher the labile DOC estimate). This is because, with lower $\Delta^{14}C$, less mass or contribution of a component is required to create the same total DOC $\Delta^{14}C$.

In order to select the most representative RDOC $\Delta^{14}C$ end-member, we explore $RDOC_{total}$ using three different end-members: first, the minimum possible RDOC $\Delta^{14}C$ end-member (-1000‰) (similar to (Beaupré & Druffel, 2009)), second, a deep LMW hydrophilic $\Delta^{14}C$ measurement from (Zigah et al., 2017) (-762‰), and finally the LMW SPE-DOC $\Delta^{14}C$ value from (Broek et al., 2020) (-573‰). The results of this experiment are shown in Figure 17, and summarized briefly here. The minimum (-1000‰) and (Zigah et al., 2017) end-members produce $RDOC_{total}$ estimates that are too low to match previous independent measurements of RDOC abundance. Using our mass-balance, $RDOC_{total}$ in the surface averages 58±6% and 63±7% for these end-members, respectively. This is on the lower bounds of previous estimates of LMW DOC abundance in the surface ocean (65-75%, shown as dotted area in Figure 17) (Benner et al. 1992; Ogawa and Ogura 1992; Amon and Benner 1994). Using the (Broek et al., 2020) end-member produces an $RDOC_{total}$ estimate that fits within this range (70±8%). Calculating deep ocean $RDOC_{total}$ similarly shows that end-members -1000‰ and -762‰ produce $RDOC_{total}$ estimates of 66±3% and 74±2%, respectively. This range is far lower than previous estimates of RDOC that range from 80% (Amon & Benner, 1994; Benner et al., 1992) to 95% (Hansell, 2013). The endmember

suggested by Broek and co-workers (2020) yields an estimate of 88±2%, which fits in this previously reported range, within error. When converting to units of concentration, this end-member also yields concentrations of labile DOC (average = 4±1 μM) within range of deep Pacific ocean [UDOC] (ultrafiltered DOC) and [HMW DOC] concentrations (4-6 μM) (Benner et al., 1997; Broek et al., 2017; Kaiser & Benner, 2009) depicted in Figure 18. We therefore use the (Broek et al. 2020) end-member to estimate $RDOC_{total}$ in each meridional zone, discussed in Section 5.2.3.

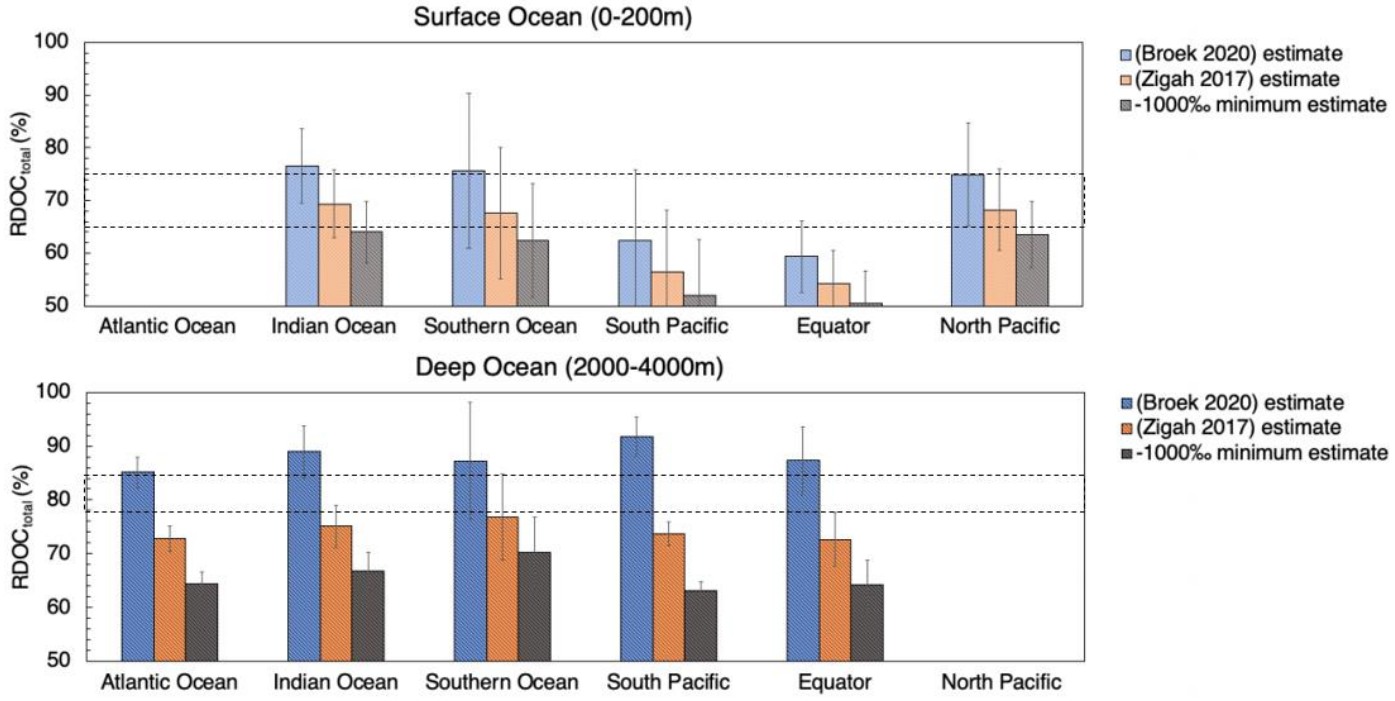

Figure 17. Mass-balance modeled $RDOC_{total}$ using three different end-members for RDOC in the non-retained fraction ($\Delta^{14}C_{refractoryendmember}$ in Eqn 3). Using the end-member -573‰ yields an estimate that falls within the range of previous independent estimates (Benner et al. 1992; Ogawa and Ogura 1992; Amon and Benner 1994), depicted by the dotted-rectangle.

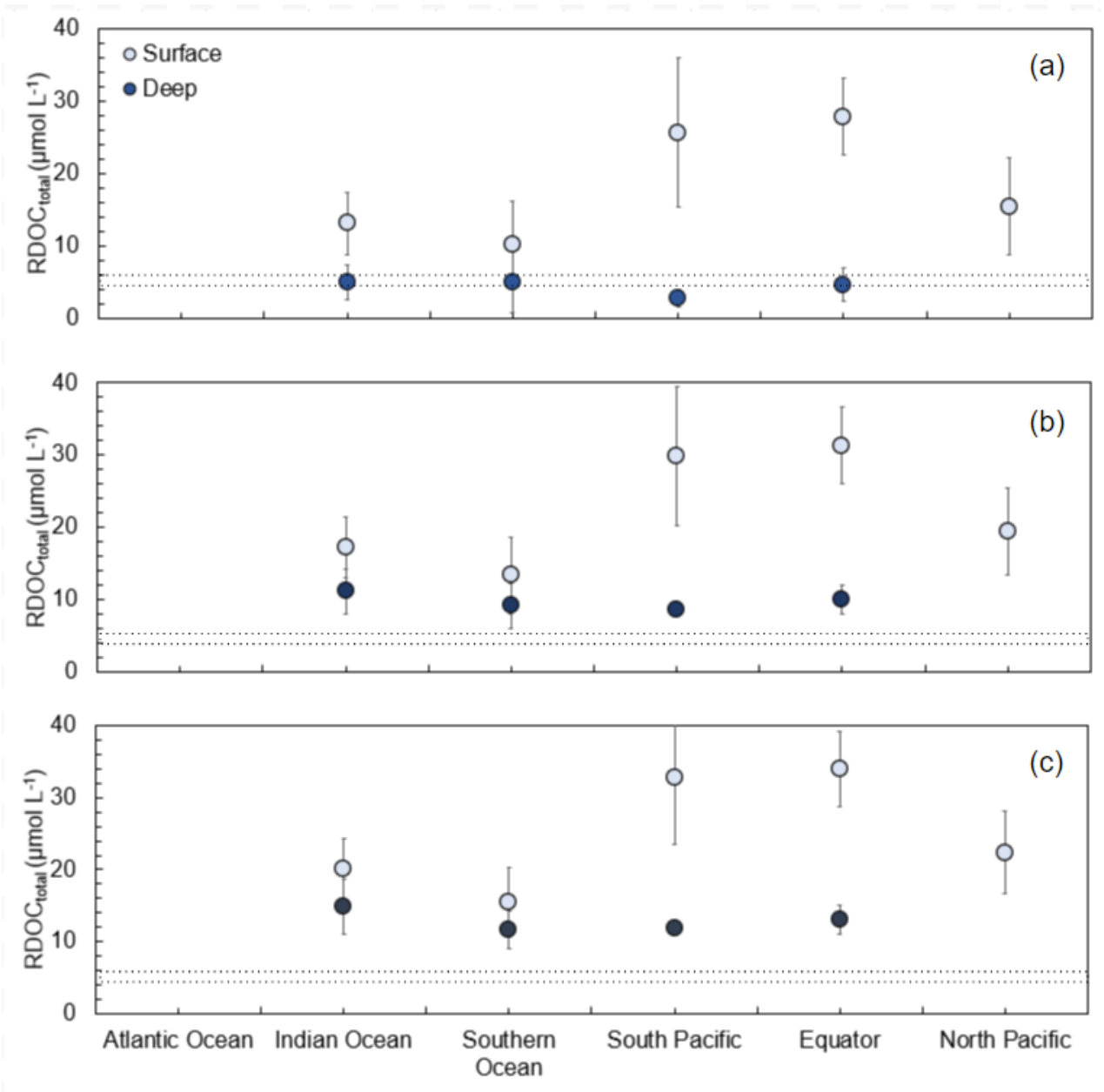

Figure 18. Derived concentrations of labile DOC, using the estimated percent abundance of $RDOC_{total}$ and measured total [DOC]. Using the end-member -573‰ from (Broek et al., 2020) yields an estimate of labile DOC in the deep ocean that falls within the range of previously reported measurements (Benner et al., 1997; Broek et al., 2017; Kaiser & Benner, 2009). Error bars represent propagated error throughout the mass-balance model.

3.5.2.2 Surface and deep ocean estimates of $RDOC_{total}$

Figure 18 shows the results of our mass-balance estimate of $RDOC_{total}$ in each ocean region, using the refractory end-member -573‰, in terms of percent abundance (a) and derived concentration (b). Global deep ocean $RDOC_{total}$ estimates range 85±3% (Atlantic Ocean) to 92±4% (South Pacific). All deep ocean $RDOC_{total}$ estimates are equal within error (88±3%) and within two standard deviations of the previous RDOC estimate of 95% (Hansell, 2013). Together the consistency of global RDOC percent relative abundance are consistent with SPE-DOC comprising a major fraction of the ocean's ubiquitous and isotopically homogenous RDOC "background" pool – a key assumption shaping the "two-pool" model paradigm of DOC cycling (Williams & Druffel, 1987).

Our estimates of RDOC are largely driven by similarities between SPE-DOC $\Delta^{14}C$ and total DOC $\Delta^{14}C$. When these values are more similar, $\Delta^{14}C_{non\text{-}retained}$ (Equation 2) remains further from the DIC $\Delta^{14}C$ (labile end-member), and $RDOC_{total}$ increases. When SPE-DOC $\Delta^{14}C$ is much lower than total DOC $\Delta^{14}C$, $\Delta^{14}C_{non\text{-}retained}$ values approach DIC $\Delta^{14}C$ (the labile end-member) and $RDOC_{total}$ decreases. Such is the case in the surface South Pacific and Equatorial Pacific.

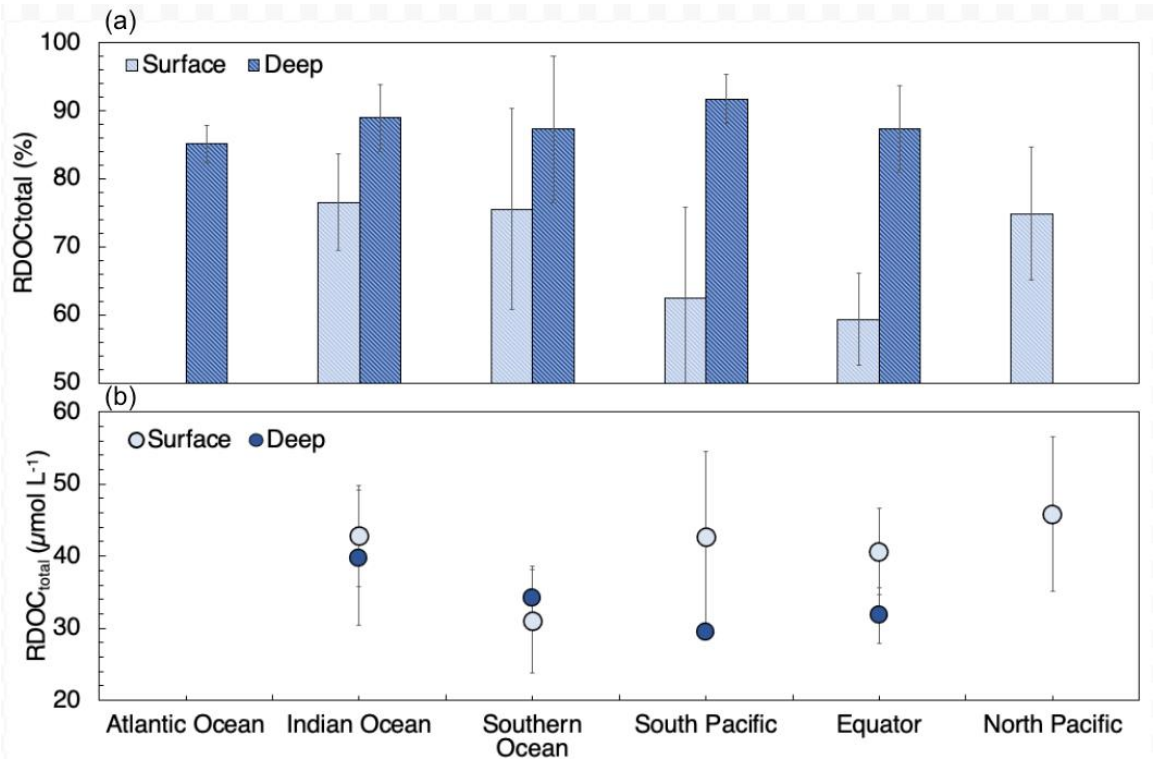

Figure 19. Estimated abundances of RDOC in different ocean regions, (a) expressed as percent abundance and (b) concentration. Error bars all represent propagated error through the mass-balance model. The deep North Pacific Ocean was not modeled due to anomalously high [SPE-DOC] recoveries.

The question remains: what is driving the difference between SPE-DOC $\Delta^{14}C$ and DOC $\Delta^{14}C$, and therefore low $RDOC_{total}$, in the South Pacific and Equatorial surface oceans*?* Total [DOC] and DOC $\Delta^{14}C$ both increase in the Southern Hemisphere subtropical gyre (Druffel et al., 2021). While [SPE-DOC] and SPE-DOC $\Delta^{14}C$ are also highest in these regions, the magnitude of increase in total DOC is enough to create larger offsets between SPE-DOC and total DOC $\Delta^{14}C$ in the South Pacific and Equatorial surface ocean (See Table 8). This is due to the addition of more fresh, labile DOC superimposed on the RDOC pool. Normalizing to units of concentration (Figure 18(b)) shows more clearly how surface and deep ocean $RDOC_{total}$ are similar. [$RDOC_{total}$] in the surface and deep ocean are 41±6% and 34±4%, the same within error. Higher concentrations of *total* DOC at the surface in the South Pacific and Equatorial region dampen $RDOC_{total}$ *percent* abundance (Figure 19a). This echoes the surface mass-balance proposed by

(Williams & Druffel, 1987), in which labile DOC is superimposed on RDOC that is similar to the deep pool.

3.6. Conclusion

This work provides the first basin-scale transect of [SPE-DOC] and SPE-DOC $\Delta^{14}C$ in the Pacific and Indian Oceans. Pacific Ocean [SPE-DOC] and SPE-DOC $\Delta^{14}C$ values show meridional variability in both the surface and deep ocean. In the Indian Ocean, [SPE-DOC] and SPE-DOC $\Delta^{14}C$ values are variable at the surface but constant at depth. This work fills in spatial gaps in SPE-DOC sampling, and provides high-resolution direct comparisons of SPE-DOC and total DOC concentrations and radiocarbon values. These comparisons are used to develop a mass-balance model and estimate RDOC abundance in the surface and deep ocean. This work independently derives a model of deep RDOC that is consistent with the two-pool model under the constrains of more meridional measurements. By matching our estimates of labile DOC and $RDOC_{total}$ to other independent estimates, this study provides support that RDOC in the non-retained DOC pool may have a $\Delta^{14}C$ signature similar to that of LMW SPE-DOC in (Broek et al., 2020). Although our results show that RDOC may be approximated as one well-mixed pool, these estimates of [RDOC] at different latitudes may be useful to future ocean biogeochemical models that attempt to resolve recalcitrant DOC cycling with higher resolution.

3.7. References

Aluwihare, L. I., Repeta, D. J., & Chen, R. F. (2002). Chemical composition and cycling of dissolved organic matter in the Mid-Atlantic Bight. *Deep Sea Research Part II: Topical Studies in Oceanography*, *49*(20), 4421–4437. https://doi.org/10.1016/S0967-0645(02)00124-8

Amon, R. M. W., & Benner, R. (1994). Rapid cycling of high-molecular-weight dissolved organic matter in the ocean. *Letters to Nature*, *369*, 549–551.

Beaupré, S. R. (2015). The Carbon Isotopic Composition of Marine DOC. In *Biogeochemistry of Marine Dissolved Organic Matter* (pp. 335–368). Elsevier. https://doi.org/10.1016/B978-0-12-405940-5.00006-6

Beaupré, S. R., & Druffel, E. R. M. (2009). Constraining the propagation of bomb-radiocarbon through the dissolved organic carbon (DOC) pool in the northeast Pacific Ocean. *Deep Sea Research Part I: Oceanographic Research Papers*, *56*(10), 1717–1726. https://doi.org/10.1016/j.dsr.2009.05.008

Benner, R., & Herndl. (2011). Bacterially Derived Dissolved Organic Matter in the Microbial Carbon Pump. In *Microbial Carbon Pump in the Ocean* (pp. 46–48). Science AAAS.

Benner, R., Pakulski, J. D., McCarthy, M. D., Hedges, J. I., & Hatcher, P. G. (1992). Bulk Chemical Characteristics of Dissolved Organic Matter in the Ocean. *Science*, *255*(5051), 1561–1564.

Benner, R., Biddanda, B., Black, B., & McCarthy, M. (1997). Abundance, size distribution, and stable carbon and nitrogen isotopic compositions of marine organic matter isolated by tangential-flow ultrafiltration. *Marine Chemistry*, *57*, 243–263.

Bercovici, S. K., Koch, B. P., Lechtenfeld, O. J., McCallister, S. L., Schmitt-Kopplin, P., & Hansell, D. A. (2018). Aging and Molecular Changes of Dissolved Organic Matter Between Two Deep Oceanic End-Members. *Global Biogeochemical Cycles*, *32*(10), 1449–1456. https://doi.org/10.1029/2017GB005854

Bercovici, S. K., McNichol, A. P., Xu, L., & Hansell, D. A. (2018). Radiocarbon Content of Dissolved Organic Carbon in the South Indian Ocean. *Geophysical Research Letters*, *45*(2), 872–879. https://doi.org/10.1002/2017GL076295

Broek, T. A. B., Walker, B. D., Guilderson, T. P., & McCarthy, M. D. (2017). Coupled ultrafiltration and solid phase extraction approach for the targeted study of semi-labile high molecular weight and refractory low molecular weight dissolved organic matter. *Marine Chemistry*, *194*, 146–157. https://doi.org/10.1016/j.marchem.2017.06.007

Broek, T. A. B., Walker, B. D., Guilderson, T. P., Vaughn, J. S., Mason, H. E., & McCarthy, M. D. (2020). Low Molecular Weight Dissolved Organic Carbon: Aging, Compositional Changes, and Selective Utilization During Global Ocean Circulation. *Global Biogeochemical Cycles*, *34*(6), 1–20. https://doi.org/10.1029/2020GB006547

Brophy, J. E., & Carlson, D. J. (1989). Production of biologically refractory dissolved organic carbon by natural seawater microbial populations. *Deep Sea Research Part A. Oceanographic Research Papers*, *36*(4), 497–507. https://doi.org/10.1016/0198-0149(89)90002-2

Coppola, A. I., & Druffel, E. R. M. (2016). Cycling of black carbon in the ocean. *Geophysical Research Letters*, *43*(9), 4477–4482. https://doi.org/10.1002/2016GL068574

Dittmar, T., Koch, B., Hertkorn, N., & Kattner, G. (2008). A simple and efficient method for the solid-phase extraction of dissolved organic matter (SPE-DOM) from seawater. *Limnology and Oceanography: Methods*, *6*(6), 230–235.

Druffel, E. R. M., & Bauer, J. E. (2000). Radiocarbon distributions in Southern Ocean dissolved and particulate organic matter. *Geophysical Research Letters*, *27*(10), 1495–1498. https://doi.org/10.1029/1999GL002398

Druffel, E. R. M., & Griffin, S. (2015). Radiocarbon in dissolved organic carbon of the South Pacific Ocean. *Geophysical Research Letters*, *42*(10), 4096–4101. https://doi.org/10.1002/2015GL063764

Druffel, E. R. M., Griffin, S., Coppola, A. I., & Walker, B. D. (2016). Radiocarbon in dissolved organic carbon of the Atlantic Ocean. *Geophysical Research Letters*, *43*(10), 5279–5286. https://doi.org/10.1002/2016GL068746

Druffel, E. R. M., Williams, P. M., Bauer, J. E., & Ertel, J. R. (1992). Cycling of dissolved and particulate organic matter in the open ocean. *Journal of Geophysical Research*, *97*(C10), 15639. https://doi.org/10.1029/92JC01511

Druffel, E. R. M., Griffin, S., Wang, N., Garcia, N. G., McNichol, A. P., Key, R. M., & Walker, B. D. (2019). Dissolved Organic Radiocarbon in the Central Pacific Ocean. *Geophysical Research Letters*, *46*(10), 5396–5403. https://doi.org/10.1029/2019GL083149

Druffel, E. R. M., Bauer, J. E., Griffin, S., Beaupré, S. R., & Hwang, J. (2008). Dissolved inorganic radiocarbon in the North Pacific Ocean and Sargasso Sea. Deep Sea Research Part I: Oceanographic Research Papers, 55(4), 451–459. https://doi.org/10.1016/j.dsr.2007.12.007

Druffel, E.R.M. (2021). DOC-14C data from P18 cruise legs 1 and 2 in 2016/17. expo code 33RO20161119, https://doi.org/10.7289/v5cv4g1w

Fiedler, P. C., & Talley, L. D. (2006). Hydrography of the eastern tropical Pacific: A review. *Progress in Oceanography*, *69*(2–4), 143–180. https://doi.org/10.1016/j.pocean.2006.03.008

Flerus, R., Lechtenfeld, O. J., Koch, B. P., McCallister, S. L., Schmitt-Kopplin, P., Benner, R., Kaiser, K., & Kattner, G. (2012). A molecular perspective on the ageing of marine dissolved organic matter. *Biogeosciences*, *9*(6), 1935–1955. https://doi.org/10.5194/bg-9-1935-2012

Follett, C. L., Repeta, D. J., Rothman, D. H., Xu, L., & Santinelli, C. (2014). Hidden cycle of dissolved organic carbon in the deep ocean. *Proceedings of the National Academy of Sciences*, *111*(47), 16706–16711. https://doi.org/10.1073/pnas.1407445111

Guo, L., Santschi, P. H., Cifuentes, L. A., Trumbore, S. E., & Southon, J. (1996). Cycling of high-molecular-weight dissolved organic matter in the Middle Atlantic Bight as revealed by carbon isotopic 13C and 14C signatures. *Limnology and Oceanography*, *41*(6), 1242–1252. https://doi.org/10.4319/lo.1996.41.6.1242

Hansell, D. A. (2013). Recalcitrant Dissolved Organic Carbon Fractions. *Annual Review of Marine Science*, *5*(1), 421–445. https://doi.org/10.1146/annurev-marine-120710-100757

Hansell, D. A., Carlson, C. A., Repeta, D. J., & Schlitzer, R. (2009). Dissolved organic matter in the ocean: A controversy stimulates new insights. *Oceanography*, *22*(4), 202–211.

Hedges, J. I. (1992). Global biogeochemical cycles: Progress and problems. *Marine Chemistry*, *39*(1–3), 67–93. https://doi.org/10.1016/0304-4203(92)90096-S

Hertkorn, N., Harir, M., Koch, B. P., Michalke, B., & Schmitt-Kopplin, P. (2013). High-field NMR spectroscopy and FTICR mass spectrometry: Powerful discovery tools for the molecular level characterization of marine dissolved organic matter. *Biogeosciences*, *10*(3), 1583–1624. https://doi.org/10.5194/bg-10-1583-2013

Kaiser, K., & Benner, R. (2009). Biochemical composition and size distribution of organic matter at the Pacific and Atlantic time-series stations. *Marine Chemistry*, *113*(1–2), 63–77. https://doi.org/10.1016/j.marchem.2008.12.004

Lechtenfeld, O. J., Kattner, G., Flerus, R., McCallister, S. L., Schmitt-Kopplin, P., & Koch, B. P. (2014). Molecular transformation and degradation of refractory dissolved organic matter in the Atlantic and Southern Ocean. *Geochimica et Cosmochimica Acta*, *126*, 321–337. https://doi.org/10.1016/j.gca.2013.11.009

Lewis, C. B., Walker, B. D., & Druffel, E. R. M. (2020). Isotopic and optical heterogeneity of solid phase extracted marine dissolved organic carbon. *Marine Chemistry*, *219*. https://doi.org/10.1016/j.marchem.2020.103752

Loh, A. N., Bauer, J. E., & Druffel, E. R. M. (2004). Variable ageing and storage of dissolved organic components in the open ocean. *Nature*, *430*(7002), 877–881. https://doi.org/10.1038/nature02780

McNichol, A. P., & Aluwihare, L. I. (2007). The Power of Radiocarbon in Biogeochemical Studies of the Marine Carbon Cycle: Insights from Studies of Dissolved and Particulate Organic Carbon (DOC and POC). *Chemical Reviews*, *107*(2), 443–466. https://doi.org/10.1021/cr050374g

Medeiros, Patricia. M., Seidel, M., Powers, L. C., Dittmar, T., Hansell, D. A., & Miller, W. L. (2015). Dissolved organic matter composition and photochemical transformations in the northern North Pacific Ocean: North Pacific Ocean DOM. *Geophysical Research Letters*, *42*(3), 863–870. https://doi.org/10.1002/2014GL062663

Moreno, A. R., Garcia, C. A., Larkin, A. A., Lee, J. A., Wang, W.-L., Moore, J. K., Primeau, F. W., & Martiny, A. C. (2020). Latitudinal gradient in the respiration quotient and the implications for ocean oxygen availability. *Proceedings of the National Academy of Sciences*, *117*(37), 22866–22872. https://doi.org/10.1073/pnas.2004986117

Ogawa, H., Fukuda, R., & Koike, I. (1999). Vertical distributions of dissolved organic carbon and nitrogen in the Southern Ocean. *Deep Sea Research Part I: Oceanographic Research Papers*, *46*(10), 1809–1826. https://doi.org/10.1016/S0967-0637(99)00027-8

Ogawa, H., & Ogura, N. (1992). Comparison of two methods for measuring dissolved organic carbon in sea water. *Letters to Nature*, *356*, 696–698.

Repeta, D. J., & Aluwihare, L. I. (2006). Radiocarbon analysis of neutral sugars in high-molecular-weight dissolved organic carbon: Implications for organic carbon cycling. *Limnology and*

Oceanography, *51*(2), 1045–1053. https://doi.org/10.4319/lo.2006.51.2.1045

Santos, G. M., Southon, J. R., Griffin, S., Beaupre, S. R., & Druffel, E. R. M. (2007). Ultra small-mass AMS 14C sample preparation and analyses at KCCAMS/UCI Facility. *Nuclear Instruments and Methods in Physics Research Section B: Beam Interactions with Materials and Atoms*, *259*(1), 293–302. https://doi.org/10.1016/j.nimb.2007.01.172

Santschi, P. H., Balnois, E., Wilkinson, K. J., Zhang, J., Buffle, J., & Guo, L. (1998). Fibrillar polysaccharides in marine macromolecular organic matter as imaged by atomic force microscopy and transmission electron microscopy. *Limnology and Oceanography*, *43*(5), 896–908. https://doi.org/10.4319/lo.1998.43.5.0896

Stuiver, M., & Polach, H. A. (1977). Discussion reporting of 14 C data. *Radiocarbon*, *19*(3), 355–363.

Talley, L. (2013). Closure of the Global Overturning Circulation Through the Indian, Pacific, and Southern Oceans: Schematics and Transports. *Oceanography*, *26*(1), 80–97. https://doi.org/10.5670/oceanog.2013.07

Walker, B. D., Primeau, F. W., Beaupré, S. R., Guilderson, T. P., Druffel, E. R. M., & McCarthy, M. D. (2016). Linked changes in marine dissolved organic carbon molecular size and radiocarbon age. *Geophysical Research Letters*, *43*(19), 9. https://doi.org/10.1002/2016GL070359

Walker, B.D., Beaupré, S. R., Guilderson, T. P., Druffel, E. R. M., & McCarthy, M. D. (2011). Large-volume ultrafiltration for the study of radiocarbon signatures and size vs. Age relationships in marine dissolved organic matter. *Geochimica et Cosmochimica Acta*, *75*(18), 5187–5202. https://doi.org/10.1016/j.gca.2011.06.015

Walker, B. D., & Xu, X. (2018). An improved method for the sealed-tube zinc graphitization of microgram carbon samples and 14C AMS measurement. *Nuclear Instruments and Methods in Physics Research Section B: Beam Interactions with Materials and Atoms*. https://doi.org/10.1016/j.nimb.2018.08.004

Walker, B. D., Beaupré, S. R., Guilderson, T. P., McCarthy, M. D., & Druffel, E. R. M. (2016). Pacific carbon cycling constrained by organic matter size, age and composition relationships. *Nature Geoscience*, *9*(12), 888–891. https://doi.org/10.1038/ngeo2830

Williams, P. M., & Druffel, E. R. M. (1987). Radiocarbon in dissolved organic matter in the central North Pacific Ocean. *Letters to Nature*, *330*(6145), 246–248. https://doi.org/10.1038/330246a0

Xu, X., Trumbore, S. E., Zheng, S., Southon, J. R., McDuffee, K. E., Luttgen, M., & Liu, J. C. (2007). Modifying a sealed tube zinc reduction method for preparation of AMS graphite targets: Reducing background and attaining high precision. *Nuclear Instruments and Methods in Physics Research Section B: Beam Interactions with Materials and Atoms*, *259*(1), 320–329. https://doi.org/10.1016/j.nimb.2007.01.175

Zigah, P. K., McNichol, A. P., Xu, L., Johnson, C., Santinelli, C., Karl, D. M., & Repeta, D. J. (2017). Allochthonous sources and dynamic cycling of ocean dissolved organic carbon revealed by carbon isotopes: Carbon Isotopes of Marine DOC. *Geophysical Research Letters*, *44*, 2407–2415. https://doi.org/10.1002/2016GL071348

Ziolkowski, L. A., & Druffel, E. R. M. (2010). Aged black carbon identified in marine dissolved organic carbon. *Geophysical Research Letters*, *37*(16), n/a-n/a. https://doi.org/10.1029/2010GL043963

3.8. Supporting Information for Chapter 3

Additional Detail about algebraic derivation of Section 3.5.2 mass-balance model

The total amount of RDOC is a function of the amount of SPE-DOC, *and* the amount of RDOC in the "non-retained" portion.

Step 1.: Solve for the radiocarbon signature of the non-retained portion.

Variables:

Total DOC $\Delta^{14}C$: from UV-oxidation measurements

SPE-DOC $\Delta^{14}C$: from values in this work

$Frac_{SPE\text{-}DOC}$: SPE-DOC recovery

$Frac_{non\text{-}retained}$: 1- SPE-DOC recovery (if SPE-DOC recovery was 40%, non-retained was 60%).

Non-retained $\Delta^{14}C$: the unknown radiocarbon signature of DOC that was not isolated on the resin.

X = the fraction of labile C within "non-retained" portion (unknown)

Y = the fraction of RDOC within the "non-retained" portion (unknown)

$\Delta^{14}C_X$= the radiocarbon signature of labile C (based on surface ocean DIC $\Delta^{14}C$ signatures)

$\Delta^{14}C_Y$= the radiocarbon value of the RDOC ((-573±6‰),based on LMW-DOC measurement from (Broek et al. 2020))

$\Delta^{14}C_{nr}$ = the radiocarbon signature of the "non-retained" portion. This value was calculated via a mass balance between SPE-DOC $\Delta^{14}C$, DOC $\Delta^{14}C$, and the SPE-DOC recovery

$$S1.\ Bulk\ DOC\ \Delta^{14}C = (SPE{-}DOC\ \Delta^{14}C * Frac_{SPE-DOC}) + (\Delta^{\mathbf{14}}\boldsymbol{C_{nr}} * Frac_{nonretained})$$

$$S2.\ \Delta^{\mathbf{14}}\boldsymbol{C_{nr}} = \frac{Bulk\ DOC^{14}C - (SPE{-}DOC\ \Delta^{14}C * Frac_{SPE-DOC})}{(Frac_{nonretained})}$$

Step 2. The radiocarbon signature of the non-retained portion are still very low, indicating there may still be an abundance of DOM with RDOC signature. If we know what the Δ^{14}C of the labile material should be (based on known surface ocean DIC Δ^{14}C values), we can estimate the relative abundance of labile and refractory material within the "non-retained" portion.

$$S3.\ \mathbf{14}_{\boldsymbol{C_{nr}}} = (X * 14_{C_X}) + (Y * 14_{C_Y})$$

S4. 1 = X + Y,

Solving for Y:

Set X = 1-Y, substitute into equation S3.

$$14_{C_{nr}} = ((1 - Y) * 14_{C_X}) + (Y * 14_{C_Y})$$

$$14_{C_{nr}} = (14_{C_X} - Y * 14_{C_X}) + (Y * 14_{C_Y})$$

$$\left(\frac{1}{Y}\right) 14_{C_{nr}} = \left(\frac{1}{Y}\right)(14_{C_X} - Y * 14_{C_X}) + (Y * 14_{C_Y})$$

$$\left(\frac{1}{Y}\right)14_{C_{nr}} = \left(\frac{1}{Y}\right)14_{C_X} - 14_{C_X} + 14_{C_Y}$$

$$\left(\frac{1}{Y}\right)14_{C_{nr}} - \left(\frac{1}{Y}\right)14_{C_X} = -14_{C_X} + 14_{C_Y}$$

$$\left(\frac{1}{Y}\right)(14_{C_{nr}} - 14_{C_X}) = -14_{C_X} + 14_{C_Y}$$

$$\left(\frac{1}{Y}\right) = \frac{(14_{C_Y} - 14_{C_X})}{(14_{C_{nr}} - 14_{C_x})}$$

$$\boldsymbol{Y = \frac{14_{C_{nr}} - 14_{C_X}}{14_{C_Y} - 14_{C_X}}}$$

Y is the relative abundance of RDOC within the "non-retained" pool. The total amount of RDOC is the amount in SPE-DOC, for example: (50% + (Y*(1-50%)).

$$\boldsymbol{Total\ refractory}\ \% = \left(\left(\frac{[SPE - DOC]}{[DOC]}\right) * 100\right) + (Y * \left(1 - \left(\frac{[SPE - DOC]}{[DOC]}\right) * 100\right)$$

Chapter 4: Low SPE-DOC stable carbon isotopic signatures driven by the ocean microbial carbon pump

4.1 Abstract

Oceanic storage of marine DOC plays a key role in long-term carbon sequestration from the atmosphere. The ^{14}C age of DOC suggests it can be stored in the deep ocean for over 6500 ^{14}C years. It is believed that most recalcitrant molecules are transformed by bacteria from large bio-molecules into smaller recalcitrant DOC forms. One example is carboxyl-rich aliphatic material (CRAM). However, the precise mechanisms of this transformation remain unconstrained. SPE is used to isolate the hydrophobic, low molecular weight, refractory portion of marine DOC. Here we show that stable carbon isotopic signatures ($\delta^{13}C$) of SPE-DOC in the Pacific and Indian Oceans are significantly lower than those of total DOC. We hypothesize that this $\delta^{13}C$ isotopic results from the MCP that preferentially respires portions of large biomolecules with high $\delta^{13}C$ values to CO_2, leaving the residual pool with low values. This may be a core mechanism driving the marine DOC $\delta^{13}C$ signature, and adds new evidence to the argument that the MCP may be a primary driver of deep ocean DOC storage.

4.2 Introduction

DOC is the largest pool of organic carbon in the ocean (Hansell et al., 2009), about the same magnitude as CO_2 in the atmosphere. The majority of DOC is produced during phytoplankton photosynthesis in the surface ocean although a small amount of allochthonous DOC comes from terrestrial runoff (Opsahl & Benner, 1997). Radiocarbon measurements of DOC in the deep ocean reveal ^{14}C ages of 4000-6500 years (Druffel et al. 1992; Williams and Druffel 1987), indicating a significant portion is recalcitrant and survives multiple ocean overturning cycles. This discovery highlighted the importance of marine DOC for long-term carbon storage; however, the predominant mechanism leading to DOC recalcitrance is still under investigation. Understanding this mechanism is fundamental to our understanding of the ocean's role in the global carbon cycle and climate.

The processes governing marine DOC cycling are complex. During photosynthesis, plankton synthesize HMW DOC (Aluwihare & Repeta, 1999), including major biomolecular groups such as carbohydrates, nucleic acids, lipids, and vitamins. (Aluwihare & Repeta, 1999; Aluwihare et al., 2002; Benner et al., 1992; Sannigrahi et al., 2005; Zigah et al., 2014). Up to half of this primary production is released directly into the water column as DOC (30-50%) (Ducklow et al. 1995). Other processes, such as grazing of phytoplankton, "sloppy feeding", and viral lysis add yet more DOC to the mix (Brussaard et al., 2008; Jiao et al., 2010; Suttle, 2007; Wilhelm & Suttle, 1999).

The HMW DOC pool cycles on timescales of weeks to several decades (Amon & Benner, 1994, 1996; Repeta & Aluwihare, 2006; Santschi et al., 1995; Walker et al., 2016) and comprises 24-28% of the total DOC pool (Benner et al. 1997; Skoog and Benner 1997). Heterotrophic bacteria use HMW DOC as substrate for remineralization to inorganic carbon and nutrients, or secondary production of organic matter. Secondary production of DOC results in organic matter that is lower molecular weight (LMW DOC), abundant in carboxyl-rich alicyclic molecules (CRAM) with lower O/C and H/C ratios than those in larger biomolecules (Hertkorn et al., 2013; Hertkorn et al., 2006; Lechtenfeld et al., 2015). These chemical characteristics make LMW DOC recalcitrant in the deep ocean (RDOC), allowing it to accumulate high net abundances (68-75% of total DOC) (Skoog & Benner, 1997), and low $\Delta^{14}C$ values (Broek et al. 2017; Zigah et al. 2014,). These characteristics are commonly found in SPE-DOC (Hertkorn et al. 2006; Lechtenfeld et al. 2014; 2015). Although DOC molecular-level characterization has shown that heterotrophic bacteria facilitate the net transition from HMW to LMW DOC (Ogawa, 2001), and RDOC, the magnitude with which this process effects the DOC pool remains undetermined, and can be constrained by carbon isotope studies.

A key tool to understand mechanisms driving biogeochemical cycles is $\delta^{13}C$ measurements. The $\delta^{13}C$ value of HMW and LMW DOC is influenced by reversible equilibrium fractionation and non-reversible kinetic isotope effects. Different photosynthetic pathways have well known isotope effects that cause distinct $\delta^{13}C$ signatures. C_3 photosynthesis results in organic matter that is lower in $\delta^{13}C$ (depleted

in ^{13}C) relative to C_4 photosynthesis (-30‰ to -25‰ versus -16‰ to -10‰, respectively) (Hayes, 2001). Marine phytoplankton photosynthesis yields a $\delta^{13}C$ value in-between, around -21‰ (Williams and Gordon 1970) and can be dependent on growth rate, temperature and CO_2 concentration, and taxa (Goericke and Fry 1994; Hinga et al., 1994.; Wilkes et al. 2018; Rau et al. 1982; Rau et al. 1989). Source appropriation using $\delta^{13}C$ of bulk material alone can be difficult. For example, a two-component mixture of C_3 and C_4 biomass could mimic the marine phytoplankton signature, and lead to incorrect source appropriation (Pancost & Boot, 2004). Compound specific studies of terrestrial biomarkers, such as lignin phenols, reveal extremely low concentrations (Opsahl & Benner, 1998), indicating that the vast majority of marine DOC is phytoplankton derived. This example is insightful because it reveals the limits in simple $\delta^{13}C$ end-member mixing models and the power of compound specific analyses to deconvolute complex biogeochemical cycling processes.

Compound specific isotope analyses have been made on amino acids, cellulose, lignin, proteins and carbohydrates in terrestrial and marine dissolved organic matter (Abelson and Hoering 1961; Benner et al. 1987; Degens et al. 1968; van Dongen et al. 2002). Summarized well in Close (2018), the $\delta^{13}C$ values organic matter follows the order: carbohydrates > proteins ≈ nucleic acids > lipids. This order is echoed in degradation rates; nucleic acids, carbohydrates and proteins are degraded much faster than lipids (LaRowe & Van Cappellen, 2011; Rodger Harvey et al., 1995). Preferential remineralization of the compounds with high $\delta^{13}C$ values results in depletion of the remaining DOC pool. This effect has been shown through decreasing $\delta^{13}C$ values of POC with depth in the Eastern Tropical North Pacific Ocean (Jeffrey et al., 1983). Microbial respiration also effects $\delta^{13}C$ values of organic carbon, depending on factors such as oxygen availability, growth stage, substrate or even ice cover in polar seas (Abraham et al., 1998; Gong & Hollander, 1997; Macko & Estep, 1984; Shah et al., 2013; Teece et al., 1999). Overall, respiration effects on DOC are significantly lower than primary biosynthesis (<1‰) (Beaupre 2015); the predominant way bacteria influence total DOC $\delta^{13}C$ values is through the compounds they choose to remineralize.

In this study, $\delta^{13}C$ values of SPE-DOC are presented for a meridional transect of two ocean basins from 70°S to 45°N.Through comparisons to bulk DOC $\delta^{13}C$, it is shown that observed offsets of SPE-DOC and total DOC $\delta^{13}C$ is ubiquitous in the Eastern Pacific and Western Indian Ocean at all depths. This study provides new, basin-scale observations supporting the microbial carbon pump (MCP) and preferential remineralization of labile DOC with high $\delta^{13}C$ values as a primary mechanism leading to low LMW DOC $\delta^{13}C$ values, its recalcitrance, and the storage of DOC in the deep ocean.

4.3 Methods

Field sampling methods and laboratory sampling preparation follow those described in Chapter 3. Stable carbon isotopic measurements ($\delta^{13}C$) were made using a Gas Bench II and Thermo Electron Delta Plus mass spectrometer, and corrected using calibrated isotopic standards (NIST NBS-19). Measurements are reported as standard permille (‰) relative to V-PDB (Vienna Pee-Dee Belemnite) scale. $\delta^{13}C$ measurements are corrected for the presence of C_{ex} as described in Chapter 2, with C_{ex} having a measured mass of 9±2 µg C. Because the known size of C_{ex} is so small relative to our sample size, (0.2%), corrected $\delta^{13}C$ values are the same as raw measured $\delta^{13}C$ values.

4.4 Results and discussion

4.4.1 SPE-DOC $\delta^{13}C$ values and identifiable trends

Corrected SPE-DOC $\delta^{13}C$ values are shown in Figure 20(a) and (b) for the surface and deep ocean, respectively, and shown in Table 8. The mean and standard deviation of total DOC $\delta^{13}C$ measurements collected within the SPE-DOC sampling range (0-200m in (a) and 2000-4000m in (b)) are represented by the dashed line and shaded regions. Surface ocean measurements of SPE-DOC $\delta^{13}C$ in the North Pacific Ocean (P16N) are all equal within error (-22.6±0.1‰). P18 surface SPE-DOC $\delta^{13}C$ values range from -22.4±0.2‰ at 69°S to -23.4±0.2‰ at 20°N (average -22.9±0.3‰, n = 9). The low $\delta^{13}C$ value at 20°N corresponds to an extremely low SPE-DOC $\Delta^{14}C$ value (-543±57‰) from the same sample

(Chapter 3). Values are high in the center and southern edge of the Southern Hemisphere subtropical gyre (-22.5±0.2‰ to -22.6±0.2‰), and the highest surface value (-22.4±0.2‰ at 69°S) is found at the southernmost station. Surface SPE-DOC $\delta^{13}C$ values in the Indian Ocean increase from south to north. SPE-DOC $\delta^{13}C$ is -23.2±0.2‰ at 29.5°S, and increases to -22.0‰ at 17°N.

Deep Pacific Ocean SPE-DOC $\delta^{13}C$ values from P18 are equal within error between 69°S and 24°S, ranging from -22.5‰ to -22.3‰ (average = -22.4±0.1, n=5). Values are lower between 15°S and 20°N, ranging from -23.2‰ to -22.8‰ (average = -23.0±0.2‰, n = 4). Deep ocean SPE-DOC $\delta^{13}C$ values from the P16N cruise in the central Pacific range from -22.5‰ at 16°S to -23.2±0.2‰ at 30°N (average -22.8±0.3‰ n=4). In the Indian Ocean deep waters, SPE-DOC $\delta^{13}C$ values range -22.2‰ to -22.7‰ (average -22.5±0.2‰ n=5), decreasing from south to north.

In the surface Pacific Ocean, SPE-DOC $\delta^{13}C$ values may be linked to regional biogeochemistry. High nutrients, high DIC, and low oxygen are all indicators of the upwelling of older, deeper water, and strong microbial respiration (Capone & Hutchins, 2013). These conditions are found in the oxygen deficient zone in the Eastern Tropical North Pacific Ocean (20°N, Figure 21), and corresponds to our lowest surface SPE-DOC $\delta^{13}C$ value. Thus, higher oxygen concentrations may indicate less remineralization has occurred. Our highest surface Pacific Ocean SPE-DOC $\delta^{13}C$ value corresponds to high oxygen concentrations in the Southern Ocean (69°S to 60°S, Figure 21). Links between remineralization strength and $\delta^{13}C$ value are further discussed in Section 4.4.2.

In the surface Indian Ocean, a similar decrease in $\delta^{13}C$ toward the oxygen minimum zone is not seen (Figure 22). This may be due to our weighted average sampling depth (represented by the y-axis in Figure 22) being shallower than the core of the oxygen minimum zone, which begins at ~150m north of 10°N.

A few other processes must be briefly addressed that may contribute slightly to low SPE-DOC $\delta^{13}C$ values.. First, it is unlikely that extraneous carbon (C_{ex}) with a low $\delta^{13}C$ value is contributing to

systematic low $\delta^{13}C$ values in SPE-DOC, as described briefly in Section 4.3. Our samples were corrected for the mass and isotopic composition of C_{ex} according to (Lewis et al. 2020). Second, the SPE process likely sorbs dissolved black carbon (DBC) which has high double-bond equivalence and polycyclic aromatic rings (Koch et al. 2005; Hertkorn et al. 2013). These thermogenically produced compounds may have low $\delta^{13}C$ values if their sources were wildfires (containing low C_3 photosynthesis $\delta^{13}C$ signature) or fossil fuels. However, recent observations have shown that DBC in the ocean has marine-like $\delta^{13}C$, and at the observed concentrations, DBC is too dilute in seawater to be the major contributor to low $\delta^{13}C$ in SPE-DOC (0.6 – 3 μM) (Coppola & Druffel, 2016; Wagner et al., 2019). Fluvial sources of carbon to the ocean would provide a source of low $\delta^{13}C$ organic matter as well. Terrestrial organic matter may sorb onto the SPE resin because of high concentrations of aromatic carbon and phenols (Hedges, 1992). Previous studies show that 0.7% of total DOC in the Pacific Ocean is of terrestrial origin (Opsahl & Benner, 1997). With average SPE-DOC recoveries of 46±8%, if SPE captured all terrestrial DOC, this would comprise 1.52±.05% of SPE-DOC. This may be a contributing factor but likely not the driving mechanism behind low SPE-DOC $\delta^{13}C$. Future studies that combine analysis of lignin phenol with SPE-DOC isotope characterizations may confirm this.

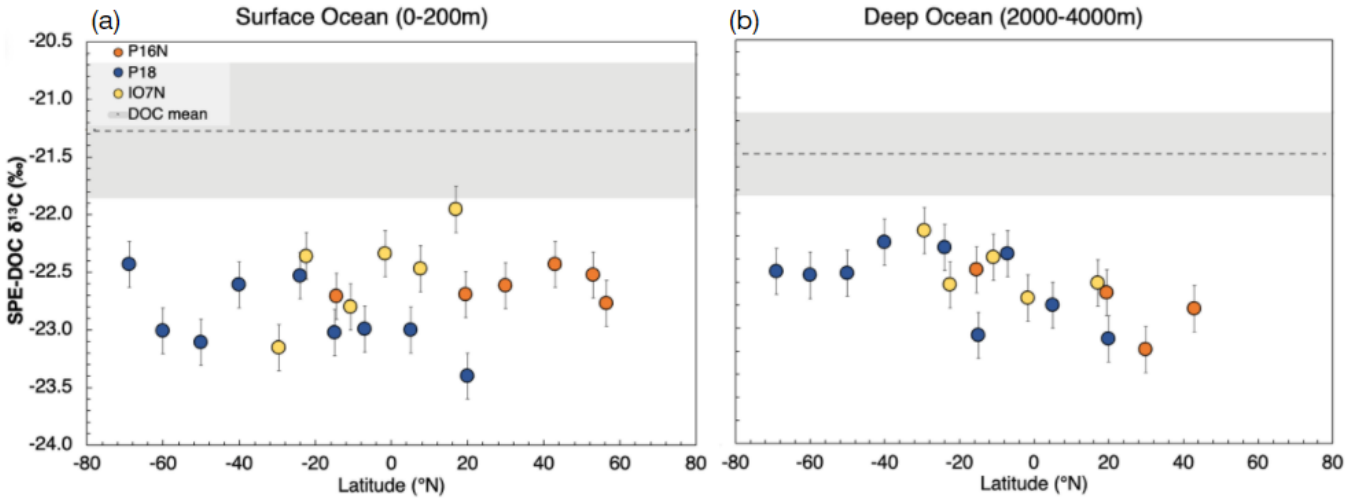

Figure 20. SPE-DOC $\delta^{13}C$ values from P16N, P18, and IO7N from the surface ocean (a) and deep ocean (b). The dashed line indicates the mean total DOC $\delta^{13}C$ values from the sampling depths (0-200m in the surface ocean and 2000-4000m in the deep ocean). The shaded areas represents the standard deviation of the means. (n = 50 and 68 for the surface and deep ocean respectively.)

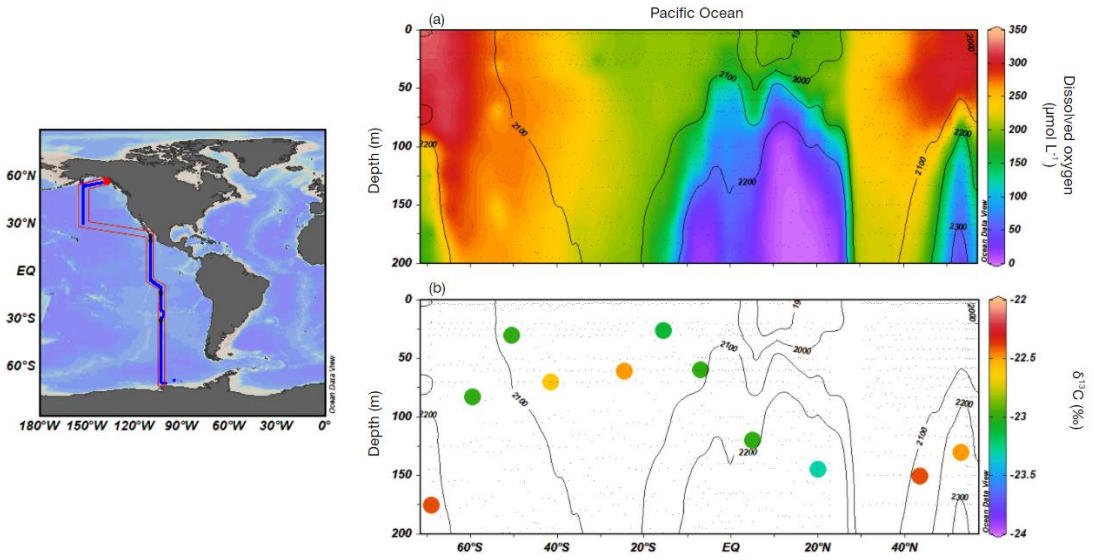

Figure 21. Top panel (a) shows dissolved oxygen concentrations in the surface Pacific Ocean sampled on P18; contour lines depict total carbon concentrations, [DIC] (µmol kg^{-1}). The bottom panel (b) shows SPE-DOC as a function of latitude and depth with $\delta^{13}C$ values denoted by the colorbar. The same DIC contours from (a) are overlaid. In the surface Pacific Ocean, SPE-DOC may be linked to regional biogeochemistry, with lower $\delta^{13}C$ values in regions with lower oxygen.

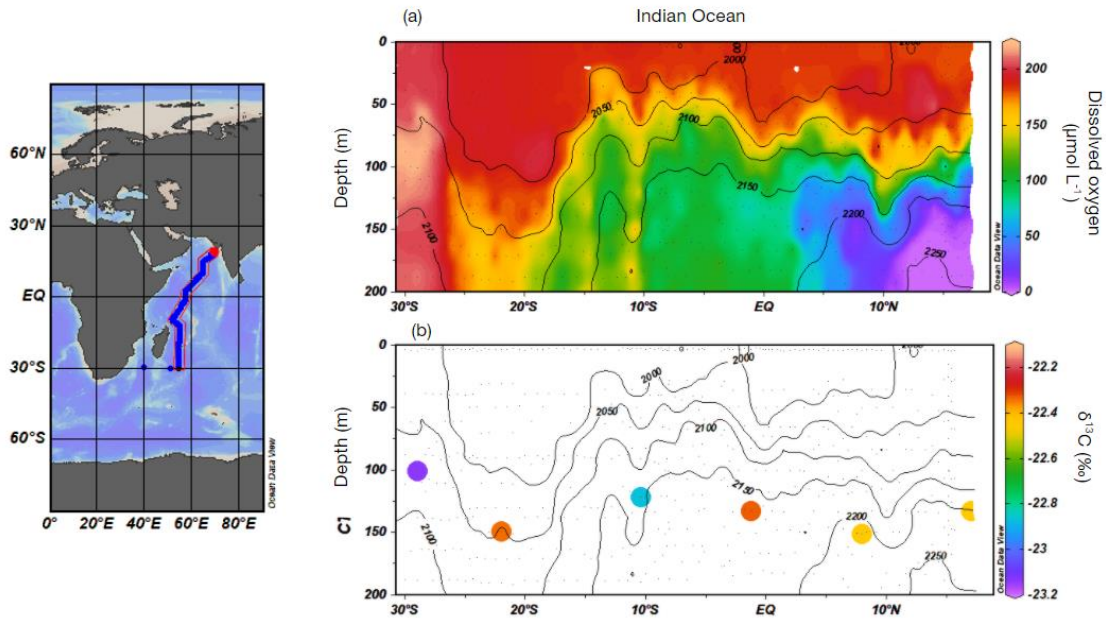

Figure 22. Top panel (a) shows dissolved oxygen concentrations in the surface Indian Ocean sampled on IO7N; contour lines depict total carbon concentrations, [DIC] (µmol kg^{-1}). The bottom panel shows SPE-DOC as a function of latitude and depth with $\delta^{13}C$ values denoted by the colorbar. The same DIC contours from (a) are overlaid.

4.4.2 Basin-scale offset between SPE-DOC and total DOC $\delta^{13}C$

The average of all available DOC $\delta^{13}C$ values from P16N (Druffel et al., 2019), P18 and IO7N (Druffel, 2021) is -21.4±0.5‰. Extracting DOC $\delta^{13}C$ values from the sampling depth ranges for SPE-DOC (0-200m and 2000-4000m) yields means of -21.3±0.7‰ and -21.5±0.4‰ in the surface and deep ocean, respectively. This is depicted by the dotted line and shaded regions of Figure 20. The difference between SPE-DOC $\delta^{13}C$ and total DOC $\delta^{13}C$ values was tested for statistical significance using a two-tailed student's t-test at 99% confidence. Significant differences were found when comparing SPE-DOC and total DOC $\delta^{13}C$ values from each cruise at both depths and when all available data were aggregated (all SPE-DOC $\delta^{13}C$ measurements vs all total DOC $\delta^{13}C$ measurements) (DF = 83, t-value = 14.02, p = 0.01). This dataset shows that previously reported differences between SPE-DOC $\delta^{13}C$ and total DOC $\delta^{13}C$ (Broek et al., 2017, 2020; Coppola & Druffel, 2016) are systematic on a basin-scale. It also links the recalcitrant characteristics of SPE-DOC (Hertkorn et al., 2006; Lechtenfeld et al., 2014) with low $\Delta^{14}C$ values ((Broek et al. 2020; 2017; Zigah et al. 2014; Lechtenfeld et al. 2014, Chapter 3) and now, low $\delta^{13}C$ values.

What is causing the systematic depletion of $\delta^{13}C$ values in SPE-DOC, and what does it mean for our understanding of ocean biogeochemistry? As described in the Introduction, processes that can influence organic matter $\delta^{13}C$ values are myriad and complex. One or many biogeochemical processes that decrease $\delta^{13}C$ in SPE-DOC is overcoming other processes that may increase $\delta^{13}C$. The most likely cause for the low SPE-DOC $\delta^{13}C$ offset is the MCP.. Marine heterotrophic bacteria are a dominant presence throughout the oceans (Pomeroy et al., 2007), and effectively "monopolize the utilization" of DOM (Jiao et al., 2010). Microbes consume large biomolecules such as carbohydrates, proteins, and amino acids (Keil & Kirchman, 1993; Reintjes et al., 2017) with high $\delta^{13}C$ values, and leave the residual pool low in $\delta^{13}C$. This is similar to decreasing $\delta^{13}C$ in POC with depth reported by (Jeffrey et al., 1983). A difference with depth is not found here because SPE largely isolates the background refractory DOM

pool in both the surface and deep ocean (Chapter 3). Instead, our results point to a general decrease in $\delta^{13}C$ with increasing microbial respiration, and water mass age. This can be seen by the comparison of $\delta^{13}C$ and dissolved oxygen in the surface Pacific Ocean (Section 4.4.1). In older water masses with low oxygen due to remineralization, SPE-DOC $\delta^{13}C$ is more likely to be lower because the majority of HMW DOC (high $\delta^{13}C$) has been stripped out.

Another explicit link between SPE-DOC and the MCP is the presence of CRAM, which has been experimentally shown to be produced by heterotrophic bacteria in laboratory experiments (Lechtenfeld et al., 2015), and is consistently observed in the SPE fraction (Broek et al. 2020; Hertkorn et al. 2013; Lechtenfeld et al. 2014). This, along with the presence of D-amino acids in LMW DOC (Kaiser & Benner, 2008; McCarthy et al., 1998), all point to the MCP fingerprint.

4.5 Conclusion

We present SPE-DOC $\delta^{13}C$ values from the Pacific and Indian Ocean and show that SPE-DOC has systematically low $\delta^{13}C$ values relative to total DOC. Through the preferential remineralization of HMW DOC with high $\delta^{13}C$ and high $\Delta^{14}C$, microbes lower the $\delta^{13}C$ signature of DOC and produce CRAM, changing the DOC pool from HMW to LMW, ^{13}C-rich to ^{13}C-depleted, and high $\Delta^{14}C$ to low $\Delta^{14}C$. This link between size and reactivity (age) has been reported previously using radiocarbon (Walker et al., 2016a, 2016b; Guo et al., 1996; Walker et al., 2011; Loh et al., 2004). This study shows that these connections extend to the $\delta^{13}C$ signature of DOC isotopes. We suggest that the MCP is the dominant mechanism in controlling the RDOC cycle. Future studies that aim to understand how DOC biogeochemistry will respond to perturbations to the global carbon cycle will be aided by these isotopic constraints.

4.6 References

Abelson, P., & Hoering, T. C. (1961). Carbon isotope fractionation in formation of amino acids by photosynthetic organisms. *Proceedings of the National Academy of Sciences*, *47*(5), 623–632.

Abraham, W.-R., Hesse, C., & Pelz, O. (1998). Ratios of Carbon Isotopes in Microbial Lipids as an Indicator of Substrate Usage. *Applied and Environmental Microbiology*, *64*(11), 4202–4209. https://doi.org/10.1128/AEM.64.11.4202-4209.1998

Aluwihare, L. I., & Repeta, D. J. (1999). A comparison of the chemical characteristics of oceanic DOM and extracellular DOM produced by marine algae. *Marine Ecology Progress Series*, *186*, 13.

Aluwihare, L. I., Repeta, D. J., & Chen, R. F. (2002). Chemical composition and cycling of dissolved organic matter in the Mid-Atlantic Bight. *Deep Sea Research Part II: Topical Studies in Oceanography*, *49*(20), 4421–4437. https://doi.org/10.1016/S0967-0645(02)00124-8

Amon, R. M. W., & Benner, R. (1994). Rapid cycling of high-molecular-weight dissolved organic matter in the ocean. *Letters to Nature*, *369*, 549–551.

Amon, R. M. W., & Benner, R. (1996). Bacterial utilization of different size classes of dissolved organic matter. *Limnology and Oceanography*, *41*(1), 41–51. https://doi.org/10.4319/lo.1996.41.1.0041

Benner, R., Pakulski, J. D., McCarthy, M. D., Hedges, J. I., & Hatcher, P. G. (1992). Bulk Chemical Characteristics of Dissolved Organic Matter in the Ocean. *Science*, *255*(5051), 1561–1564.

Benner, R., Biddanda, B., Black, B., & McCarthy, M. (1997). Abundance, size distribution, and stable carbon and nitrogen isotopic compositions of marine organic matter isolated by tangential-flow ultrafiltration. *Marine Chemistry*, *57*, 243–263.

Benner, R., Fogel, M. L., Sprague, E. K., & Hodson, R. E. (1987). Depletion of 13C in lignin and its implications for stable carbon isotope studies. *Nature*, *329*(6141), 708–710. https://doi.org/10.1038/329708a0

Broek, T. A. B., Walker, B. D., Guilderson, T. P., & McCarthy, M. D. (2017). Coupled ultrafiltration and solid phase extraction approach for the targeted study of semi-labile high molecular weight and refractory low molecular weight dissolved organic matter. *Marine Chemistry*, *194*, 146–157. https://doi.org/10.1016/j.marchem.2017.06.007

Broek, T. A. B., Walker, B. D., Guilderson, T. P., Vaughn, J. S., Mason, H. E., & McCarthy, M. D. (2020). Low Molecular Weight Dissolved Organic Carbon: Aging, Compositional Changes, and Selective Utilization During Global Ocean Circulation. *Global Biogeochemical Cycles*, *34*(6), 1–20. https://doi.org/10.1029/2020GB006547

Brussaard, C. P., Wilhelm, S. W., Thingstad, F., Weinbauer, M. G., Bratbak, G., Heldal, M., Kimmance, S. A., Middelboe, M., Nagasaki, K., Paul, J. H., Schroeder, D. C., Suttle, C. A., Vaque, D., & Wommack, K. E. (2008). Global-scale processes with a nanoscale drive: The role of marine viruses. *The ISME Journal*, 4.

Capone, D. G., & Hutchins, D. A. (2013). Microbial biogeochemistry of coastal upwelling regimes in a changing ocean. *Nature Geoscience*, *6*, 711–717. https://doi.org/10.1038/NGEO1916

Coppola, A. I., & Druffel, E. R. M. (2016). Cycling of black carbon in the ocean. *Geophysical Research Letters*, *43*(9), 4477–4482. https://doi.org/10.1002/2016GL068574

Degens, E. T., Behrendt, M., Gotthardt, B., & Reppmann, E. (1968). Metabolic fractionation of carbon isotopes in marine plankton—II. Data on samples collected off the coasts of Peru and Ecuador. *Deep Sea Research and Oceanographic Abstracts*, *15*, 11–20.

Druffel, E. R. M., Williams, P. M., Bauer, J. E., & Ertel, J. R. (1992). Cycling of dissolved and particulate organic matter in the open ocean. *Journal of Geophysical Research*, *97*(C10), 15639. https://doi.org/10.1029/92JC01511

Druffel, E.R.M. (2021). DOC-14C data from P18 cruise legs 1 and 2 in 2016/17. expo code 33RO20161119, https://doi.org/10.7289/v5cv4g1w

Druffel, E. R. M., Griffin, S., Wang, N., Garcia, N. G., McNichol, A. P., Key, R. M., & Walker, B. D. (2019). Dissolved Organic Radiocarbon in the Central Pacific Ocean. *Geophysical Research Letters*, *46*(10), 5396–5403. https://doi.org/10.1029/2019GL083149

Ducklow, H., Quinby, H. L., & Carlson, C. A. (1995). Bacterioplankton dynamics in the equatorial Pacific during the 1992 El Nino. *Deep Sea Research II*, *42*.

Goericke, R., & Fry, B. (1994). Variations of marine plankton δ^{13} C with latitude, temperature, and dissolved CO_2 in the world ocean. *Global Biogeochemical Cycles*, *8*(1), 85–90. https://doi.org/10.1029/93GB03272

Gong, C., & Hollander, D. J. (1997). Differential contribution of bacteria to sedimentary organic matter in oxic and anoxic environments, Santa Monica Basin, California. *Organic Geochemistry*, *26*(9),

545–563.

Guo, L., Santschi, P. H., Cifuentes, L. A., Trumbore, S. E., & Southon, J. (1996). Cycling of high-molecular-weight dissolved organic matter in the Middle Atlantic Bight as revealed by carbon isotopic 13C and 14C signatures. *Limnology and Oceanography*, *41*(6), 1242–1252. https://doi.org/10.4319/lo.1996.41.6.1242

Hansell, D. A., Carlson, C. A., Repeta, D. J., & Schlitzer, R. (2009). Dissolved organic matter in the ocean: A controversy stimulates new insights. *Oceanography*, *22*(4), 202–211.

Hayes, J. M. (2001). Fractionation of the Isotopes of Carbon and Hydrogen in Biosynthetic Processes. *Mineralogical Society of America*, 31. https://doi.org/nosams.whoi.edu/jmh/

Hedges, J. I. (1992). Global biogeochemical cycles: Progress and problems. *Marine Chemistry*, *39*(1–3), 67–93. https://doi.org/10.1016/0304-4203(92)90096-S

Hertkorn, N., Benner, R., Frommberger, M., Schmitt-Kopplin, P., Witt, M., Kaiser, K., Kettrup, A., & Hedges, J. I. (2006). Characterization of a major refractory component of marine dissolved organic matter. *Geochimica et Cosmochimica Acta*, *70*(12), 2990–3010. https://doi.org/10.1016/j.gca.2006.03.021

Hertkorn, N., Harir, M., Koch, B. P., Michalke, B., & Schmitt-Kopplin, P. (2013). High-field NMR spectroscopy and FTICR mass spectrometry: Powerful discovery tools for the molecular level characterization of marine dissolved organic matter. *Biogeosciences*, *10*(3), 1583–1624. https://doi.org/10.5194/bg-10-1583-2013

Hinga, K. R., Arthur, M. A., Pilson, M. E. Q., & Whitaker, D. (1994). Carbon isotope fractionation by marine phytoplankton in culture: The effects of CO2 concentration, pH, temperature, and species. *Global Biogeochemical Cycles*, *8*(1), 91–102.

Jeffrey, A. W. A., Pflaum, R. C., Brooks, J. M., & Sackett, W. M. (1983). Vertical trends in particulate organic carbon 13C:12C ratios in the upper water column. *Deep Sea Research*, *30*.

Jiao, N., Herndl, G. J., Hansell, D. A., Benner, R., Kattner, G., Wilhelm, S. W., Kirchman, D. L., Weinbauer, M. G., Luo, T., Chen, F., & Azam, F. (2010). Microbial production of recalcitrant dissolved organic matter: Long-term carbon storage in the global ocean. *Nature Reviews Microbiology*, *8*, 539–599.

Kaiser, K., & Benner, R. (2008). Major bacterial contribution to the ocean reservoir of detrital organic carbon and nitrogen. *Limnology and Oceanography*, *53*, 99–112.

Keil, R. G., & Kirchman, D. L. (1993). Dissolved combined amino acids: Chemical form and utilization by marine bacteria. *Limnology and Oceanography*, *38*(6), 1256–1270. https://doi.org/10.4319/lo.1993.38.6.1256

LaRowe, D. E., & Van Cappellen, P. (2011). Degradation of natural organic matter: A thermodynamic analysis. *Geochimica et Cosmochimica Acta*, *75*(8), 2030–2042. https://doi.org/10.1016/j.gca.2011.01.020

Lechtenfeld, O. J., Hertkorn, N., Shen, Y., Witt, M., & Benner, R. (2015). Marine sequestration of carbon in bacterial metabolites. *Nature Communications*, *6*(1), 8. https://doi.org/10.1038/ncomms7711

Lechtenfeld, O. J., Kattner, G., Flerus, R., McCallister, S. L., Schmitt-Kopplin, P., & Koch, B. P. (2014). Molecular transformation and degradation of refractory dissolved organic matter in the Atlantic and Southern Ocean. *Geochimica et Cosmochimica Acta*, *126*, 321–337. https://doi.org/10.1016/j.gca.2013.11.009

Lewis, C. B., Walker, B. D., & Druffel, E. R. M. (2020). Isotopic and optical heterogeneity of solid phase extracted marine dissolved organic carbon. *Marine Chemistry*, *219*. https://doi.org/10.1016/j.marchem.2020.103752

Loh, A. N., Bauer, J. E., & Druffel, E. R. M. (2004). Variable ageing and storange of dissolved organic components in the open ocean. *Letters to Nature*, *430*, 877–881.

Macko, S. A., & Estep, M. L. F. (1984). Microbial alteration of stable nitrogen and carbon isotopic compositions of organic matter. *Organic Geochemistry*, *6*, 787–790.

McCarthy, M. D., Hedges, J. I., & Benner, R. (1998). *Major Bacterial Contribution to Marine Dissolved Organic Nitrogen*. *281*, 5.

Ogawa, H. (2001). Production of Refractory Dissolved Organic Matter by Bacteria. *Science*, *292*(5518), 917–920. https://doi.org/10.1126/science.1057627

Opsahl, S., & Benner, R. (1997). Distribution and cycling of terrigenous dissolved organic matter in the ocean. *Nature*, *386*(6624), 480–482. https://doi.org/10.1038/386480a0

Opsahl, S., & Benner, R. (1998). Photochemical reactivity of dissolved lignin in river and ocean waters. *Limnology and Oceanography*, *43*(6), 1297–1304. https://doi.org/10.4319/lo.1998.43.6.1297

Pancost, R. D., & Boot, C. S. (2004). The palaeoclimatic utility of terrestrial biomarkers in marine sediments. *Marine Chemistry*, *92*, 239–261. https://doi.org/doi:10.1016/j.marchem.2004.06.029

Pomeroy, L., leB. Williams, P., Azam, F., & Hobbie, J. (2007). The Microbial Loop. *Oceanography*,

20(2), 28–33. https://doi.org/10.5670/oceanog.2007.45

Rau, G. H., Sweeney, R. E., & Kaplan, I. R. (1982). Plankton 13C:12C ratio changes with latitude: Differences between northern and southern oceans. *Deep-Sea Research*, *29*(8A), 1035–1039.

Rau, G. H., Takahashi, T., & Marais, D. J. D. (1989). Latitudinal Variations in plankton d13C: implications for CO2 and productivity in past oceans. *Letters to Nature*, *341*, 516–518.

Reintjes, G., Arnosti, C., Fuchs, B. M., & Amann, R. (2017). An alternative polysaccharide uptake mechanism of marine bacteria. *The ISME Journal*, *11*(7), 1640–1650. https://doi.org/10.1038/ismej.2017.26

Repeta, D. J., & Aluwihare, L. I. (2006). Radiocarbon analysis of neutral sugars in high-molecular-weight dissolved organic carbon: Implications for organic carbon cycling. *Limnology and Oceanography*, *51*(2), 1045–1053. https://doi.org/10.4319/lo.2006.51.2.1045

Rodger Harvey, H., Tuttle, J. H., & Tyler Bell, J. (1995). Kinetics of phytoplankton decay during simulated sedimentation: Changes in biochemical composition and microbial activity under oxic and anoxic conditions. *Geochimica et Cosmochimica Acta*, *59*(16), 3367–3377. https://doi.org/10.1016/0016-7037(95)00217-N

Sannigrahi, P., Ingall, E. D., & Benner, R. (2005). Cycling of dissolved and particulate organic matter at station Aloha: Insights from 13C NMR spectroscopy coupled with elemental, isotopic and molecular analyses. *Deep-Sea Research I*, *52*, 1429–1444. https://doi.org/doi:10.1016/j.dsr.2005.04.001

Santschi, P. H., Honeyman, B., Cifuentes, L., Guo, L., Baskaran, M., Trumbore, S., Southon, J., & Bianchi, T. S. (1995). Isotopic evidence for the contemporary origin of high-molecular weight organic matter in oceanic environments. *Geochimica et Cosmochimica Acta*, *59*, 7.

Shah, S. R., Griffith, D. R., Galy, V., McNichol, A. P., & Eglinton, T. I. (2013). Prominent bacterial heterotrophy and sources of ¹³C-depleted fatty acids to the interior Canada Basin. *Biogeosciences*, *10*(11), 7065–7080. https://doi.org/10.5194/bg-10-7065-2013

Skoog, A., & Benner, R. (1997). Aldoses in various size fractions of marine organic matter: Implications for carbon cycling. *Limnology and Oceanography*, *42*(8), 1803–1813. https://doi.org/10.4319/lo.1997.42.8.1803

Suttle, C. A. (2007). *Marine viruses—Major players in the global ecosystem*. 12.

Teece, M. A., Fogel, M. L., Dollhopf, M. E., & Nealson, K. H. (1999). Isotopic fractionation associated with biosynthesis of fatty acids by a marine bacterium under oxic and anoxic conditions. *Organic Geochemistry*, *30*(12), 1571–1579. https://doi.org/10.1016/S0146-6380(99)00108-4

van Dongen, B., Schouten, S., & Sinninghe Damsté, J. (2002). Carbon isotope variability in monosaccharides and lipids of aquatic algae and terrestrial plants. *Marine Ecology Progress Series*, *232*, 83–92. https://doi.org/10.3354/meps232083

Wagner, S., Brandes, J., Spencer, R. G. M., Ma, K., Rosengard, S. Z., Moura, J. M. S., & Stubbins, A. (2019). Isotopic composition of oceanic dissolved black carbon reveals non-riverine source. *Nature Communications*, *10*(1), 5064. https://doi.org/10.1038/s41467-019-13111-7

Walker, B. D., Primeau, F. W., Beaupré, S. R., Guilderson, T. P., Druffel, E. R. M., & McCarthy, M. D. (2016). Linked changes in marine dissolved organic carbon molecular size and radiocarbon age. *Geophysical Research Letters*, *43*(19), 9. https://doi.org/10.1002/2016GL070359

Walker, B.D., Beaupré, S. R., Guilderson, T. P., Druffel, E. R. M., & McCarthy, M. D. (2011). Large-volume ultrafiltration for the study of radiocarbon signatures and size vs. Age relationships in marine dissolved organic matter. *Geochimica et Cosmochimica Acta*, *75*(18), 5187–5202. https://doi.org/10.1016/j.gca.2011.06.015

Walker, B. D., Beaupré, S. R., Guilderson, T. P., McCarthy, M. D., & Druffel, E. R. M. (2016). Pacific carbon cycling constrained by organic matter size, age and composition relationships. *Nature Geoscience*, *9*(12), 888–891. https://doi.org/10.1038/ngeo2830

Wilhelm, S. W., & Suttle, C. A. (1999). Viruses and Nutrient Cycles in the Sea. *BioScience*, *49*(10), 8.

Wilkes, E. B., Lee, R. B. Y., McClelland, H. L. O., Rickaby, R. E. M., & Pearson, A. (2018). Carbon isotope ratios of coccolith–associated polysaccharides of Emiliania huxleyi as a function of growth rate and CO2 concentration. *Organic Geochemistry*, *119*, 1–10. https://doi.org/10.1016/j.orggeochem.2018.02.006

Williams, P. M., & Gordon, L. I. (1970). Carbon-13: Carbon-12 ratios in dissolved and particulate organic matter in the sea. *Deep Sea Research and Oceanographic Abstracts*, *17*, 19–27.

Williams, P. M., & Druffel, E. R. M. (1987). Radiocarbon in dissolved organic matter in the central

North Pacific Ocean. *Letters to Nature*, *330*(6145), 246–248. https://doi.org/10.1038/330246a0

Zigah, P. K., Minor, E. C., Abdulla, H. A. N., Werne, J. P., & Hatcher, P. G. (2014). An investigation of size-fractionated organic matter from Lake Superior and a tributary stream using radiocarbon, stable isotopes and NMR. *Geochimica et Cosmochimica Acta*, *127*, 264–284. https://doi.org/10.1016/j.gca.2013.11.037

Chapter 5: Conclusions and future research

Motivated by the facts that deep ocean DOC has the same mass as atmospheric carbon (Hansell et al., 2009) and ^{14}C ages of thousands of years (Williams and Druffel 1987), marine geochemists have focused efforts to understand the mechanisms controlling this long-term carbon sink in the global ocean, and its connection to global climate. What processes lead to the dilute concentrations of ~40 µM and low $\Delta^{14}C$ values below 1000 m depth? The canonical "two-pool" model presented by Williams and Druffel (1987) described a surface system with a 1:1 mixture of RDOC and labile DOC, and a well-mixed deep ocean of RDOC. Although this general framework has held up, as time progressed, more details about the mechanisms that control the flux of carbon from the surface to depth, from labile to refractory, and from high-molecular weight (HMW) to low molecular weight (LMW) have emerged. Advanced instrumentation such as NMR spectroscopy, FT-ICR MS, compound specific isotope studies, and the advancement of isotope measurements of very small samples, have allowed a more detailed understanding of marine DOC cycling.

This dissertation improved our understanding of the sources and cycling of RDOC through $\delta^{13}C$ and $\Delta^{14}C$ measurements of solid-phase extracted DOC (SPE-DOC). The following topics were addressed.

5.1 Isotopic heterogeneity in elutions of marine solid-phase extracted DOC

Solid-phase extraction (SPE) is commonly used to isolate the hydrophobic portion of DOC that is typically low-molecular weight, and refractory. This technique was popularized for its ease of use and high recoveries of carbon (Dittmar et al., 2008). Although this technique was reported increasingly in the scientific literature, there was little information about the mass or isotopic composition of extraneous carbon (C_{ex}) associated with the SPE resin. Additionally, there was also a lack of information about the use of 6 mL methanol recommended for SPE elutions. At the outset of this work, we implemented the use of SPE method at-sea to extract DOC for future isotopic analyses, but needed to know how much our isotopic measurements would be affected by SPE C_{ex}.

In Chapter 2 of this dissertation, the characteristics of the SPE method are explored using spectrophotometry, $\delta^{13}C$ and $\Delta^{14}C$ analyses, and an indirect isotopic assessment of C_{ex}. Seawater from the Newport Beach Pier (NBP), CA extracted using the SPE method was tested using spectrophotometry to determine the elution volume needed to establish the methanol baseline. We determined that ~32 mL was required for elution, and this volume was used for future experiments. Four sets of subsequent SPE extractions and elutions were used to analyze the changes in $\delta^{13}C$ and $\Delta^{14}C$ throughout the elution. The heterogeneity of $\delta^{13}C$ and $\Delta^{14}C$ values indicated that marine-like SPE-DOC with low $\Delta^{14}C$ values elute first, and terrestrial-like SPE-DOC with higher $\Delta^{14}C$ values eluted later, with highest values obtained at around 6-7 mL.

This result is significant because 1) the isotopic heterogeneity is shown in triplicate, indicating this is a robust result that can be reproduced, and 2) the isotopic composition of a sample may depend on the volume of methanol used. In our case, the majority of SPE-DOC mass eluted with the $\Delta^{14}C$ minimum around 3 mL. The relatively small amount of material with high $\Delta^{14}C$ values did not change the weighted average $\Delta^{14}C$ values. However, this study may serve as a proof of concept that such sequential elutions can be used to gain new understanding of heterogeneity of a given sample, and that some material could be missed if the elution is too low in volume.

Another significant result of this study is the indirect isotopic characterization of the mass of C_{ex} related to the SPE method. The mass of Cex is 9.8±5.5 µg C with a $\Delta^{14}C$ of -997‰. These values are used in the blank-corrections SPE-DOC samples in this dissertation. However, future SPE-DOC analyses should re-constrain C_{ex} as it may vary between users and laboratories.

5.2 Basin-scale depletion of SPE-DOC $\Delta^{14}C$

Chapter 3 of this dissertation focuses on characterizing the basin-scale offset in $\Delta^{14}C$ values between SPE-DOC and total DOC. Seawater from two GO-SHIP Repeat Hydrography Cruises in the Pacific Ocean and one in the Indian Ocean were used to create a database of SPE-DOC

radiocarbon ($\Delta^{14}C$) values at 0-200 m and 2000-4000 m. These SPE-DOC $\Delta^{14}C$ values were compared directly to total DOC $\Delta^{14}C$ and the $\Delta^{14}C$ value of the non-retained fraction was calculated. Although the non-retained fraction has higher $\Delta^{14}C$ than total DOC $\Delta^{14}C$, it is still much lower than DIC $\Delta^{14}C$. This indicates that a residual amount of RDOC exists in the non-retained portion and may have escaped solid-phase extraction due to hydrophobicity or other unidentified characteristics.

Assuming that SPE-DOC approximates RDOC, and that non-retained DOC is a two-component mixture of more RDOC and labile DOC, a simple mass-balance model is used to estimate the percent abundance of $RDOC_{total}$ at different regions. Percent abundance of $RDOC_{total}$ refers to the sum of RDOC in the SPE-DOC and non-retained portions. Estimates of $RDOC_{total}$ in the deep ocean are the same within error. In the surface ocean, estimates of $RDOC_{total}$ are more variable. When percent abundance of $RDOC_{total}$ is normalized to units of concentration (μmol L^{-1}), $RDOC_{total}$ is less variable. Surface ocean $RDOC_{total}$ is variable in terms of percent, but not concentration, in the surface ocean because of variable overlying concentrations of labile and semi-labile DOC, especially in the tropics and subtropical gyres. This result is reminiscent of the two-pool model, and provides new support for this theory of DOC cycling. Estimates of $RDOC_{total}$ abundance in the deep ocean average 88±3%, within two standard deviations of the previous RDOC estimate of 95% (Hansell 2013). These latitudinal estimates of RDOC may aid future biogeochemical models that resolve DOC cycling with higher resolution.

5.3 Basin-scale depletion of SPE-DOC $\delta^{13}C$ supports evidence of the predominant ocean microbial carbon pump

The $\Delta^{14}C$ measurements described in Section 5.2 have accompanying stable carbon isotopic ($\delta^{13}C$) measurements. Similar to the relationship between SPE-DOC and total DOC $\Delta^{14}C$ values, SPE-DOC is lower in $\delta^{13}C$ across the Pacific and Indian Oceans. Lower values have been shown previously in a few measurements; however, they have been sparse both spatially and temporally. The dataset presented in Chapter 4 shows this phenomenon is present systematically in the global Pacific and Indian ocean. The

likely reason for this pattern is the preferential remineralization of large biomolecules with high $\delta^{13}C$ values, leaving the DOC pool with small bacterial remineralization products such as CRAM, and with lower $\delta^{13}C$ values. These compounds are also refractory in nature, allowing them to avoid degradation and become older (low $\Delta^{14}C$ values). The influence of the microbial carbon pump has been demonstrated previously (Jeffrey et al., 1983; Jiao et al., 2010; Lechtenfeld et al., 2015). However, this is the first instance in which $\delta^{13}C$ and $\Delta^{14}C$ values, on a basin-scale, have been used as evidence to support this mechanism in controlling the ocean carbon cycle.

5.4 Future work

What is the role of dissolved black carbon in the low $\Delta^{14}C$ values of marine DOC?

This dissertation has found key isotopic evidence that supports the MCP as a driving mechanism behind long-term DOC storage. However, individual molecules with significantly low $\Delta^{14}C$ may also contribute to the observed age of total DOC. Compound specific isotope analyses can be used to identify the concentration and isotopic characteristics of individual molecular classes. One key molecular class that requires more constraints is dissolved black carbon (DBC). Black carbon (BC) is formed during the incomplete combustion of fossil fuels and biomass. Masiello (1998) found that BC in deep sea sediments had ^{14}C ages 13,900 years older than non-BC sedimentary organic carbon deposited at the same time, indicating BC was an ancient component of DOC. Ziolkowski and Druffel (2010) and Coppola and Druffel (2016) found DBC was 4,800±620 ^{14}C years old in the surface ocean and 23,000±3000 ^{14}C years old in the deep ocean. There are few measurements of DBC that are sparse spatially.

A new dataset of [DBC] and DBC $\delta^{13}C$ and $\Delta^{14}C$ values from samples that were collected on the GO-SHIP cruises mentioned above will be key pieces of information in our understanding of the role pyrogenic carbon and its low $\Delta^{14}C$ values play in low total DOC $\Delta^{14}C$ signature. Interestingly, new research has suggested that oceanic DBC has marine-like $\delta^{13}C$ values (Wagner et al., 2019), in contrast to the previous paradigm that such molecules must be pyrogenic or hydrothermal in nature due to their high

double bond equivalences (Dittmar & Koch, 2006; Dittmar & Paeng, 2009). This potential GO-SHIP dataset of DBC could also include $\delta^{13}C$ values to compare with this intriguing work.

Characterization of non-retained DOC

About 60% of the DOC pool is viewed on a molecular level only indirectly through differences between SPE-DOC and total DOC. Through this approach, the $\delta^{13}C$, $\Delta^{14}C$, and C/N values of this non-retained DOC pool has been estimated (Broek et al. 2020; Zigah et al. 2017, this work). However, no study has yet directly observed the molecular characteristics of this sub-pool that avoids isolation on solid-phase extraction resins likely due to hydrophilic properties. In the non-retained DOC pool, the observed $\delta^{13}C$, $\Delta^{14}C$, and C/N values could arise from a number of different combinations of DOC from the biological pump, MCP, fluvial sources, or chemosynthesis in the deep ocean. Molecular characterization of the non-retained DOC pool is important for our complete understanding of DOC cycling.

Until new techniques are developed to directly observe the non-retained DOC, studies that combine all available techniques to compare DOC sub-pools may provide a wider window through which to view the non-retained DOC. This includes the combination of FT-ICR MS and carbon isotope measurements, which are often reported in separate studies. Table 1 (Introduction) outlines many noteworthy studies that use SPE-DOC for further molecular characterization; however, FT-ICR MS analyses are often not used alongside isotopic measurements. These are both powerful analytical tools in their own right; but may lead to new discoveries when combined.

5.5 Conclusion

In summary, this dissertation advanced our understanding of commonly used SPE protocols and how isotopic characteristics of SPE-DOC change during elutions. An updated SPE protocol was used to create a high-resolution dataset of SPE-DOC $\delta^{13}C$ and $\Delta^{14}C$ values on three GO-SHIP Repeat Hydrography Cruises that span the Pacific Ocean and western Indian Ocean. Through direct comparison

with total DOC isotopic measurements, systematically low SPE-DOC $\delta^{13}C$ and $\Delta^{14}C$ suggest that the MCP drives long-term storage of DOC in the deep ocean through the selective respiration of large biomolecules with high $\delta^{13}C$, and the production of RDOC that has low $\Delta^{14}C$.

5.6 References

Broek, T. A. B., Walker, B. D., Guilderson, T. P., Vaughn, J. S., Mason, H. E., & McCarthy, M. D. (2020). Low Molecular Weight Dissolved Organic Carbon: Aging, Compositional Changes, and Selective Utilization During Global Ocean Circulation. *Global Biogeochemical Cycles*, *34*(6), 1–20. https://doi.org/10.1029/2020GB006547

Coppola, A. I., & Druffel, E. R. M. (2016). Cycling of black carbon in the ocean. *Geophysical Research Letters*, *43*(9), 4477–4482. https://doi.org/10.1002/2016GL068574

Dittmar, T., Koch, B., Hertkorn, N., & Kattner, G. (2008). A simple and efficient method for the solid-phase extraction of dissolved organic matter (SPE-DOM) from seawater. *Limnology and Oceanography: Methods*, *6*(6), 230–235.

Dittmar, T., & Koch, B. P. (2006). Thermogenic organic matter dissolved in the abyssal ocean. *Marine Chemistry*, *102*(3–4), 208–217. https://doi.org/10.1016/j.marchem.2006.04.003

Dittmar, T., & Paeng, J. (2009). A heat-induced molecular signature in marine dissolved organic matter. *Nature Geoscience*, *2*(3), 175–179. https://doi.org/10.1038/ngeo440

Hansell, D. A., Carlson, C. A., Repeta, D. J., & Schlitzer, R. (2009). Dissolved organic matter in the ocean: A controversy stimulates new insights. *Oceanography*, *22*(4), 202–211.

Jeffrey, A. W. A., Pflaum, R. C., Brooks, J. M., & Sackett, W. M. (1983). Vertical trends in particulate organic carbon 13C:12C ratios in the upper water column. *Deep Sea Research*, *30*(9A), 971–983.

Jiao, N., Herndl, G. J., Hansell, D. A., Benner, R., Kattner, G., Wilhelm, S. W., Kirchman, D. L., Weinbauer, M. G., Luo, T., Chen, F., & Azam, F. (2010). Microbial production of recalcitrant dissolved organic matter: Long-term carbon storage in the global ocean. *Nature Reviews Microbiology*, *8*, 539–599.

Lechtenfeld, O. J., Hertkorn, N., Shen, Y., Witt, M., & Benner, R. (2015). Marine sequestration of carbon in bacterial metabolites. *Nature Communications*, *6*(1), 8. https://doi.org/10.1038/ncomms7711

Masiello, C. A. (1998). Black Carbon in Deep-Sea Sediments. *Science*, *280*(5371), 1911–1913. https://doi.org/10.1126/science.280.5371.1911

Wagner, S., Brandes, J., Spencer, R. G. M., Ma, K., Rosengard, S. Z., Moura, J. M. S., & Stubbins, A. (2019). Isotopic composition of oceanic dissolved black carbon reveals non-riverine source. *Nature Communications*, *10*(1), 5064. https://doi.org/10.1038/s41467-019-13111-7

Williams, P. M., & Druffel, E. R. M. (1987). Radiocarbon in dissolved organic matter in the central North

Pacific Ocean. *Letters to Nature*, *330*(6145), 246–248. https://doi.org/10.1038/330246a0

Zigah, P. K., McNichol, A. P., Xu, L., Johnson, C., Santinelli, C., Karl, D. M., & Repeta, D. J. (2017). Allochthonous sources and dynamic cycling of ocean dissolved organic carbon revealed by carbon isotopes. *Geophysical Research Letters*, *44*, 2407–2415. https://doi.org/10.1002/2016GL071348

Ziolkowski, L. A., & Druffel, E. R. M. (2010). Aged black carbon identified in marine dissolved organic carbon. *Geophysical Research Letters*, *37*(16). https://doi.org/10.1029/2010GL043963